TP-3679 E

SHIP RESISTANCE TO CONTINUOUS MOTION IN LEVEL ICE

prepared for the
TRANSPORTATION DEVELOPMENT CENTRE
TRANSPORT CANADA
Montréal, Québec, Canada

préparé pour le
CENTRE DE DÉVELOPPEMENT DES TRANSPORTS
TRANSPORTS CANADA
Montréal, Québec, Canada

CA1
DTC 801
83
S36
c.2

ar
NALD CARTER, D.Sc.,
génieur Conseil / Consulting Engineer
1281 Bishop
Sainte-Foy, Québec
G1W 3E4

Library and Information Centre/
Centre de Documentation (GSLA)
RECEIVED - REÇU LE
JUN 2 1983
Transport Canada / Transports Canada

TP-3679 E

SHIP RESISTANCE TO CONTINUOUS MOTION IN LEVEL ICE

prepared for

TRANSPORTATION DEVELOPMENT CENTRE
TRANSPORT CANADA
1000 Sherbrooke St. W.
Suite 2421
Montreal, Quebec H3A 2R3

by

Dr. Donald Carter, P.Eng.
Consulting Engineer
1281 Bishop Avenue
Ste Foy, P.Q. G1W 3E4
Tel.: (418) 656-0690

MARCH 1983

"The contents of this report reflect the views of the contractor and not necessarily the official views or policies of the Transportation Development Centre , Transport Canada."

REPORT DOCUMENTATION FORM

1. Transport Canada Report No. TP-3679 E	2. TDC Project No 4472	3. Recipient's Catalogue No

4. Title and Subtitle Ship Resistance to Continuous Motion in Level Ice.	5. Report Date MARCH 1983 6. Performing Organization Report No
7. Author(s) D.S. Carter	8. Transport Canada File No D1460-177-1
9. Performing Organization Name and Address Donald Carter, Consulting Engineer, 1281 Avenue Bishop, Ste-Foy, P.Q. G1W 3E4	10. DSS File No. 09SD.T8200-1-1529 11. DSS or Transport Canada Contract No 1SD81-00081
12. Sponsoring Agency Name and Address TRANSPORTATION DEVELOPMENT CENTRE (TDC) TRANSPORT CANADA 1000 Sherbrooke W., Suite 2421 Montreal, Quebec, H3A 2R3	13. Type of Report and Period Covered Final, May 81 March 83 14. Sponsoring Agency Code 4472
15. Supplementary Notes	16. TDC Project Officer J.E. Laframboise

17. Abstract

This report presents an analysis of the various ice failure mechanisms involved in breaking and moving through level ice and presents a method for evaluating the ship resistance to continuous motion. The mathematical model developed is sensitive to the various principal ship and ice parameters. Correlation of model results with the existing full-scale data seems relatively good.

18. Key Words Icebreaking, Ice navigation, Ice mechanics, Ice Forces,	19. Distribution Statement Limited number of copies available from TDC.

20. Security Classification (of this report) nil	21. Security Classification (of this page) nil	22. No. of Pages 142	23. Price nil

TDC/CDT 79-005

FORMULE DE DOCUMENTATION POUR RAPPORT

1. Nº du rapport Transports Canada
TP-3679 E

2. Nº de l'étude — CDT
4472

3. Nº de catalogue du destinataire

4. Titre et sous-titre
Ship Resistance To Continuous Motion in Level Ice.

5. Date du rapport
MARS 1983

6. Nº du rapport de l'organisme executant

7. Auteur(s)
D.S. Carter

8. Nº de dossier Transports Canada
D1460-177-1

9. Nom et adresse de l'organisme exécutant
Donald Carter,
Ingénieur-Conseil,
1281 Avenue Bishop,
Ste-Foy, P.Q. G1W 3E4

10. Nº de dossier — ASC
09SD.T8200-1-1529

11. Nº de contrat — ASC ou Transports Canada
1SD81-00081

12. Nom et adresse de l'organisme parrain
CENTRE DE DEVELOPPEMENT DES TRANSPORTS (CDT)
TRANSPORTS CANADA
1000 O., rue Sherbrooke, Suite 2421
Montréal, Québec, H3A 2R3

13. Genre de rapport et periode visee
Final, Mai 81 Mars 83

14. Code de l'organisme parrain
4472

15. Remarques additionnelles

16. Agent de projet — CDT
J.E. Laframboise

17. Résumé

Le présent rapport soumet une analyse des différents mécanismes de rupture d'un champ de glace uniforme et propose une méthode de calcul de la résistance à l'avancement continu d'un navire. Le modèle mathématique obtenu s'avère sensible aux caractéristiques principales du navire et de la glace. La correlation entre les résultats du modèle et les mesures effectués en nature paraît être relativement bonne.

18. Mots-clés
Brise-glace, Glace,
Mécanique des glace,
Navigation hivernale,
Poussée des glaces.

19. Diffusion
Nombre limité de copies disponibles au CDT

20. Classification de sécurité (de ce rapport)
nil

21. Classification de sécurité (de cette page)
nil

22. Nombre de pages
142

23. Prix
nil

ACKNOWLEDGEMENTS

This study began with an unsolicited proposal to Department of Supply and Services, Science Centre, in April 1981. Under Transport Canada sponsorship, and aided by Department of Supply and Services bridge funding, the project got underway in September 1981.

J.E. Laframboise was appointed scientific authority from Transport Canada and, Jean Lacelle, a D S S science procurement manager, handled the negotiation and management of the contract.

The author would like to express his thanks to all those who have given advice and assisted in the project. In particular, he wishes to express his gratitude to J.E. Laframboise and Ian Bayly, from the Transportation Development Centre, Transport Canada, for their excellent cooperation

Sincere acknowledgements are also expressed to Jean Lacelle for his assistance.

SUMMARY

This report presents a study undertaken by the Transportation Development Centre, Transport Canada, to develop a method for evaluating the total resistance to ship motion through level ice. Such a predictive model would provide the ship designer with a meaningful tool for optimizing ice passage capability.

In the initial stages of the analysis, considerable effort was devoted to represent the forebody lines of conventional icebreakers by mathematical functions. An analytical method of hull definition was required to conduct a parametric study on the influence of major ship parameters on ice resistance.

The largest ice forces encountered at each point along the bow were established by determining the intensity of the forces at which the ice cover fails. Depending on geometrical parameters and ice characteristics, the ice cover may fail by crushing, bending, or buckling whichever requires less force.

The resistance to ship motion was then obtained by integrating the elementary compression and friction forces exerted by the ice on the entire bow section. The total resistance was found to be dependent on the following ship parameters:

a.: Length of entrance of the forebody;
b.: Maximum beam;
c.: Bow opening angle;
d.: Stem angle;
e.: Flare angle at maximum beam;
f.: Coefficient of friction.

Correlation of model predictions with actual full-scale field data and model test data has been shown to be good over a wide range of ship parameters and environmental conditions.

TABLE OF CONTENTS

INTRODUCTION 1

1.: SCHEMATIC REPRESENTATION OF THE PROBLEM 3

2.: ICE FAILURE CRITERIA 9

3.: CONTINUOUS MODE OF ICEBREAKING 13
  3.1.: ICE RESISTANCE UNDER QUASI-STATIC CONDITIONS 17
    3.1.1.: ICE RESISTANCE REFERRED TO THE STEM 19
    3.1.2.: ICE RESISTANCE REFERRED TO THE SIDES 23
    3.1.3.: TOTAL ICE RESISTANCE UNDER QUASI-STATIC CONDITIONS 25
  3.2.: ICE RESISTANCE UNDER DYNAMIC CONDITIONS 29
  3.3.: ICE PRESSURE EFFECT 33
  3.4.: SNOW COVER EFFECT 35

4.: FINAL RESULTS 36

5.: COMPARISON WITH EXPERIMENTAL DATA 38
  5.1.: USCGC STATEN ISLAND 41
  5.2.: USCGC MACKINAW 43
  5.3.: CCGS LOUIS ST.LAURENT 45
  5.4.: USSR MOSKVA 47
  5.5.: CCGS WOLFE (Converted Hull) 49
  5.6.: CCGS PIERRE RADISSON 51
  5.7.: COMMENTS 56

CONCLUSIONS AND RECOMMENDATIONS 58

REFERENCES 61

Appendix "A" ICE FORCES 63
Appendix "B" COMPUTER PROGRAMS 91
Appendix "C" LOAD DISTRIBUTION 97
Appendix "D" FURTHER COMPARISONS WITH FULL SCALE DATA 109
Appendix "E" COMPARISON WITH OTHER LEVEL ICE MODELS 125
Appendix "F" OPTIMUM CHARACTERISTICS OF THE HULL-ICE INTERFACE 131

LIST OF FIGURES

Figure 1.1.: Schematic Representation of the Bow Branch of the Waterline and Symbols Used. 2

Figure 1.2.: Distance from Maximum Beam Section to Bow 4

Figure 1.3.: Typical Variation of the Calculated Flare Angle and Angle s 4

Figure 1.4.: Comparison of Elliptical Approximation to the Waterlines with the Data Measured from Lines Plans of Four Different Icebreakers 6

Figure 1.5.: Comparison of Approximation to Waterline Run Angles with Data Measured from Lines Plans of Four Different Icebreakers 6

Figure 1.6.: Comparison of Approximation to Frame Angles with Data Measured from Lines Plans of Four Different Icebreakers 7

Figure 2.1.: Schematic Representation of the Floating Truncated Wedge Formed by the Cracks Emanating from the Loaded Region 8

Figure 2.2.: Failure Criteria for Loads Applied at the Edge of a Truncated Wedge Resting on Water 10

Figure 3.1.: Fracture Load Exerted on Ship Hull by Direct Contact with Unbroken Ice Sheet or through Ice Floes 12

Figure 3.2.: Most Probable Intervals Referred to Stem and Sides. Final Integration of Elementary Forces is not Altered by the Intervals Assumed. 16

Figure 3.3.: Characteristics of the Contacting Interface Between Ice and Stem 18

Figure 3.4.: Comparison Between the Exact Solution (EQ.: 3.5) and the Approximate Solution (EQ.: 3.7) Shown as Dashed Line. 20

Figure 3.5.: Characteristics of the Contacting Interface Between the Ice and the Sides of the Bow Section 22

LIST OF FIGURES (Cont'd)

Figure 3.6.: Plot of Relative Ice Resistance versus a) Maximum Beam, B , and b) Length, L/2 , from Bow to Maximum Beam Section 26

Figure 3.7.: Plot of Relative Ice Resistance versus a) Stem Angle, β , and b) Flare Angle, γ , at Maximum Beam Section 27

Figure 3.8.: Plot of Relative Ice Resistance versus a) Bow Opening Angle, θ , and b) Coefficient of Friction 28

Figure 3.9.: Plot of Relative Ice Resistance versus Ship Speed 32

Figure 3,10.: Effect of Internal Ice Pressure on the Stress Distribution 34

Figure 5.1.: Predicted Icebreaking Resistance for USCG STATEN ISLAND as Compared to Regression Lines from Full Scale Trials and Model Tests 40

Figure 5.2.: Predicted Icebreaking Resistance for USCG MACKINAW as Compared to Regression Lines from Full Scale Trials and Model Tests 42

Figure 5.3.: Predicted Icebreaking Resistance for CCGS LOUIS ST.LAURENT as Compared to Regression Lines from Full-Scale Trials and Model Tests 44

Figure 5.4.: Predicted Icebreaking Resistance for USSR MOSKVA as Compared to Regression Lines from Full-Scale Trials and Model Tests 46

Figure 5.5.: Predicted Icebreaking Resistance for CCGS WOLFE (Converted Hull) as Compared to Measured Values in Snowless Ice Cover (0,28m) and in Ice Cover (0,46m) with Snow (0,18m) 48

Figure 5.6.: Predicted Icebreaking Resistance for CCGS WOLFE (Converted Hull) as Compared to Actual Measurements during Full-Scale Trials under Various Ice Conditions 50

LIST OF FIGURES (Cont'd)

Figure 5.7.: Predicted Icebreaking Resistance for CCGS PIERRE RADISSON as Compared to Measured Values in Deteriorated One-Year Sea Ice and in Solid Fresh and Saline Ice 52

Figure 5.8.: Predicted Icebreaking Resistance for CCGS PIERRE RADISSON as Compared to Actual Measurements during Full-Scale Trials under Dissimilar Ice Conditions 53

Figure 5.9.: Plot of Propeller Thrust Required to Overcome Level Ice Resistance versus Ship Speed. CCGS PIERRE RADISSON 54

Figure 5.10.: Typical Relationship between Ice Thickness and Speed of Advance in the Continuous Icebreaking Mode for the CCGS PIERRE RADISSON Operating at Full Power 55

Table 5.1.: Relevant Parameters of the Retained Ships and the Full-Scale Range (Minimum, Mean, Maximum) of the Test Conditions 39

LIST OF SYMBOLS

B : maximum beam (m);
E : elastic modulus (kPa);
F : force component due to side friction (kN);
H : horizontal load sufficient to cause buckling (kN);
$L^*/2$: bow section length from stem back to maximum beam (m);
L : ship's length (m);
M : bending moment sufficient to cause failure (kN-m);
M_0 : bending moment sufficient to cause failure of an ice sheet with internal pressure (kN-m);
N : force normal to the shell plating (kN);
P : load applied to the edge of the ice sheet (kN);
P_0 : failure load of an ice sheet with internal pressure (kN);
R_1 : ice resistance referred to the stem (kN);
R_2 : ice resistance referred to the sides (kN);
Re : Reynold's number based on ship's length;
R_i : resistance component due to ice forces (kN);
R_i^* : resistance in level ice under compression (kN);
R_{is} : total ice resistance under quasi-static conditions (kN);
R_{ow} : open-water resistance (kN);
R_s : snow resistance component (kN);
R_t : total resistance to continuous motion in level ice (kN);
V : ship velocity (m/s); vertical load (kN);
a_0 : semi-axis in the 0y-direction (m);
b_0 : semi-axis in the 0x-direction (m);
f : coefficient of friction between the hull and the ice;
h : thickness of the ice sheet (m);
h_s : snow cover thickness (m);
ℓ : characteristic length of the ice sheet (m) (See EQ.:2.5);
m : $\tan\theta$

LIST OF SYMBOLS (Cont'd)

r : angle between the perpendicular to the waterline and the direction of motion;

s : angle between the normal to the shell plating and the horizontal plane;

t : angle between the normal to the shell plating and the direction of motion;

$x, y, z,$: rectangular coordinates;

α : angle between the directions of motion and ice compression;

β : stem angle from horizontal;

γ : flare angle from vertical;

or water unit weight (kN/m^3);

η : water pressure expressed in equivalent of water height (m);

θ : bow opening angle;

κ : water unit weight (kN/m^3);

μ : dynamic viscosity of water;

ν : Poisson's ratio for ice;

ρ : mass density of water;

or non-dimensional radial distance;

σ : flexural strength of the ice (kPa);

σ_0 : effective internal pressure (kPa);

σ_1 : tensile strength of the ice sheet (kPa);

σ_2 : compressive strength of the ice sheet (kPa);

ϕ : opening angle of the wedge-shaped ice sheet;

χ : non-dimensional distance;

ω : deflection of the ice sheet (m);

Other symbols are defined in the text.

INTRODUCTION

Over the years, many attempts have been made to develop an expression to evaluate ship resistance to continuous motion through level ice. Unfortunately, due to the complexity of icebreaking process involving a tremendous number of variables, most models are of the empirical or semi-empirical type. These empirical or semi-empirical models tend to mirror the conditions under which they were determined including ice and ship parameters and, hence, do not lend themselves to extrapolation.

The goal of the work reported herein is to explore the possibility of deriving, on analytic grounds, a relatively simple model which would permit the desired degree of flexibility to optimize the design of capable and reliable icebreaking vessels. This analytical model should take into account the hull characteristics and environmental conditions which may influence the icebreaking resistance.

To achieve the ultimate goal of the study, the analysis has been divided into four (4) steps:

1.: Schematic representation of the problem;

2.: Consideration of possible ice failure mechanisms and derivation of appropriate ice failure criteria;

3.: Determination and integration of the incremental ice forces acting on the ship hull;

4.: Comparison of the proposed model predictions with full scale and model data available in open literature.

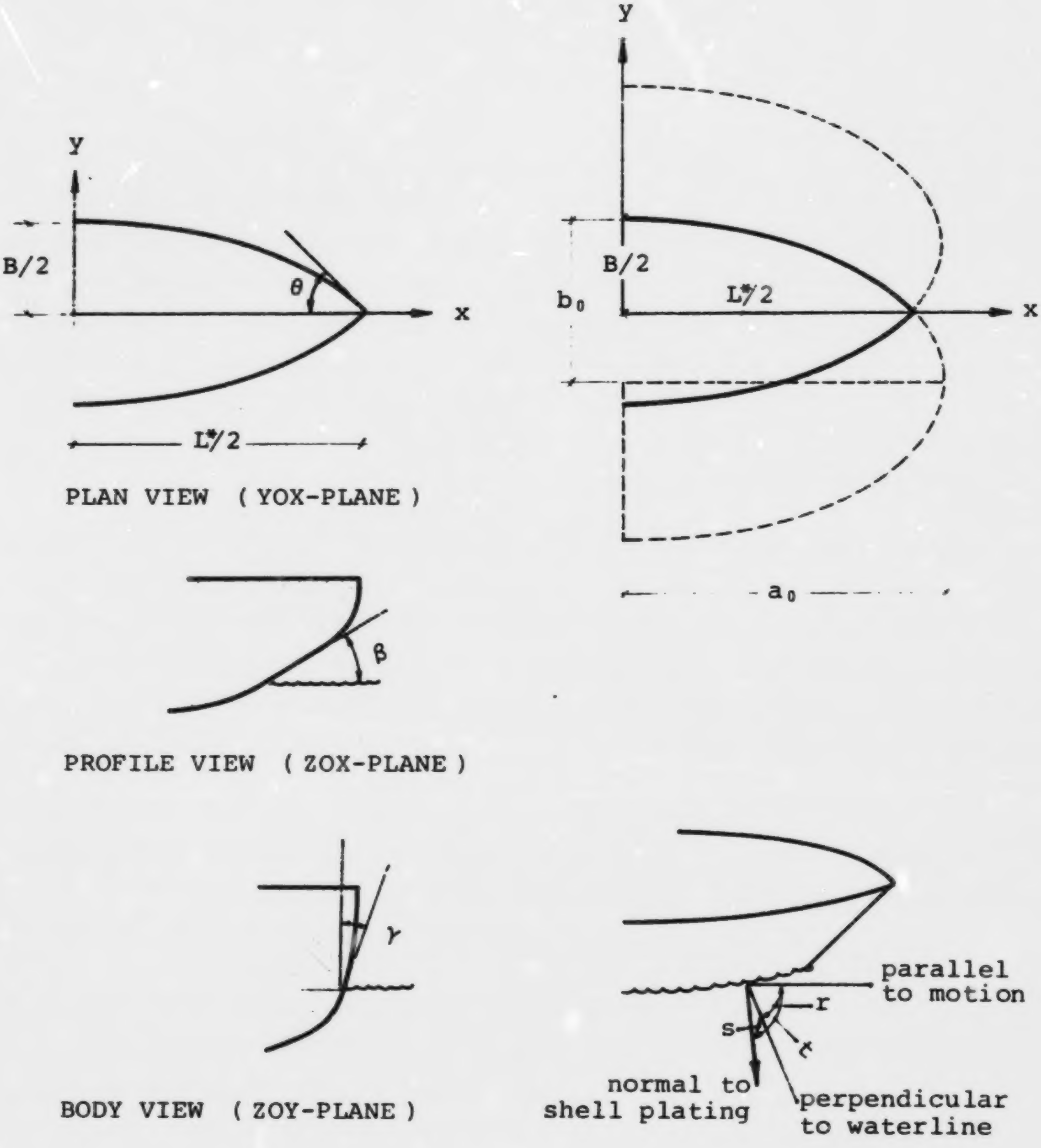
y
B/2
θ
x
L*/2
PLAN VIEW (YOX-PLANE)
y
B/2
b₀
L*/2
x
a₀
β
PROFILE VIEW (ZOX-PLANE)
γ
BODY VIEW (ZOY-PLANE)
parallel to motion
r
s
t
normal to shell plating
perpendicular to waterline

Figure 1.1.: Schematic representation of the bow branch of the waterline and symbols used.

1.: SCHEMATIC REPRESENTATION OF THE PROBLEM

To allow a systematic investigation of the effects of ship shape and size on the various mechanisms involved in breaking and moving through ice, it is very convenient to represent analytically the hull geometrical parameters.

It has been found that, for ships of conventional icebreaker form, the bow branch of the forebody waterplane can be closely represented by an arc of ellipse with semi-axes a_0 and b_0 and the center at $y = \pm(b_0 - B/2)$ where $B/2$ is the half-beam. (Figure 1.1.)

In order to fulfil the two (2) following conditions:

$$y = 0 \quad \text{at} \quad x = L^*/2$$

$$\frac{\partial y}{\partial x} = -\tan\theta \quad \text{at point } P(L^*/2, 0, 0)$$

where $L^*/2$: bow section length;

θ : bow angle;

the semi-axes of the ellipse in the plane $z = 0$ are determined as:

$$b_0 = \frac{B(mL^* - B)}{2(mL^* - 2B)}$$

$$a_0 = \left[\frac{(L^*/2)^2}{1 - \dfrac{(b_0 - B/2)^2}{b_0^2}}\right]^{\frac{1}{2}}$$

where $m = \tan\theta$.

From whence, we obtain:

$$y = \pm\left[\frac{B}{2} - b_0\left\{1 - \left(1 - \frac{x^2}{a_0^2}\right)^{\frac{1}{2}}\right\}\right]$$

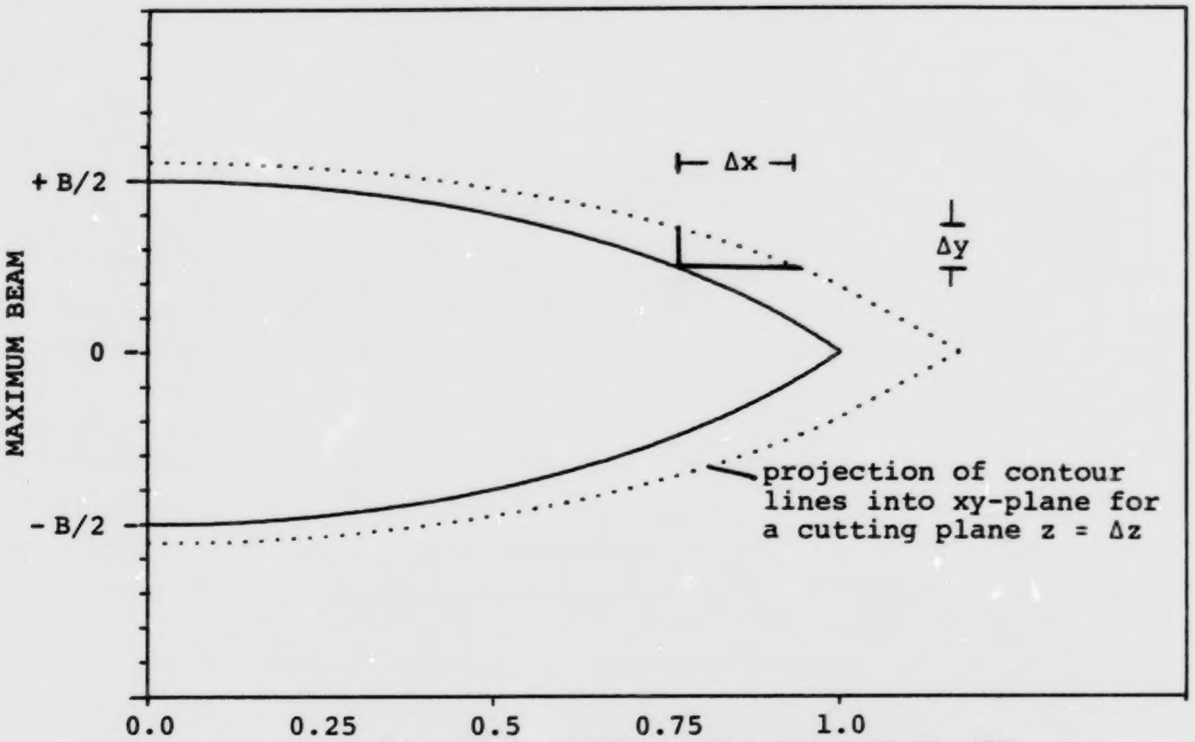
+ B/2
0
- B/2
MAXIMUM BEAM
Δx
Δy
projection of contour lines into xy-plane for a cutting plane z = Δz
0.0
0.25
0.5
0.75
1.0

Figure 1.2.: DISTANCE FROM MAXIMUM BEAM SECTION TO BOW.

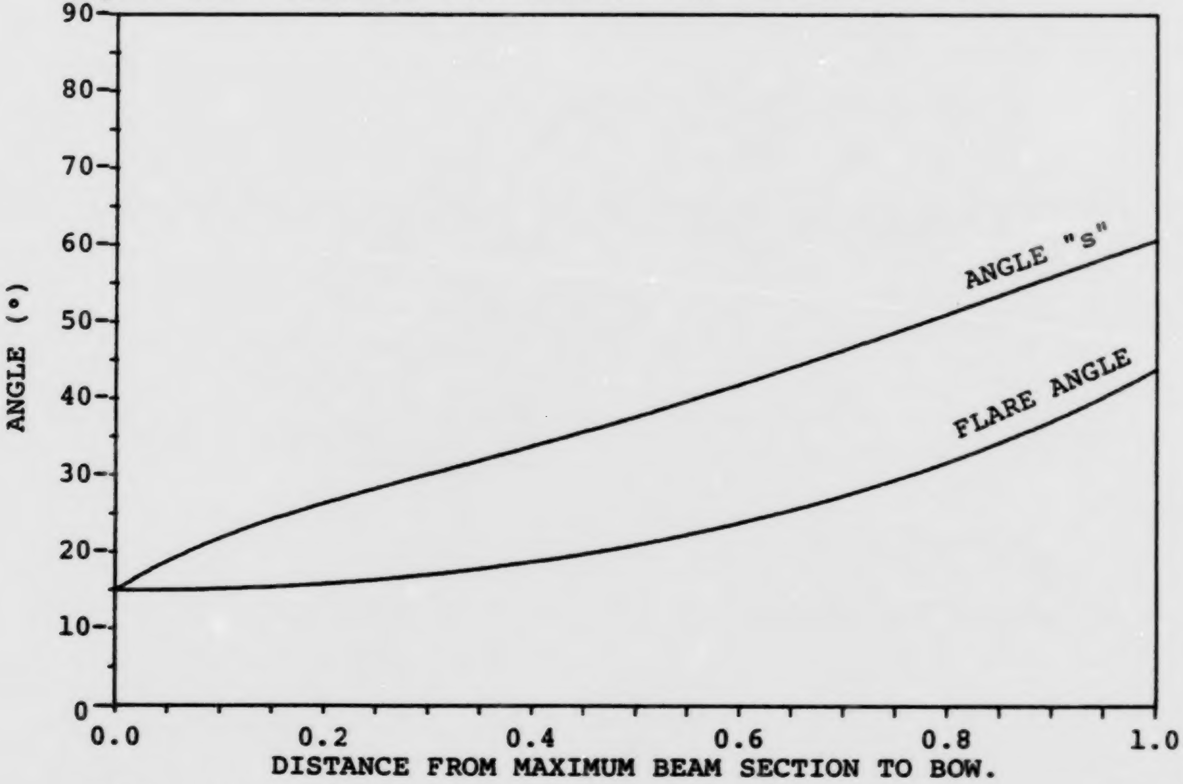

Figure 1.3.: Typical variation of the calculated flare angle and angle s.

To satisfy the two (2) conditions corresponding respectively to the bow angle, β, and to the flare angle, γ:

$$\frac{\partial x}{\partial z} = \cot \beta \quad \text{at } P\,(L^*/2,\, 0\,,\, 0\,)$$

$$\frac{\partial y}{\partial z} = \tan \gamma \quad \text{at } P\,(\,0\,,\, B/2\,,\, 0\,)$$

we determine the bow branch of the forebody in the plane $z_1 = \Delta z$ where:

$$B/2_1 = B/2 + \Delta z \tan \gamma$$

$$L^*/2_1 = L^*/2 + \Delta z \cot \beta$$

Figure 1.2 shows the superimposition of the bow branches for $z = 0$, in full line, and for $z = \Delta z$, in dashed line.

By geometrical considerations, the angles r, s, and t related to the normal at any point, $P(x,y,0)$, of the waterline are then obtained as:

$$\tan r = \frac{a_0}{b_0} \tan\left(\cos^{-1}(\,x/a_0\,)\right)$$

$$\tan s = \frac{\Delta x}{\Delta z} \cos r + \frac{\Delta y}{\Delta z} \sin r$$

$$\cos t = \cos r \cos s$$

Figure 1.3 shows a typical variation of the calculated flare angle, $\tan^{-1}(\Delta y/\Delta z)$, and the angle s comprised between the normal to the hull and the horizontal plane.

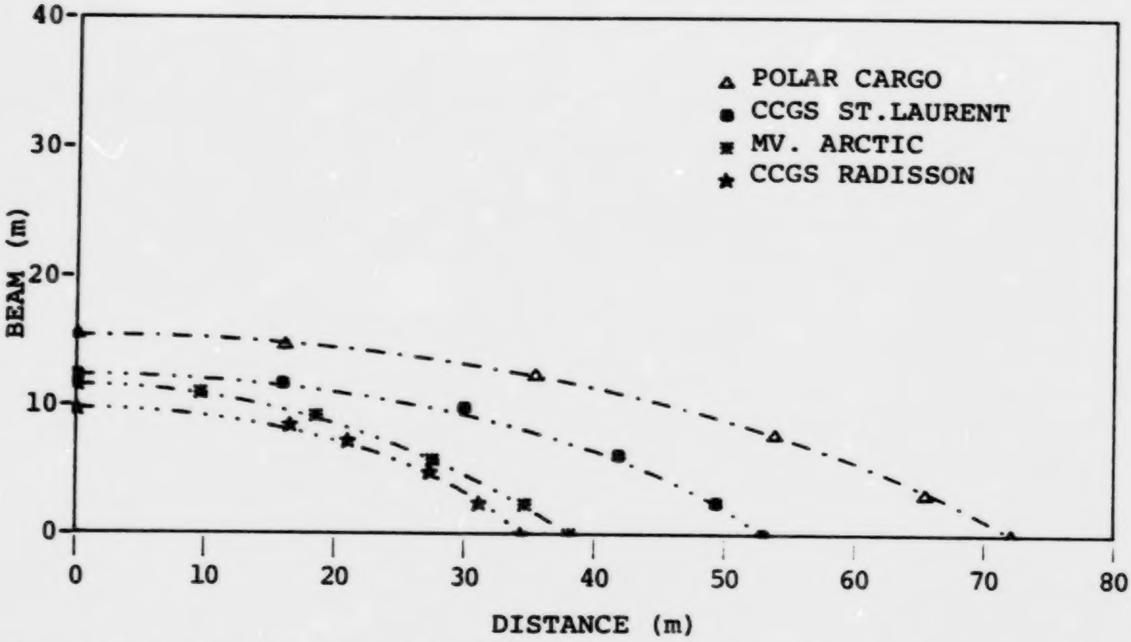

Figure 1.4.: Comparison of elliptical approximation to the waterlines with data measured from lines plans of four different icebreakers.

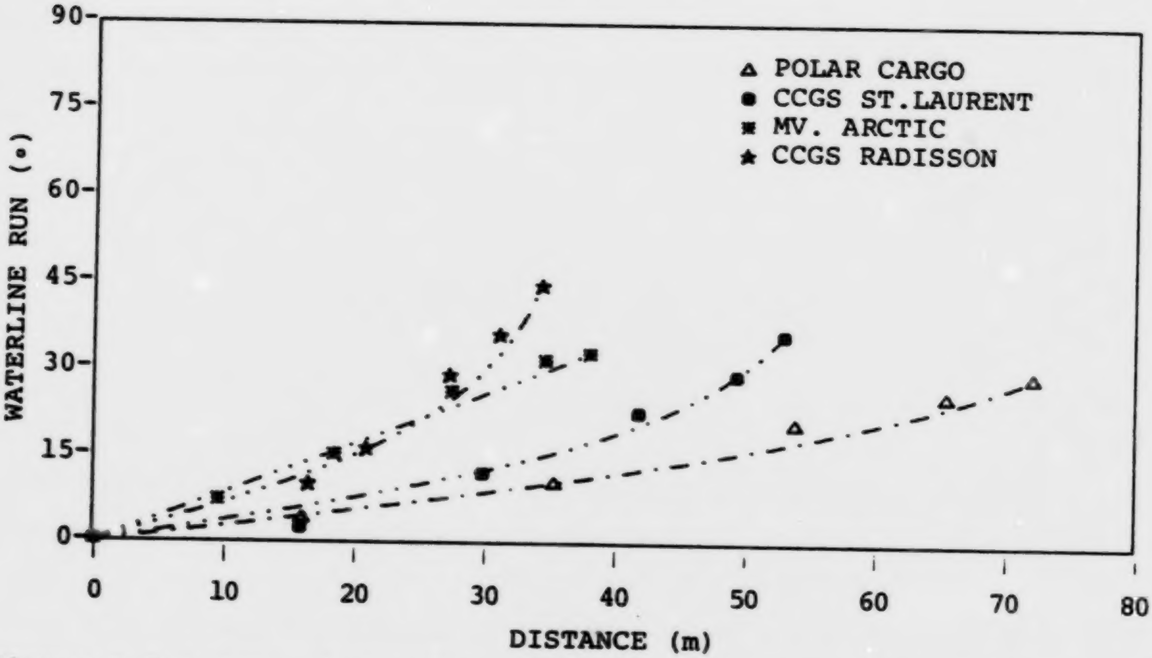

Figure 1.5.: Comparison of approximation to waterline run angles with data measured from lines plans of four different icebreakers.

The forebody waterline run angle is easily related to r as:

Waterline run angle = (90° - r)

It is now necessary to determine if the water plane shape represented by the above expressions applies to icebreaker hull forms. As a first step in this direction, Figure 1.4 shows the elliptical approximation to the waterlines of four different icebreakers along with data measured from their actual lines plan. Figures 1.5 & 1.6 show a comparison of hull angles, respectively waterline run and frame flare, with data measured from the lines plan of the four same ships.

As shown, the elliptical approximation represents satisfactorily icebreaker hull forms and, therefore, can be used for the purpose of our study.

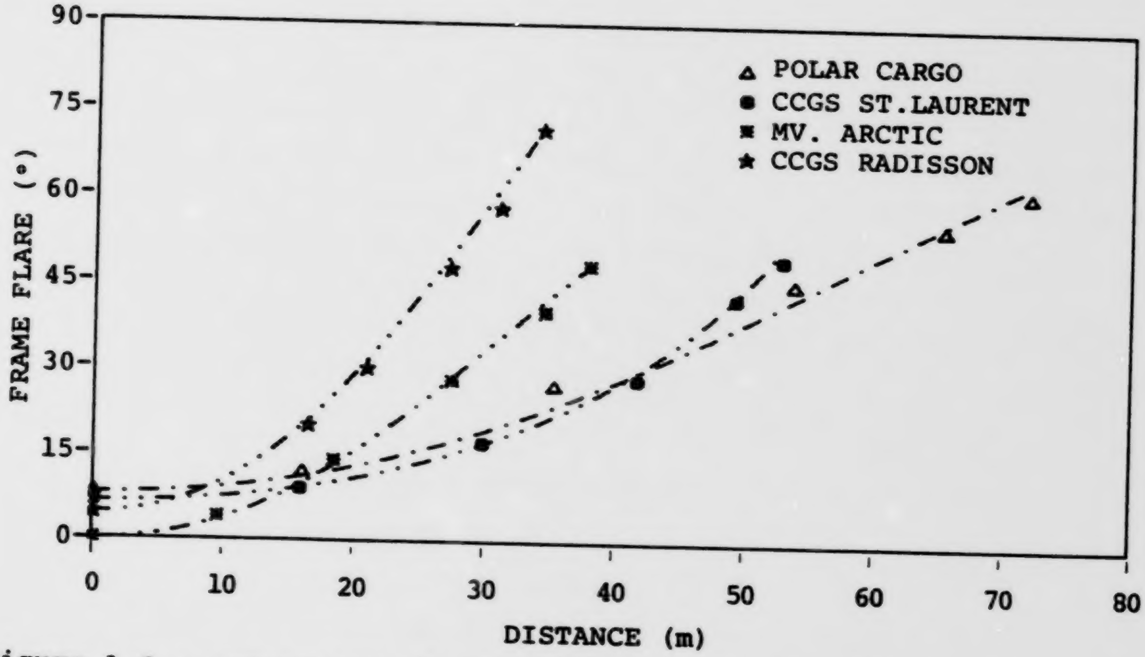

Figure 1.6.: Comparison of approximation to frame flare angles with data measured from lines plans of four different icebreakers.

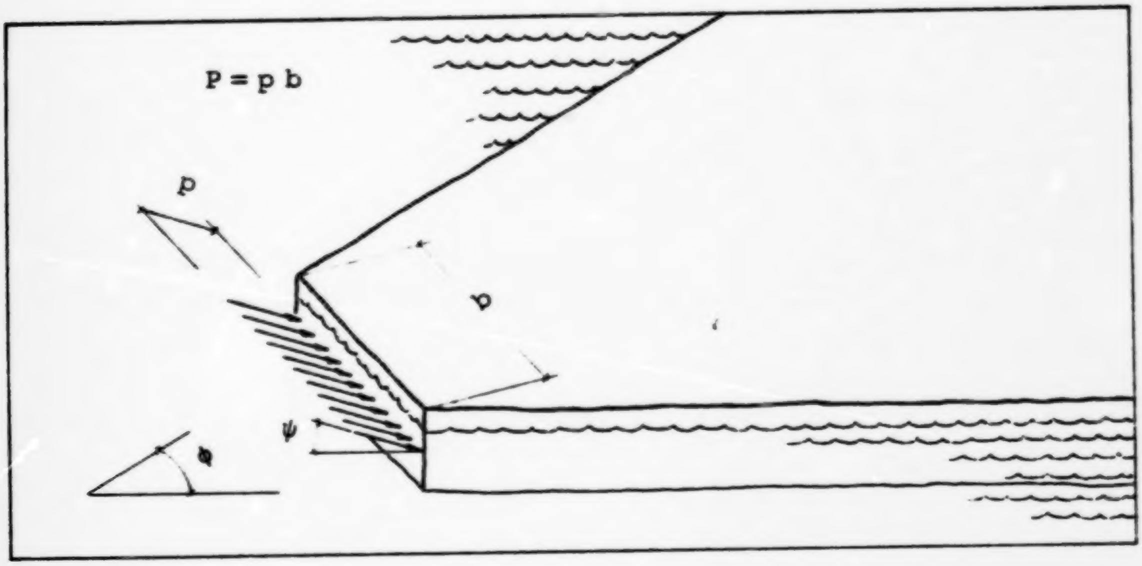

Figure 2.1.: Schematic representation of the floating truncated wedge formed by the cracks emanating from the loaded region.

2. ICE FAILURE CRITERIA

Field observations reveal that ice cover failures often occur in two steps: First, the ice cracks radially from the loaded region, and, under increasing load, this is followed either by local crushing at the contact area or by the formation of circumferential cracks that cause final failure of the inner part of the ice cover which is formed by the radial cracks.

A ice-force analysis for different loading conditions is presented in Appendix A. Our review of relevant analyses and tests has shown a marked distinction between the two situations of prime interest for engineering purposes:

a.: loads applied on the ice cover;
b.: loads applied at the edge of the ice cover.

The problem of bearing capacity of ice plates, i.e. loads applied on the ice cover, has been extensively studied both analytically and experimentally. However, no solution was available from the litterature for the determination of the largest force an ice cover may exert on a structure or a ship hull. That largest force, applied at the edge of an ice cover, is related to either the crushing or the formation of a circumferential crack in the truncated wedge (tapered beam) formed by the diverging cracks emaning from the loaded region of the ice plate. A floating truncated wedge is shown in Figure 2.1.

The type of ice cover failure depends on the relative values of the following parameters:

a.: h, the thickness of the ice cover;
b.: b, the width of the contact area;
c.: ψ, the angle between the direction of the load and the horizontal;

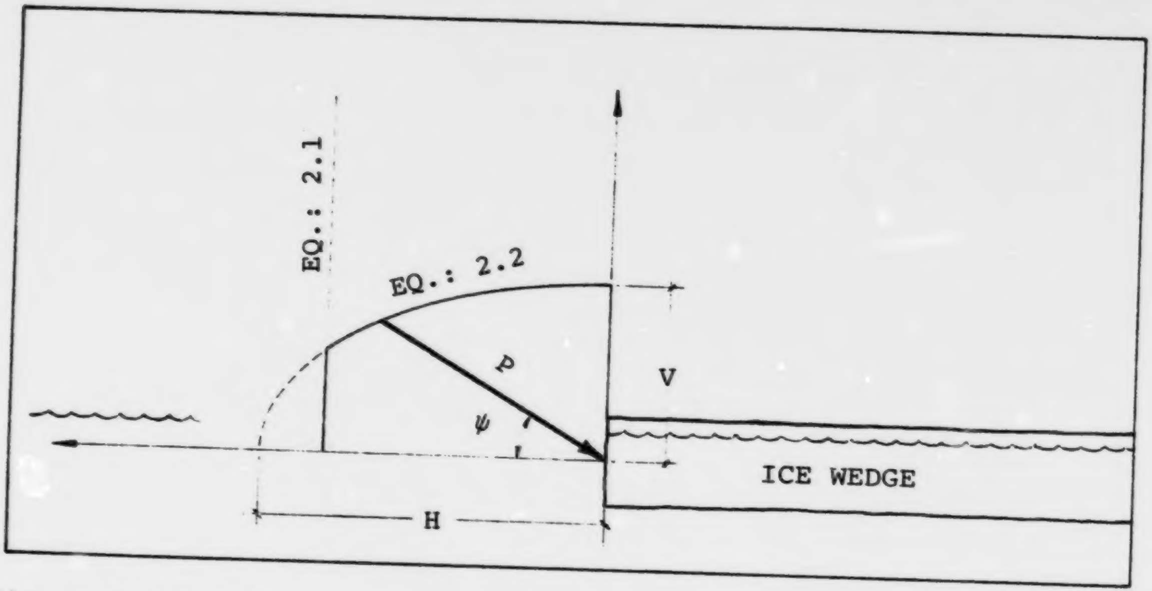
EQ.: 2.1
EQ.: 2.2
P
ψ
V
H
ICE WEDGE

Figure 2.2.: Failure criteria for loads applied at the edge of a truncated wedge resting on water.

2. ICE FAILURE CRITERIA (Cont'd)

d.: σ_1 , the tensile strength of the ice;
e.: σ_2 , the compressive strength of the ice.

Failure will occur by crushing when the load applied at the edge of the ice cover, P, will reach:

$$P = \left[\frac{\sigma_2\ h\ b}{\cos\psi}\right] \qquad \text{EQ.: 2.1}$$

Failure will occur by the combined effects of buckling and bending when the applied load, P, will reach:

$$P = \left[\frac{H^2\ V^2}{H^2 \sin^2\psi + V^2 \cos^2\psi}\right]^{\frac{1}{2}} \qquad \text{EQ.: 2.2}$$

where V: the vertical load sufficient to cause failure by bending; (Appendix A; EQ.: A.19)
H: the horizontal load sufficient to cause failure by buckling; (Appendix A; EQ.: A.25)

$$V = 0{,}5483\ (\ 0{,}5\phi\ +\ b/\ell\ )\ \sigma_1\ h^2 \qquad \text{EQ.: 2.3}$$

$$H = 1{,}5\ (\ 0{,}5\phi + b/\ell\ )\ \gamma\ \ell^3 \qquad \text{EQ.: 2.4}$$

where ϕ: the wedge opening angle at its apex (radians);
γ: the water unit weight;
ℓ: the characteristic length of the ice plate.

$$\ell = \left[\frac{E\,h^3}{12\,\gamma\,(\,1 - \upsilon^2)}\right]^{\frac{1}{4}} \qquad \text{EQ.: 2.5}$$

E being the Young's modulus and υ the Poisson's ratio for the ice.

The failure criteria for loads applied at the edge of an ice cover are represented graphically in Figure 2.2 by superimposing EQ.: 2.1 & 2.2.

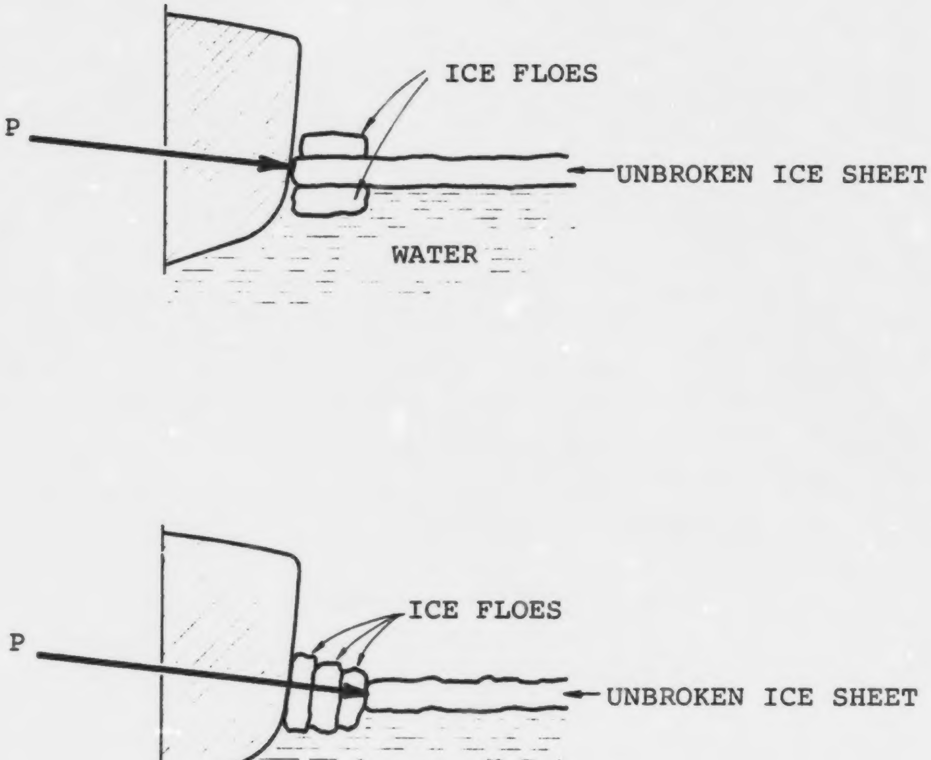
ICE FLOES
P
UNBROKEN ICE SHEET
WATER
ICE FLOES
P
UNBROKEN ICE SHEET
WATER

Figure 3.1.: Fracture load exerted on ship hull by direct contact with unbroken ice sheet or through ice floes.

3. CONTINUOUS-MODE ICEBREAKING RESISTANCE.

As an icebreaker impacts an unbroken ice field, a part of the ship kinetic energy is lost in overcoming the ice which, usually, is first crushed locally before failing at a certain distance from the contact area. The distance to the line of ice fracture is dependent upon ice characteristics and failure mode.

If applied propeller power is sufficient, the energy gained in accelerating to next impact equals that lost in overcoming the ice and the ship continues to move forward. Otherwise, motion may continue for only a few cycles before all kinetic energy is lost and the ship comes to a stop.

The ice forces acting on the ship hull are sawtooth in fashion, peaks corresponding to impacts with the solid ice field. As the ship moves through water filled with broken ice pieces of varying size, the forces exerted by the ice floes on the hull are necessarily smaller than the force resisted by the ice during breaking. An ice force cannot be larger than the force capable of breaking the ice cover.

The maximum peak load will correspond to the situation where the force capable of breaking the ice cover is applied on the whole ship forebody. This fracture load may be exerted on the hull by direct contact with the unbroken ice cover or through ice floes, as shown in Figure 3.1.

When an icebreaker progressing at some constant average speed impacts with the solid ice field, the total resistance, R_t , is the sum of the component resistances offered by the water, R_w , and by the ice, R_i . Since the presence of an ice cover may modify the open water resistance, R_{ow} , the total resistance is to be written:

$$R_t = R_i + R_{ow} + \Delta R_{ow}$$

where ΔR_{ow} is the variation of the open-water resistance resulting from the presence of the ice cover.

Experimental data show that, at the low velocity involved in icebreaking, the open-water resistance is only but a small part of the total resistance.

Since R_{ow} is usually small when compared with R_t and, furthermore, ΔR_{ow}, is probably small when compared with R_{ow}, it seems reasonable to consider the variation, ΔR_{ow}, to be a negligigle part of the total resistance which will be written:

$$R_t = R_i + R_{ow} \qquad \text{EQ.: 3.1}$$

In the absence of a more precise relation, generally determined empirically for each particular hull configuration, the open water resistance may be estimated using the formula recommended by the 1975 International Towing Tank Conference (Vance 1975).

$$R_{ow} = \frac{1}{2} \rho S V^2 (C_f + 0,0004) \qquad \text{EQ.: 3.2}$$

where: $S = 2,7 \sqrt{\text{Displacement} \times \text{Length}}$

$$C_f = \frac{0,075}{(\log_{10} Re - 2)^2}$$

Re being the Reynolds number based on ship's length defined as:

$$Re = \frac{V \times \text{length} \times \rho}{\mu}$$

where V is ship velocity; μ dynamic viscosity of water and ρ density of water.

As noted previously, the ice resistance may vary between the maximum force resisted by the ice during breaking and the force required for displacing the broken ice floes as the ship moves forward to the next impact with the unbroken pack.

The maximum ice resistance will occur when the breaking load is simultaneously applied on the entire length of the bow section of the waterline. The knowledge of this maximum peak load is required for the design of capable and reliable icebreaking vessels. It is this maximum ice resistance that will be investigated in this study.

In order to reach the aimed purpose, our continuous-mode icebreaking resistance model will be developped in two (2) steps:

1.: Mathematical description of the interaction between standard level ice and ship's hull under quasi-static conditions. This quasi-static model will take into account the ship's parameters, ice characteristics, and hull-ice friction.

2.: Modifications to quasi-static model in order to include the effects of ship's velocity, snow cover, and internal ice pressure.

In this manner, the ice resistance should be given as a function of the following parameters:

1.: ship's parameters;
2.: ice characteristics;
3.: hull-ice friction;
4.: ship's velocity;
5.: snow cover thickness;
6.: internal ice pressure.

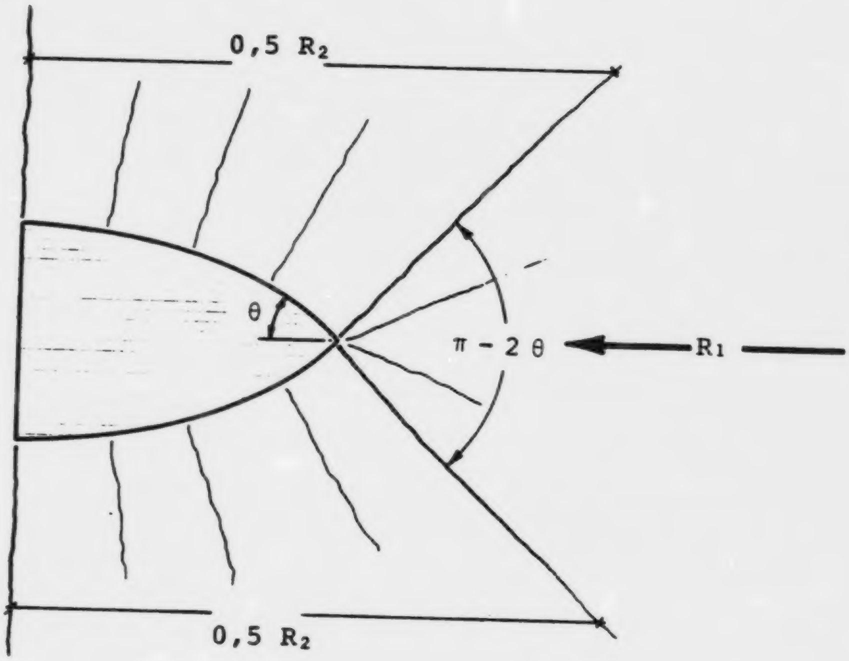
0,5 R₂
θ
π - 2 θ
R₁
0,5 R₂

Figure 3.2.: Most probable intervals referred to stem and sides. Final integration of elementary forces is not altered by the intervals assumed.

3.1.: ICE RESISTANCE UNDER QUASI-STATIC CONDITIONS.

Let us consider an icebreaker proceeding at some very low speed through a standard level ice cover. The total ice resistance corresponds then to the integration of all the individual forces exerted by the ice along the entire length of the bow section of the waterline, i.e. from the stem to the maximum beam.

From EQ.: 2.1 & 2.2, it can be seen that the breaking load depends on the direction of application, ψ, of the load. Since the direction of application of the load varies continuously in the interval comprised between the normals to the hull at the stem and at the maximum beam, it is very convenient to divide the total ice resistance into two (2) components:

$$R_{is} = R_1 + R_2$$

where: R_{is} : total ice resistance under quasi-static conditions;
R_1 : ice resistance referred to the stem;
R_2 : ice resistance referred to the sides.

The intervals corresponding respectively to R_1 and R_2 are shown in Figure 3.2.

Furthermore, it must be pointed out that, if the truncated wedge shown in Figure 2.1 is subdivided by additional radial cracks, the total fracture load which will then equal the sum of the loads on the individual wedges will remain unchanged. In other words, whatever it may be the number of wedges assumed, the total load remains uniquely a function of the total opening angle and the total width of the contact area. Therefore, the final result of the integration of the individual forces acting along the waterline will not be altered by the assumed number of radial cracks emanating from the contact area between the ice and the hull.

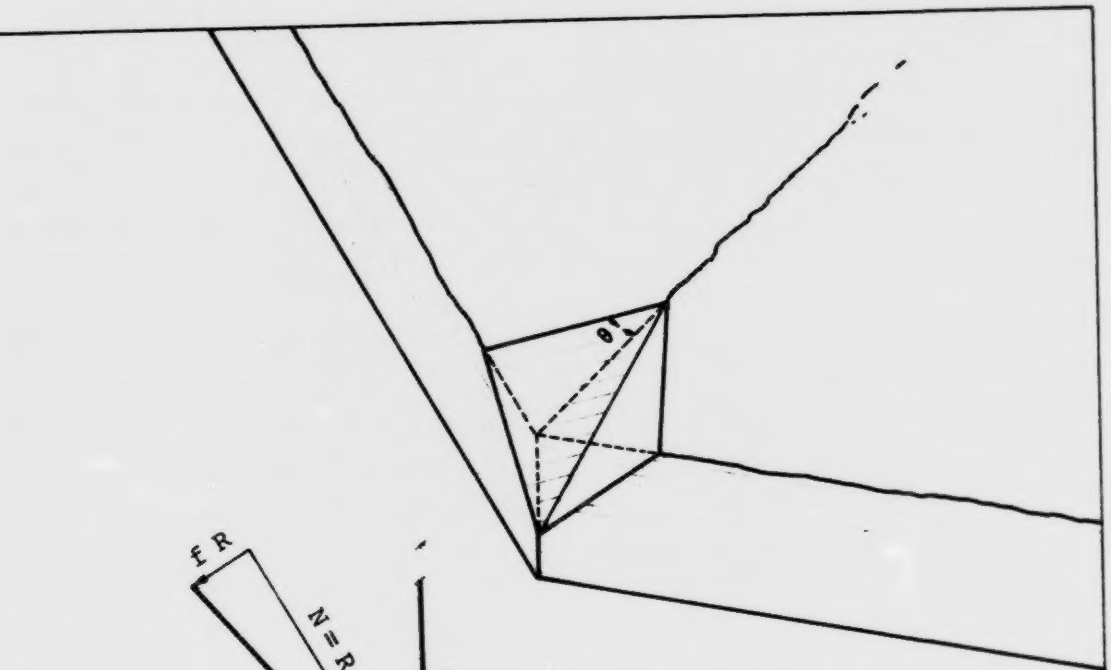

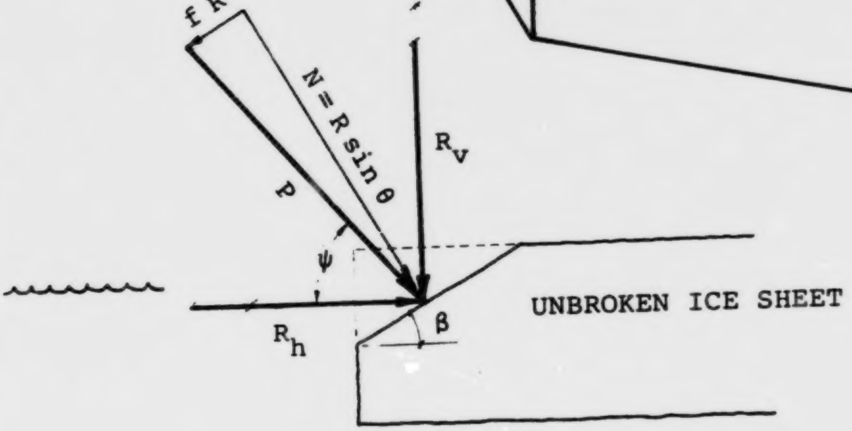
f R
N = R sin θ
P
ψ
R_v
R_h
β
UNBROKEN ICE SHEET
θ

PROFILE VIEW AND FORCE DIAGRAM

Figure 3.3.: Characteristics of the contacting interface between ice and stem.

3.1.1.: ICE RESISTANCE REFERRED TO THE STEM.

The characteristics of the contacting interface between ice and stem are shown in Figure 3.3. By trigonometric considerations, the direction of application, ψ, of the resultant force, P, is easily found from the force diagram:

$$\tan\psi = \left\{ \frac{\sin\theta \cos\beta - f \sin\beta}{\sin\theta \sin\beta + f \cos\beta} \right\} \qquad \text{EQ.: 3.3}$$

where ψ: direction of application of the resultant force;
θ: bow opening angle; β: stem angle; f: friction coefficient.

The above equation is identical to that first obtained by Runeberg in 1890.

Using the ice failure criterion given by EQ.: 2.2, the critical load, P, acting at an angle, ψ, may be written:

$$P = V \left\{ \frac{1}{\sin^2\psi + \frac{V^2}{H^2}\cos^2\psi} \right\}^{\frac{1}{2}} \qquad \text{EQ.: 3.4}$$

and the ice resistance referred to the stem, R_1, is given by:

$$R_1 = V \left\{ \frac{1}{\sin^2\psi + \frac{V^2}{H^2}\cos^2\psi} \right\}^{\frac{1}{2}} \cos\psi \qquad \text{EQ.: 3.5}$$

EQ.: 3.5 is shown as full line in Figure 3.4. Since, under practical applications, the buckling failure load, H, is much greater than the bending failure load, V, and, ψ, is usually greater than 45°, the second term of the denominator may be considered as negligible. EQ.: 3.5 then simplifies to:

$$R_1 = V \cot\psi \qquad \text{EQ.: 3.6}$$

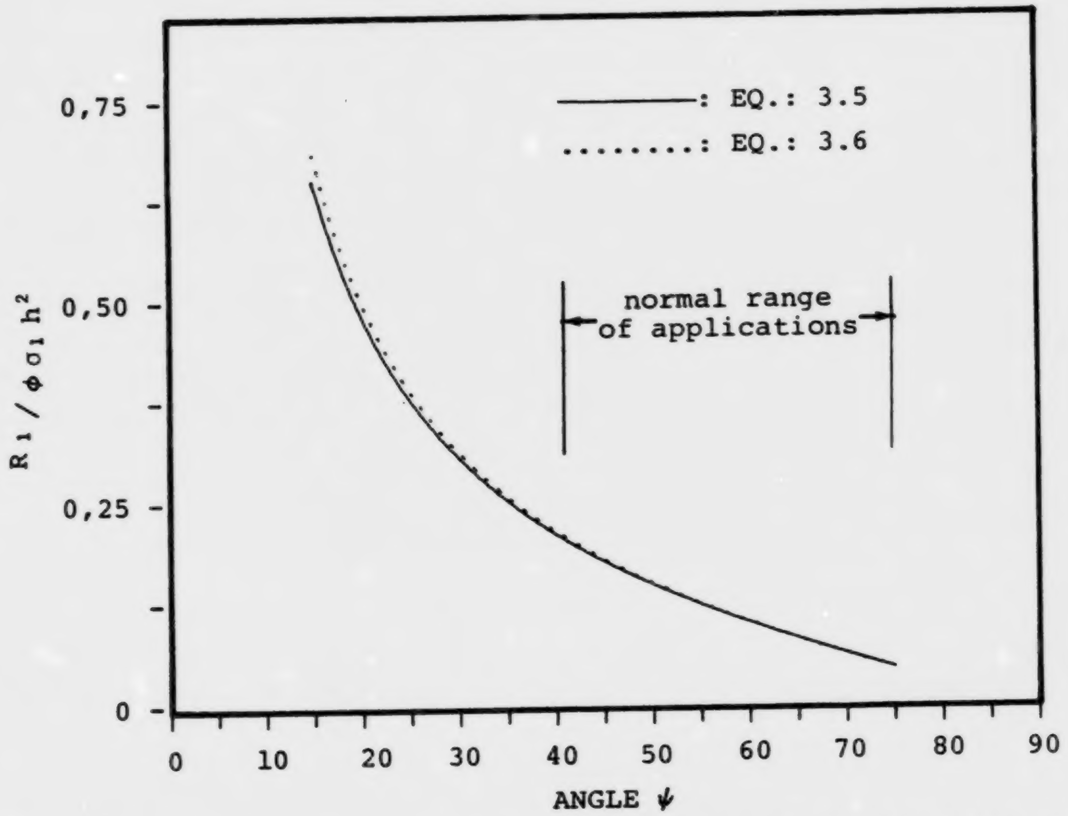

Figure 3.4.: Comparison between the exact solution (EQ.:3.5) and the approximate solution (EQ.:3.6) shown as dashed line.

EQ.: 3.5 and EQ.: 3.6 are compared in Figure 3.4

By introducing into EQ.: 3.6, the values of V and tan ψ respectively given by EQ.: 2.3 and EQ.: 3.3, we obtain the ice resistance referred to the stem under quasi-static conditions as:

$$\boxed{R_1 = 0{,}5483 \left\{ \frac{\pi}{2} - \theta \right\} \left\{ \frac{\sin\theta \sin\beta + f \cos\beta}{\sin\theta \cos\beta - f \sin\beta} \right\} \sigma_1 \; h^2}$$

EQ.: 3.7

where R_1: ice resistance referred to the stem under quasi-static conditions (kN);
θ: bow opening angle expressed in radians;
β: stem angle with the horizontal;
f: coefficient of friction between the hull and the ice;
σ_1: ice flexural strength (kPa)
h: ice thickness (m).

As seen from EQ.: 3.7, the ice resistance referred to the stem depends on the hull shape (bow opening angle and stem angle) but not on its size (forebody length and maximum beam).

For actual icebreakers, the ice resistance referred to the stem, R_1 , as estimated by EQ.: 3.7, represents about 10% of the total ice resistance under quasi-static ice resistance.

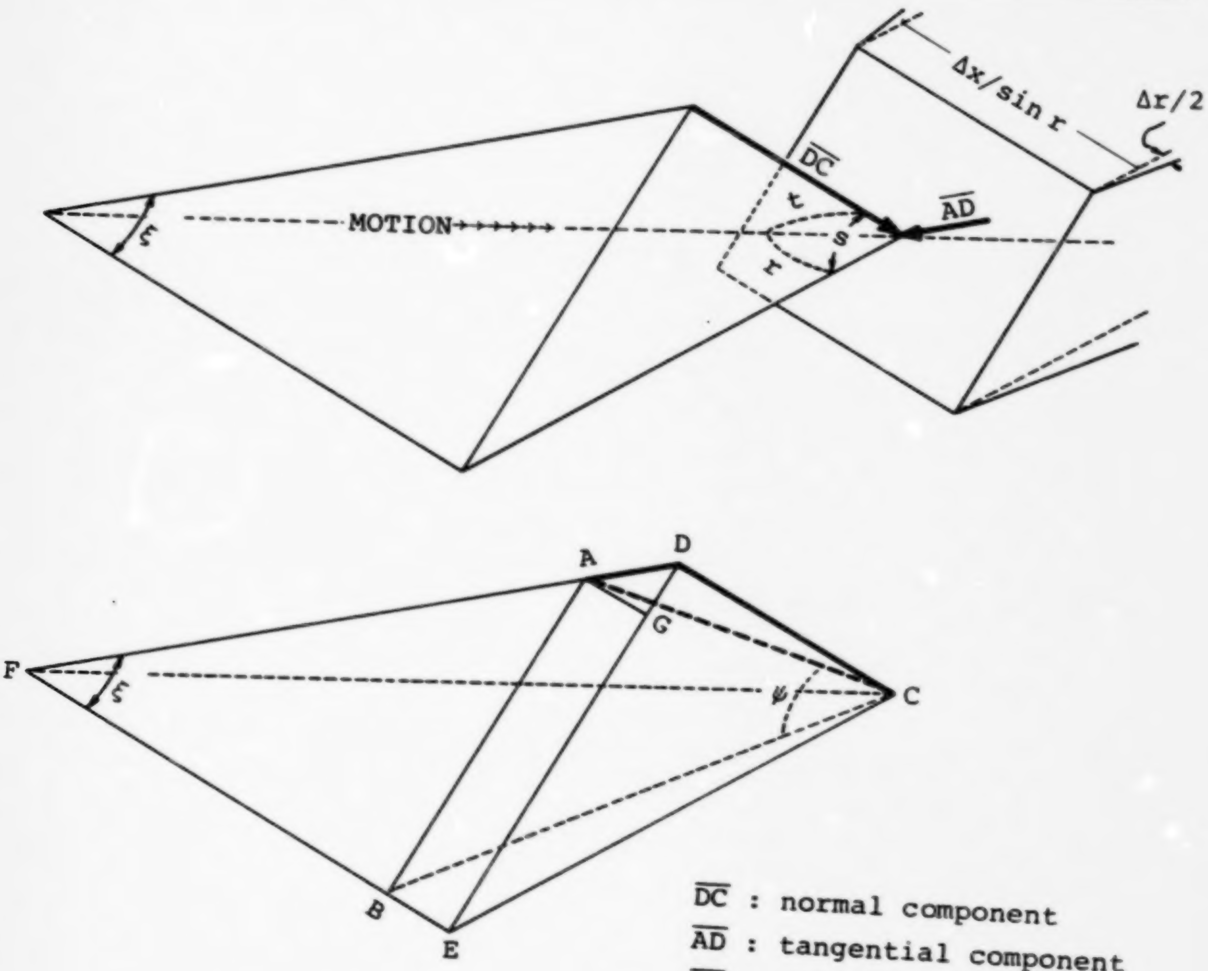

$\overline{DC}$: normal component

$\overline{AD}$: tangential component

$\overline{AC}$: resultant force

$$\tan\psi = \frac{\overline{AB}}{\overline{AC}} = \frac{\overline{DE} - \overline{DG}}{\dfrac{\overline{DC}}{\cos f'}} = \frac{\overline{DE} - \overline{AD}\sin\xi}{\overline{DC}}\cos f'$$

$$\tan\psi = \left\{\frac{\overline{DC}\tan s - f\,\overline{DC}\sin\xi}{\overline{DC}}\right\}\cos f' = \left\{1 - f\,\frac{\sin\xi}{\tan s}\right\}\cos f'\tan s$$

$$\tan\psi = \left\{1 - f\,\frac{\overline{DE}}{\overline{DF}}\,\frac{\overline{DC}}{\overline{DE}}\right\}\cos f'\tan s = \left\{1 - f\cot t\right\}\cos f'\tan s$$

$$\tan\psi = (\sin t\cos f' - \cos t\sin f')\,\frac{\tan s}{\sin t} = \frac{\sin(t-f')}{\sin t}\tan s$$

Figure 3.5.: Characteristics of the contacting interface between the ice and the bow section

3.1.2.: ICE RESISTANCE REFERRED TO THE SIDES.

The characteristics of the contacting interface between the ice and the sides of the bow section are schematically shown in Figure 3.5. The elementary force, ΔP , acting at a point (x,y) may be reduced to a component, ΔN , acting normally to the interface and a tangential component, $f.\Delta N$, parallel to the line of intersection of the tangent plane and the plane determined by the normal and the direction of motion.

The direction of application, ψ , of the elementary force, ΔP , is found by trigonometric considerations as:

$$\tan \psi = (1 - f \cot t) \tan s \cos f' \qquad \text{EQ.: 3.8}$$

where: t : angle between the normal to the shell plating at point (x,y) and the direction of motion; (EQ.: 1.6);

s : angle between the normal to the shell plating at point (x,y) and the horizontal plane; (EQ.: 1.5);

f : coefficient of friction between the hull and the ice;

f': arctan f

Knowing the direction of application of the elementary force, its critical value is then obtained from the failure criterion (EQ. 2.2) as:

$$\Delta P = 0{,}5483\, \sigma\, h^2 \left\{ 0{,}5\, \Delta r + \frac{\Delta x}{\ell \sin r} \right\} \left\{ \frac{1}{\sin^2\psi + \frac{V^2}{H^2} \cos^2\psi} \right\}^{\frac{1}{2}} \qquad \text{EQ.: 3.9}$$

where: σ : ice flexural strength (kPa);

h : ice thickness (m);

r : angle between the perpendicular to the waterline at point (x,y) and the direction of motion (EQ.:1.4);

V : bending failure load (EQ.: 2.3);
H : buckling failure load (EQ.:2.4);
ℓ : characteristic length of the ice plate (EQ.:2.5);
Δx : projection onto 0x-axis of the width of the elementary contact area.

The elementary normal component acting at point (x,y) is given by:

$$\Delta N = \Delta P \cos f' \qquad \text{EQ.: 3.10}$$

and the elementary contribution to the force acting along the centerline becomes:

$$\Delta R_2 = \Delta N\,(\cos t + f \sin t) \qquad \text{EQ.: 3.11}$$

The total ice resistance referred to the sides corresponds then to the integration of the elementary forces acting on both sides of the ship forebody. Exactly, the total resistance referred to the sides is given by an elliptic integral of the second kind. However, the total ice resistance referred to the sides can easily be found by the method of slicing.

$$R_2 = 2\sum \Delta R_2$$

It was found that the ice resistance referred to the sides, R_2 , obtained by numerical integration may be approximated very closely by the following equation when the stem angle $\beta \le 75°$:

$$R_2 = 0{,}75\,\sigma h^2 \frac{B}{\ell}\,\frac{(1+2\cos\beta)}{(\sin\theta+\cos\theta)(1+2\sin\gamma)}\left\{\tan\beta + f\left(\frac{L^*}{B}\,\frac{2}{(1+2\cos\beta)} + 1{,}732\tan\beta\right)\right\} \qquad \text{EQ.: 3.12}$$

The symbols are defined after EQ.: 3.13

3.1.3.: TOTAL ICE RESISTANCE UNDER QUASI-STATIC CONDITIONS.

Under quasi-static conditions, the total ice resistance, R_{is}, corresponds to the sum of the ice resistance referred to the stem, R_1 plus the ice resistance referred to the sides, R_2 :

$$R_{is} = R_1 + R_2 \qquad \text{EQ.: 3.13}$$

where:

$$R_1 = 0{,}5483 \left\{ \frac{\pi}{2} - \theta \right\} \left\{ \frac{\sin\theta \, \sin\beta + f \, \cos\beta}{\sin\theta \, \cos\beta - f \, \sin\beta} \right\} \sigma h^2$$

and

$$R_2 = 0{,}75 \sigma h^2 \frac{B}{\ell} \frac{(1+2\cos\beta)}{(\sin\theta+\cos\theta)(1+2\sin\gamma)} \left\{ \tan\beta + f \left(\frac{L^*}{B} \frac{2}{(1+2\cos\beta)} + 1{,}732\tan\beta \right) \right\}$$

The symbols are defined as follows:

R_{is} : total ice resistance under quasi-static conditions;
R_1 : ice resistance referred to the stem (EQ.: 3.7);
R_2 : ice resistance referred to the sides (EQ.: 3.12);
h : ice thickness;
$L^*/2$: bow section length from stem to maximum beam;
B : maximum beam;
ℓ : characteristic length of the ice plate (EQ.: 2.5);
β : stem angle with the horizontal (Figure 1.1);
γ : flare angle at maximum beam (Figure 1.1);
θ : bow opening angle (Figure 1.1);
f : coefficient of friction;
σ : ice flexural strength.

Since $R_1 << R_2$, R_{is} is not significantly influenced by the directions of the radial cracks emanating from the stem, i.e. the interval referred to the stem. Typical examples of the relative influence of relevant parameters are shown in Figures 3.6 to 3.8.

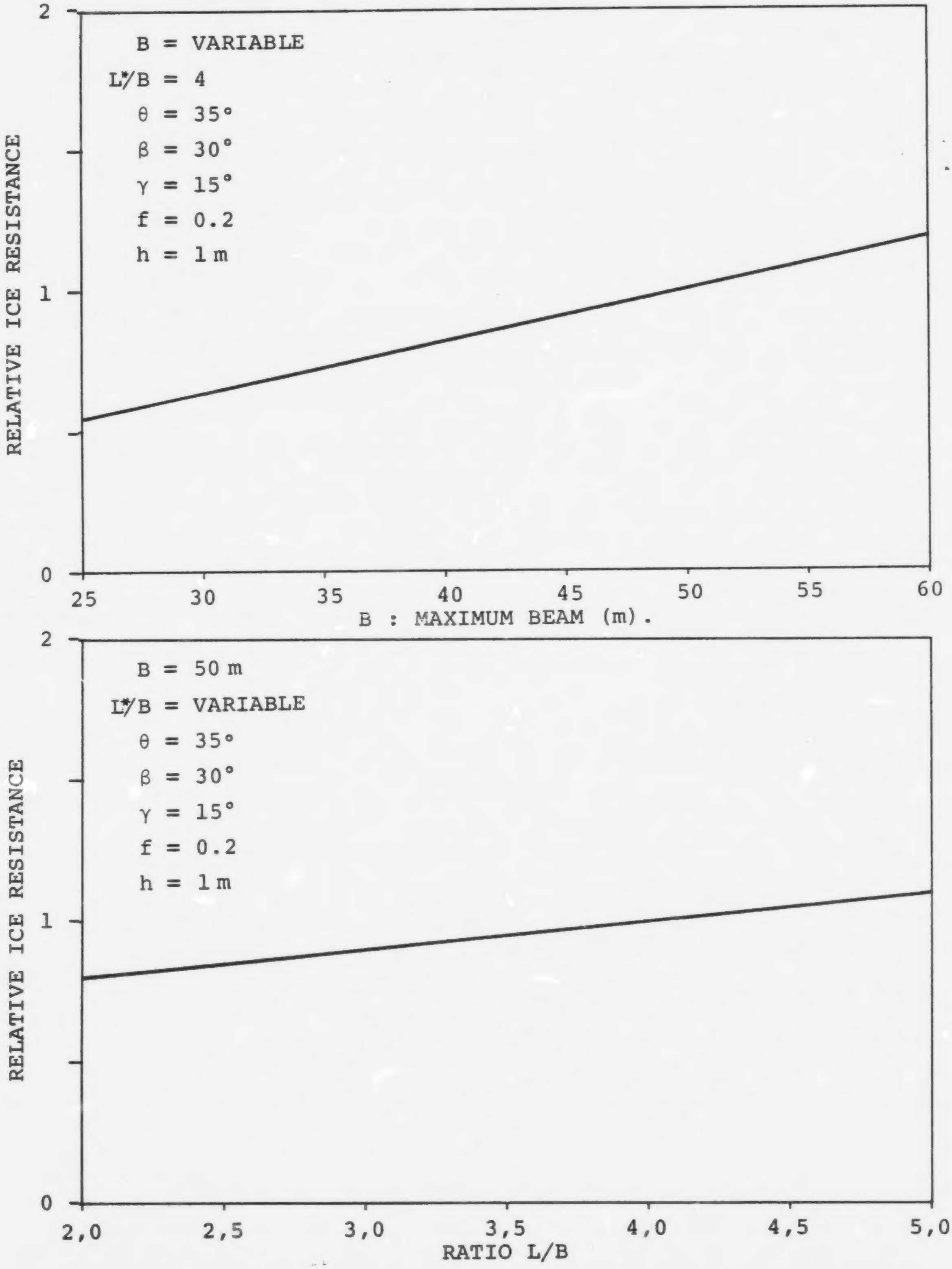

Figure 3.6.: Plot of relative ice resistance versus a) maximum beam , B , and b) length , L*/2 , from bow to maximum beam section.

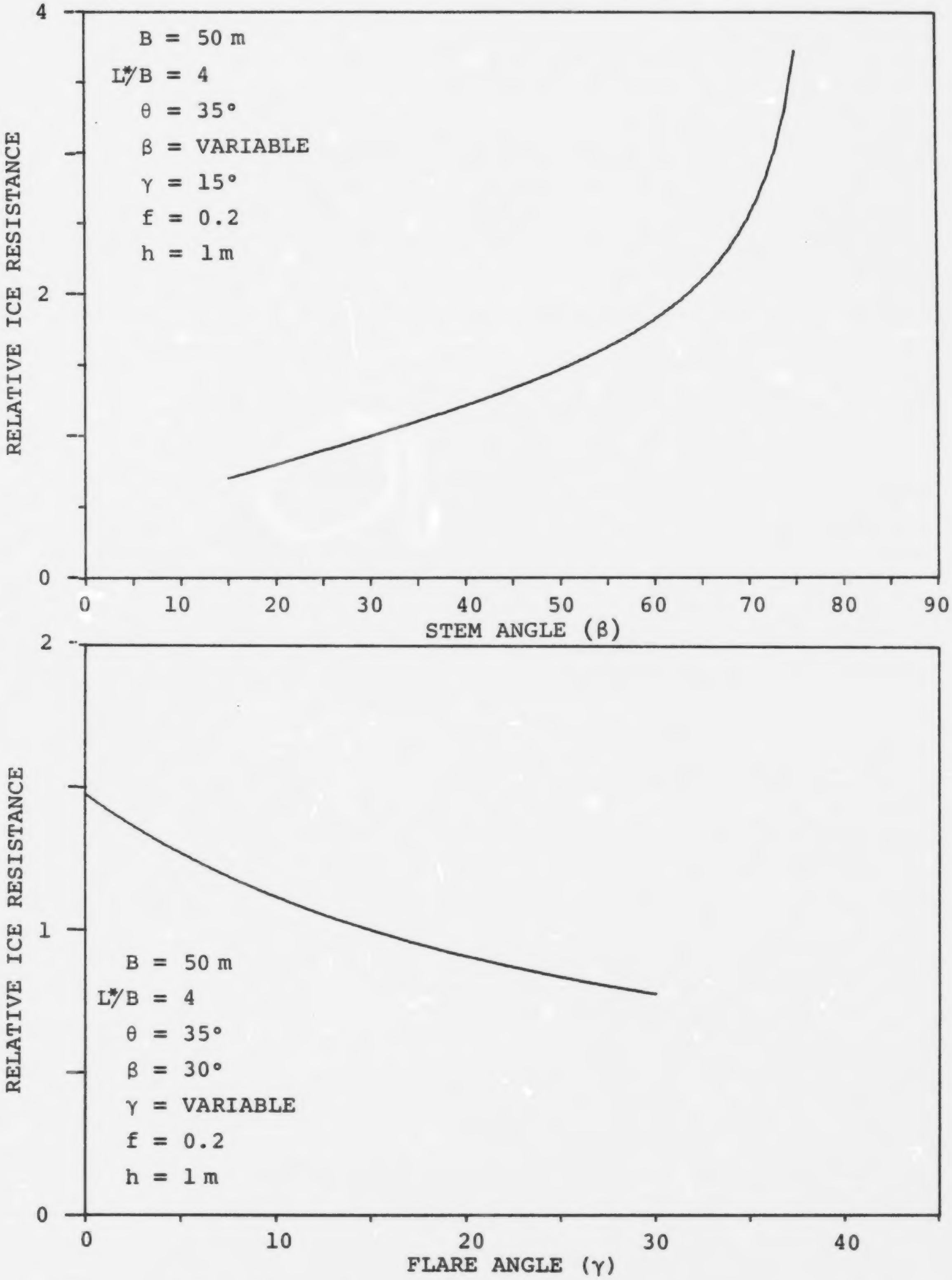

Figure 3.7.: Plot of relative ice resistance versus a) stem angle β and b) flare angle , γ , at maximum beam section.

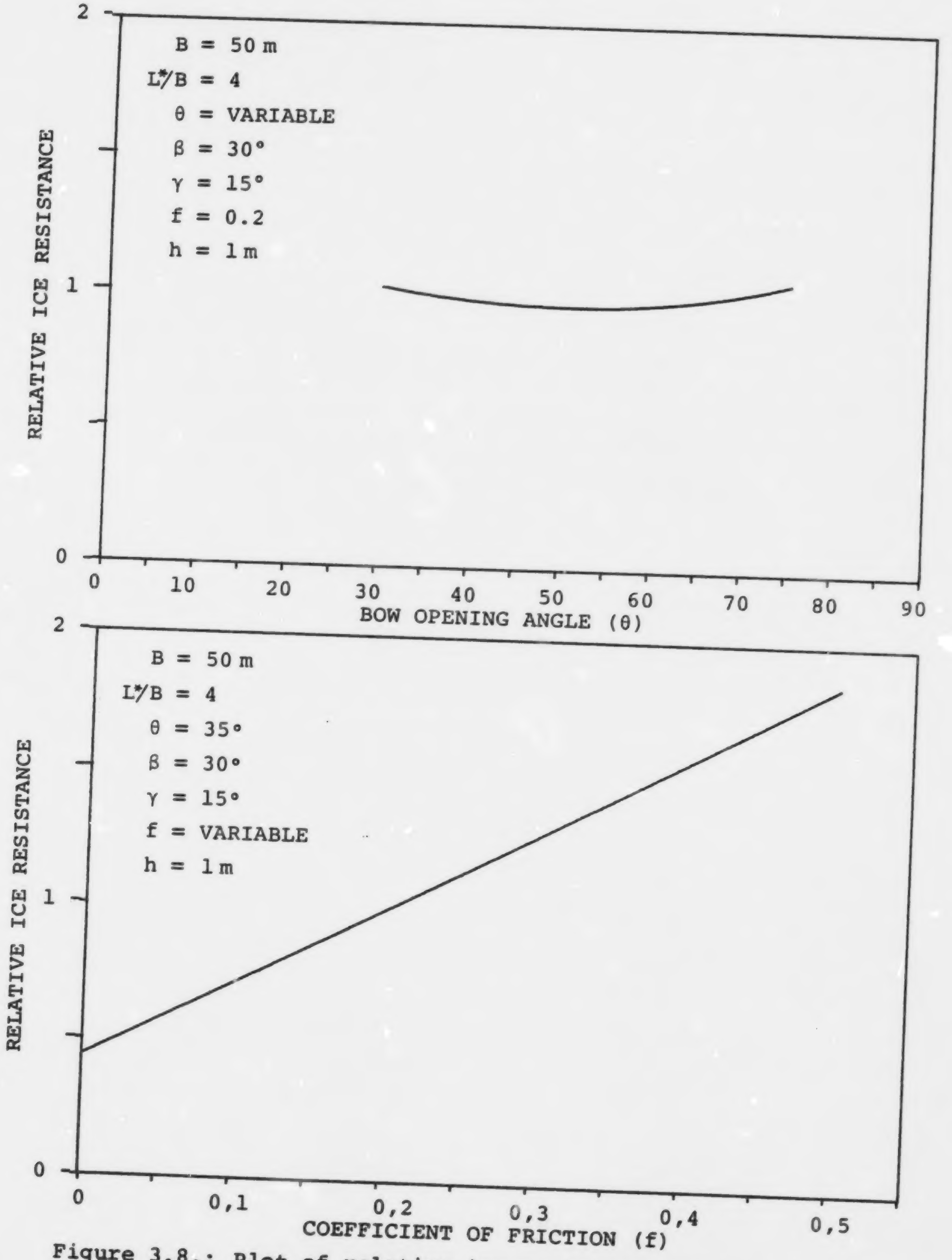

Figure 3.8.: Plot of relative ice resistance versus a) bow opening angle , θ , and b) coefficient of friction , f .

3.2.: ICE RESISTANCE UNDER DYNAMIC CONDITIONS.

Between two consecutive impacts with the unbroken ice sheet, the ship moves through water that is filled with broken ice pieces of varying size. Velocity then affects mainly the resistance due to submersion and displacement of broken ice floes and the frictional resistance between hull and ice floes.

However, since we consider, in this study, the ice resistance at the instant of impact, we have to estimate the influence of velocity on the breaking resistance of an ice sheet.

The dynamic equation describing the response of a floating wedge was obtained by Carter (1975) as:

$$\frac{d^4\omega}{d\chi^4} + \frac{2}{\chi}\,\frac{d\omega^3}{d\chi^3} + \kappa\,(\,\omega + \eta\,) = 0 \qquad \text{EQ.: 3.14}$$

where: ω : wedge deflection;

χ : x/ℓ , ℓ being the characteristic length (EQ.: 2.5);

κ : water unit weight;

η : pressure exerted on the ice by the ship-generated wave expressed in equivalent of water height;

This equation is identical to the static equation (EQ.: A.11) except that the water reaction is replaced by the water reaction plus the pressure due to the ship-generated wave.

In order to evaluate the upper bound for the velocity effect, we will make three (3) very conservative assumptions:

1.: the wave generated by the ship is not damped by the presence of an ice cover;

2.: The uplifting pressure keeps its maximum value on the entire length of the bow section;

3.: From the hull to the line of ice fracture, the ratio of the equivalent wave profile, $\eta(x)$, to the deflection, $\omega(x)$, remains constant. Since both the deflection and the equivalent wave profile decrease with the distance and, furthermore, the distance to the line of ice fracture is relatively small, it is not thought that this assumption is significant when compared to the variations of the flexural strength, elastic modulus, and thickness of real ice sheets.

The third assumption leads to a very useful simplification:

$$\kappa' = \kappa \left(1 + \frac{\eta(x)}{\omega(x)} \right) = \kappa \left(1 + \frac{\eta^*}{\omega^*} \right) = \text{constant}$$

where η^*: maximum amplitude of the ship-generated wave;
ω^*: maximum deflection of the ice sheet.

EQ.: 3.14 may then be rewritten:

$$\frac{d^4\omega}{d\chi^4} + \frac{2}{\chi}\frac{d^3\omega}{d\chi^3} + \kappa'\omega = 0 \qquad \text{EQ.: 3.15}$$

This equation is identical to the static equation (EQ.:A.11) except that κ must be replaced by κ'.

Knowing that, under static conditions, the failure load is directly proportional to $1/\ell^2$ and, from EQ.: 2.5, that ℓ is directly proportional to $1/\kappa^{0.25}$, the ice resistance, under dynamic conditions, may be written:

$$R_{id} = R_{is} \left(\frac{\kappa'}{\kappa} \right)^{\frac{1}{2}}$$

or

$$R_{id} = R_{is} \left(1 + \frac{\eta^*}{\omega^*} \right)^{\frac{1}{2}} \qquad \text{EQ.: 3.16}$$

where R_{id} : ice resistance under dynamic conditions;

R_{is} : ice resistance under quasi-static conditions.

From the data summarized by Sorensen (1973) for a wide variety of ship forms, it is seen that the height of the wave near a vessel is reasonably approximated by:

$$\eta^* = 0{,}016\ V^2 \qquad \text{EQ.: 3.17}$$

where V is the ship speed.

The deflection of the ice cover, near the vessel, is obtained from Nevel's work (1961) and given by:

$$\omega^* = 0{,}04\ \frac{\sigma h^2}{\ell^2} \qquad \text{EQ.: 3.18}$$

By introducing EQ.: 3.17 & 3.18 into EQ.: 3.16, the level ice resistance to continuous motion of a ship is obtained as:

$$R_{id} = R_{is}\left(1 + \frac{0{,}4\ V^2\ \ell^2}{\sigma\ h^2}\right)^{\frac{1}{2}} \qquad \text{EQ.: 3.19}$$

The influence of the ship speed on the ice resistance is shown in Figure 3.9 for typical ice thicknesses.

As shown in Figure 3.9, the effect of velocity on the ice breaking resistance increases with increasing ice thickness. Therefore our simplified approach predicts that a smaller effect of velocity will be observed in model tests than in full scale tests.

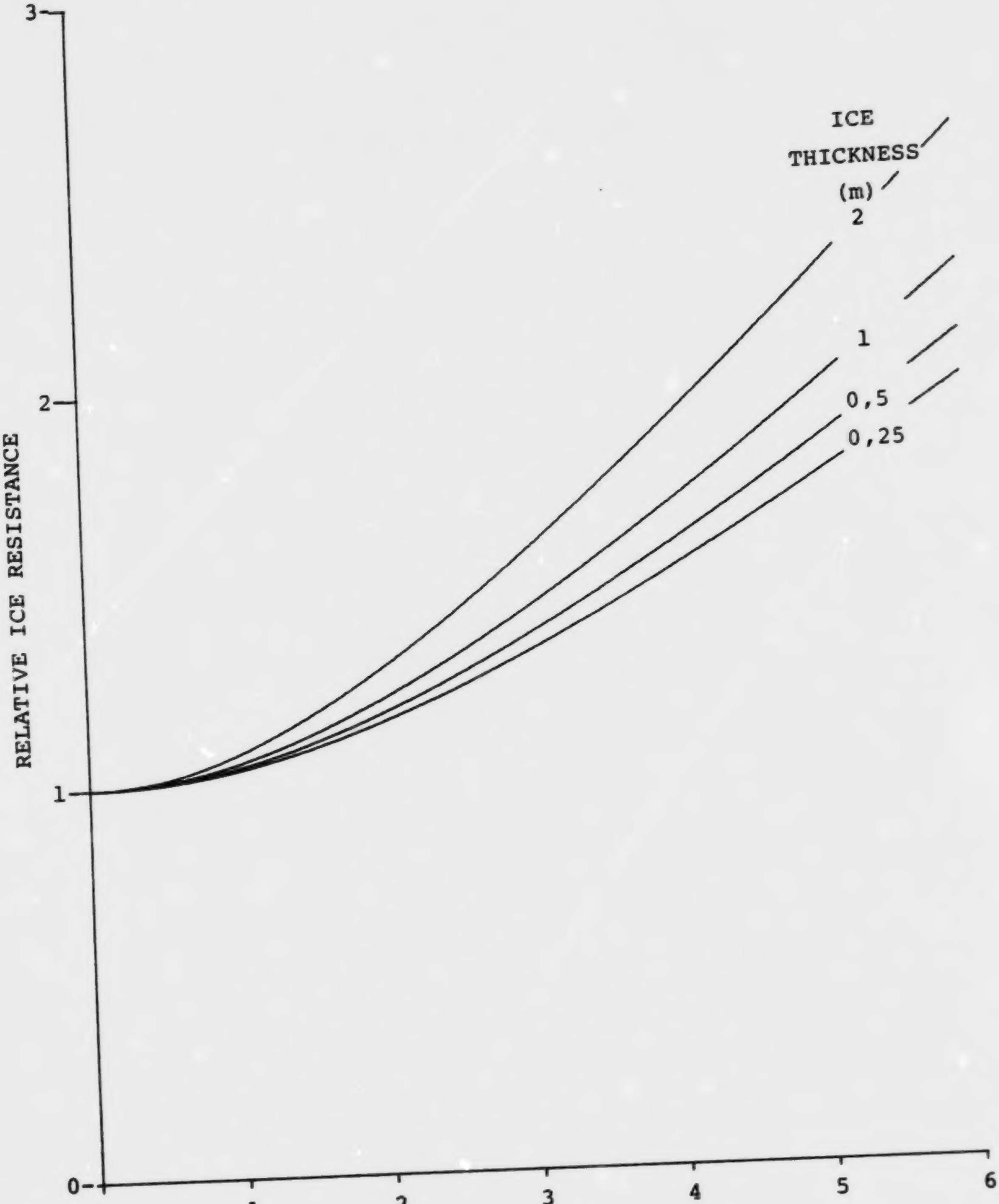

Figure 3.9.: Plot of relative ice resistance versus ship speed.

3.3.: ICE PRESSURE EFFECT.

Field observations indicate that the frictional stresses exerted by winds or currents generate internal ice pressure which may be transmitted over considerable distances. As noted by Edwards et alt. (1979), during the MANHATTAN voyage, ice compression proved to cause a major resistance component, expending 20 to 40% of the total thrust.

Let us consider the upper limits of forces to be expected due to ice compression against the hull sides of a ship moving through a level ice cover. It should be noted that ice compression may cause an additional resistance to failure and an additional side friction.

The effective ice pressure, σ_0 , against ship side is given by:

$$\sigma_0 = \sigma_{0_{max}} \sin^2 \alpha$$

where α is the contact angle between the directions of ship motion and ice compression.

As shown in Figure 3.10, to develop the failure stress, σ , the bending moment which is proportional to the applied load has to be increased by a factor:

$$\frac{\sigma + \sigma_0}{\sigma} = \frac{M_0}{M} = \frac{P_0}{P}$$

The additional side friction is evaluated by:

$$F = \sigma_0 h (2L - L^*) f$$

where L is ship's length and F the additional side friction.

Introducing the above equations into EQ.: 3.19, the resistance in level ice under compression is then rewritten as:

$$R_i^* = R_i \left\{ \frac{\sigma + \sigma_0}{\sigma} \right\} + \sigma_0 h \left(2L - L^* \right) f \qquad \text{EQ.: 3.20}$$

where: R_i^* : resistance of a level ice cover with internal compression;

R_i : resistance of a standard level ice cover;

P_0 : failure load of an ice cover under compression;

M_0 : bending moment causing the failure of an ice cover under compression.

It should be noted that the internal horizontal pressure in the ice sheet which eventually can reach the ridging or rafting limit may, as shown by EQ.: 3.20, increase the resistance by factors such as those observed during the MANHATTAN voyage. Unfortunately, to our knowledge, there are presently no available data which could allow a proper assessment of the model proposed to account for the effect of internal ice pressure.

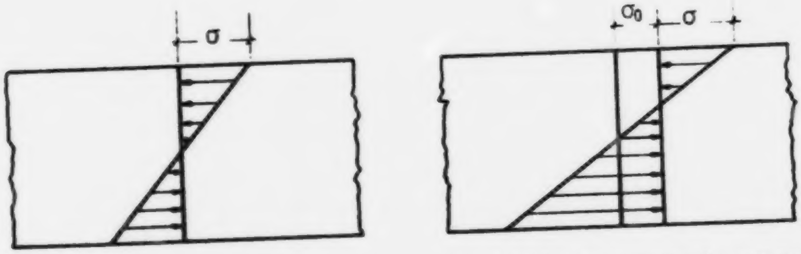

a) without internal pressure b) with internal pressure

Figure 3.10.: Effect of an internal ice pressure on the stress distribution.

3.4.: SNOW COVER EFFECT.

Full scale data on the USCGC STATEN ISLAND (Lewis and Edwards 1970) and on the USCGC MACKINAW (Edwards et alt. 1972) have shown that the presence of snow cover on top of the ice increases the icebreaking resistance.

The correction based upon regression analysis of these full scale data suggests that the snow resistance component, R_s , is linearly proportional to snow cover thickness, h_s :

$$R_s = 900\, h_s \qquad \text{EQ.: 3.21}$$

Due to the two ships similarity, it cannot be determined, from the above-mentioned full scale data, if the snow component is a function of the ship's shape.

It should be pointed out that the snow effect may also be compensated for by slightly increasing the coefficient of friction between the hull and the snow covered ice. Till more full scale data become available, the correction given by EQ.: 3.21 should be used.

It should be pointed out that, since the snow resistance component is but a relatively small component of the total resistance to icebreaking, even an appreciable error in calculation of this component has little effect on the total resistance.

4.: FINAL RESULTS

To sum up our investigations, the maximum resistance to ship motion through a level ice cover is obtained by introducing into EQ.: 3.1 the combined effects of the vessel characteristics and environment conditions. (EQ.: 3.13, 3.19, 3.20, 3.21)

$$\boxed{R_t = R_{is}\left\{1+\frac{0{,}4V^2\ell^2}{\sigma h^2}\right\}^{\frac{1}{2}}\left\{\frac{\sigma+\sigma_0}{\sigma}\right\}+\sigma_0 h(2L-L^*)f+900h_s+R_{ow}}$$

EQ.: 4.1

where: $R_{is} = R_1 + R_2$

$$R_1 = 0{,}5483\left\{\frac{\pi}{2}-\theta\right\}\left\{\frac{\sin\theta\sin\beta+f\cos\beta}{\sin\theta\cos\beta-f\sin\beta}\right\}\sigma h^2$$

$$R_2 = 0{,}75\,\sigma h^2\,\frac{B}{\ell}\,\frac{(1+2\cos\beta)}{(\sin\theta+\cos\theta)(1+2\sin\gamma)}\left|\tan\beta+f\left(\frac{L^*}{B}\,\frac{2}{(1+2\cos\beta)}+1{,}732\tan\beta\right)\right|$$

The symbols are defined as follows:

R_t : maximum resistance to ship motion;
R_{ow} : open-water resistance;
R_{is} : total ice resistance under quasi-static conditions;
R_1 : ice resistance referred to the stem (EQ.: 3.7);
R_2 : ice resistance referred to the sides (EQ.: 3.12);
h : ice thickness;
$L^*/2$: bow section length from stem to maximum beam;
B : maximum beam;
ℓ : characteristic length of the ice plate (EQ.: 2.5);
β : stem angle with the horizontal (Figure 1.1);
γ : flare angle at maximum beam (Figure 1.1);
θ : bow opening angle (Figure 1.1);
f : coefficient of friction;
σ : ice flexural strength.
L : ship length; V: ship velocity;
σ_0 : effective internal ice pressure;
h_s : snow cover thickness.

For standard level ice cover, i.e. no internal pressure in the ice cover, EQ.: 4.1 simplifies to:

$$\boxed{R_t = R_{is} \left(1 + \frac{0,4\, V^2\, \ell^2}{\sigma\, h^2} \right)^{\frac{1}{2}} + 900\, h_s + R_{ow}} \qquad \text{EQ.: } 4.2$$

It is our opinion that the snow component is not only dependent on snow thickness but also on other parameters such as snow density, texture etc. The snow resistance would probably be more rightly estimated by modifying the friction coefficient between the hull and the snow covered ice cover.

Since at the present time, there is no available relation between the friction coefficient and the snow conditions, the above relation is still used. It may be worthwhile noting that the snow component is relatively small so that even an appreciable error in its estimation has little effect on the total resistance.

5. COMPARISON WITH EXPERIMENTAL DATA

Since our analysis is based on a number of assumptions and simplifications, it is now essential that the analytical results be compared with experimental data. The check will be obtained by testing the goodness of prediction for data sets from full-scale trials and model tests of six (6) different icebreakers. The selection is based on the availability of the data in open literature. The relevant parameters of the retained ships and the full-scale range (minimum, mean, maximum) of the test conditions are summarized in TABLE 5.1. Further comparisons with full-scale data are given in Appendix D.

Unless otherwise stated, the open water resistance component will be estimated by the use of EQ.:3.2. The following relations, between the flexural ice strength, σ , the compressive ice strength, σ_2 , and the elastic modulus, E , will also be used:

$$\sigma_2 = 3\,\sigma \qquad \text{and} \qquad E = 5000\,\sigma$$

Continuous-mode icebreaking resistance predictions given by EQ.: 4.1 will be compared to actual measurements and, also to values estimated by the most widely used resistance equation, the Kashteljan formula: (in S.I. units)

$$R_t = 0{,}004\,\mu_0\,\sigma\,B\,h + 3{,}6\,\mu_0\,\gamma_1\,B\,h^2 + \frac{2{,}45}{\eta_2}\,B^{1.65}\,h\,V + R_{ow} \qquad \text{EQ.: 5.1}$$

where R_t : total resistance (kN);
σ : ice flexural strength (kPa);
γ_1 : ice unit weight (kN/m^3);
h : ice thickness (m);
V : ship speed (m/s);
R_{ow} : open water resistance (kN)

μ_0 and η_2 usually referred to as Kashteljan's efficiency coefficient and Shimansky's ice-cutting coefficient are given in TABLE 5.1 for the retained icebreakers.

TABLE 5.1		STATEN ISLAND	MACKINAW	ST-LAURENT	MOSKVA	WOLFE	RADISSON
SHIP PARAMETERS							
Beam	B(m):B	18,9	21,3	24,4	23,5	14,6	19,22
Forebody length×2	L*(m):L	76,2	85,4	106,2	112,4	67,1	68,9
Ship length	L(m):SL	76,2	85,4	111,7	112,4	67,1	86,1
Displacement	(m^3):DISPL	5316	5180	13180	13100	3208	6450
Bow opening angle	θ(°):TETA	30	29	36	25	31	44,5
Stem angle	β(°):BETA	25	31	32	26,5	16	18
Flare angle	γ(°):GAMMA	20	20	6,5	15,6	0	5,5
Coefficient	μ_0:MUO	1,65	1,52	1,99	1,45	1,50	1,53
Coefficient	η_2:ETA2	2,78	2,72	2,29	3,28	3,32	2,21
ENVIRONMENTAL CONDITIONS							
Ice thickness	h(m):THICK	0,12	0,09	0,30	0,45	0,25	0,23
		0,51	0,35		0,59	0,33	0,68
		0,71	0,58	1,92	0,68	0,52	1,20
Snow thickness	h_s(m):SNOW	0,00	0,00	0,03	-	0,00	0,00
		0,08	0,05	0,15	-	0,09	0,01
		0,25	0,22	0,30	-	0,18	0,13
Flexural strength	σ(kPa):TENS	226	386	315	200	146	207
		336	873	556	400	250	360
		442	1290	1650	600	570	525
Friction coefficient	f:FRICT	-	-	0,08	0,1	-	0,19
		0,2	0,145	0,20	0,2	0,2	-
		-	-	0,48	0,3	-	0,30
Ship velocity	V(m/s):VEL	0,52	0,49	0,10	0,0	0,29	0,00
		2,06	3,66	3,00	1,5	1,60	2,62
		4,57	7,22	5,51	4,8	3,45	6,82

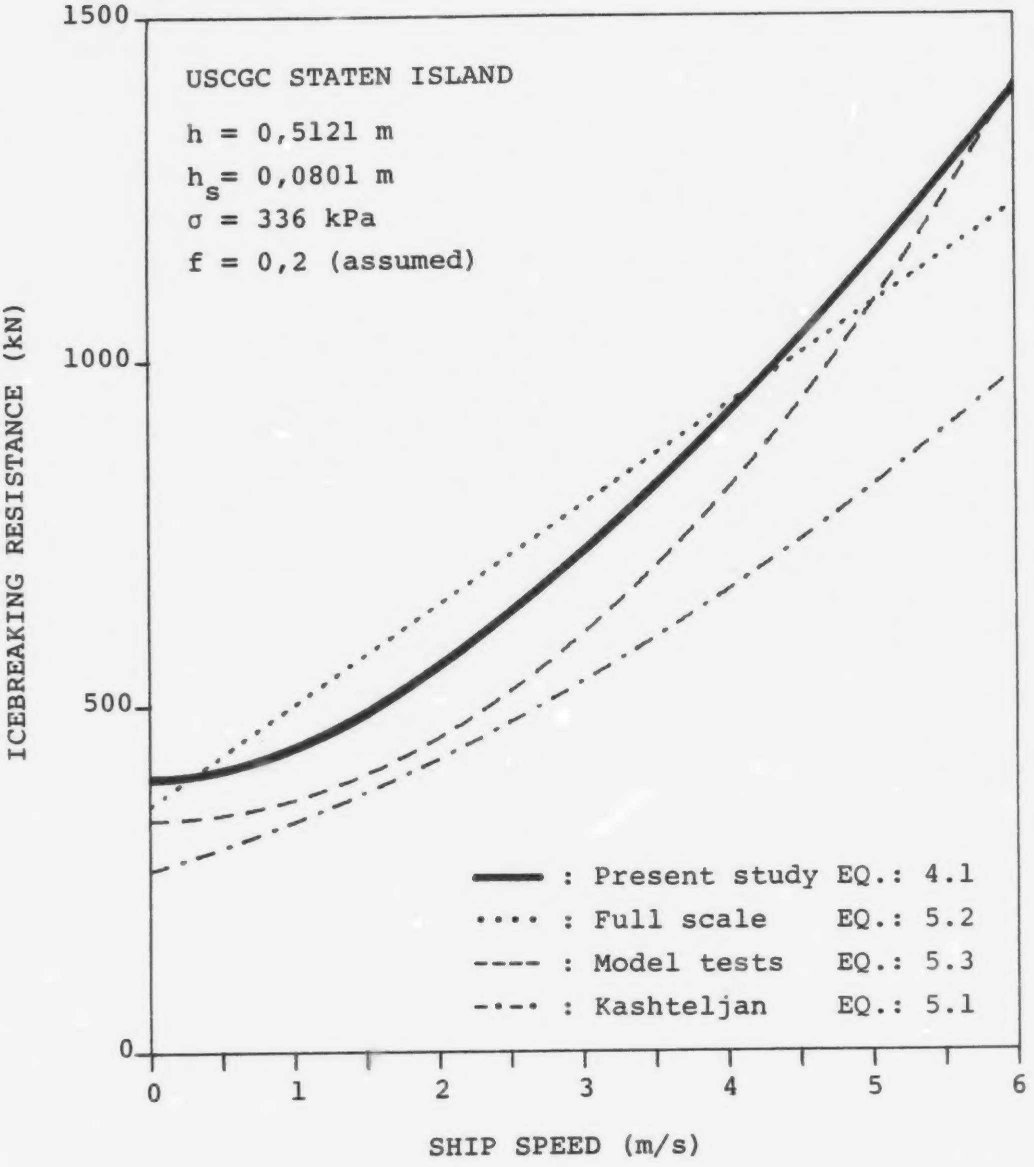

Figure 5.1.: Predicted icebreaking resistance for USCGC STATEN ISLAND as compared to regression lines from full scale trials and model tests.

5.1.: USCGC STATEN ISLAND

Source of data: Lewis J.W., and Edwards R.Y.Jr. 1970

For the 28 full-scale continuous icebreaking data point, the authors report a best fitting regression equation of the form: (rewritten in S.I. units)

$$R_t = {}^{-}103,881 + 19,289\,V + 21,236\,h_s + 158\,V\,h + 1500\,h^2$$

EQ.: 5.2

where R_t: total resistance (kN);
V : ship velocity (m/s);
h_s: snow thickness (m);
h : ice thickness (m).

By performing a regression and variance analysis of all data collected on a model in freshwater and saltwater ice, the authors obtained for the model tests the following equation: (Scale 1/36)

$$R_t = 0,474\,\sigma\,h^2 + 6,71\,\rho_1\,g\,B\,h^2 + 3,3969\,\rho_1\,B\,h\,V^2$$

EQ.: 5.3

where σ : ice flexural strength (kPa);
ρ_1: ice density (0,9);
g : gravitational acceleration ($9,81 m/s^2$);
B : maximum beam (m);
h : ice thickness (m);
V : ship velocity (m/s).

In Figure 5.1, predictions given by EQ.: 4.1 are compared with:
a.: full scale data represented by EQ.: 5.2;
b.: model tests data represented by EQ.: 5.3;
c.: Kashteljan formula;
for the mean values of the environmental conditions prevailing during the full-scale trials.

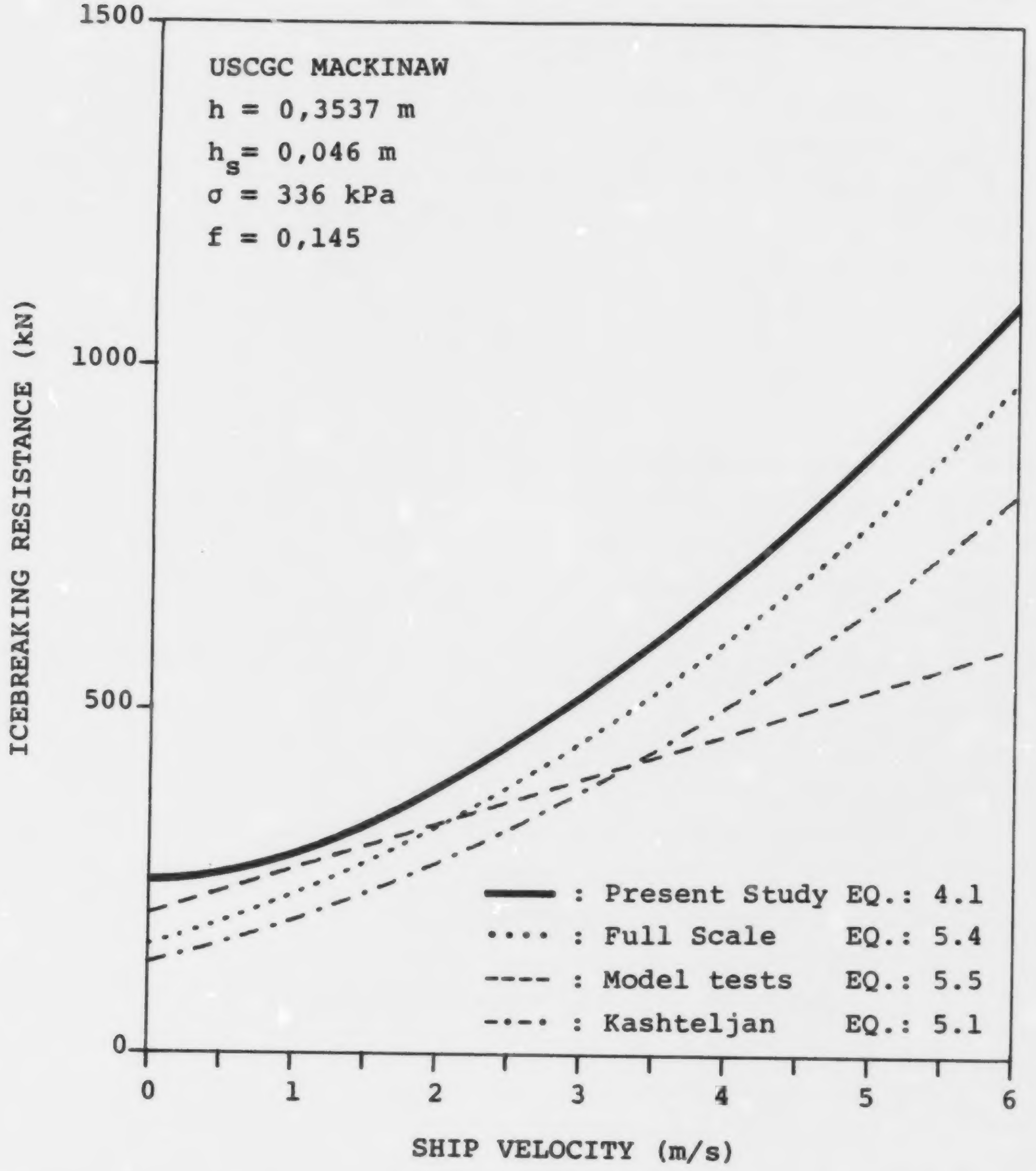

Figure 5.2.: Predicted icebreaking resistance for USCGC MACKINAW as compared to regression lines from full scale trials and model tests.

5.2.: USCGC MACKINAW

Source of data: Edwards,R.Y.Jr., et alt.,1972

For the 136 full-scale continuous icebreaking data points, the authors report a best fitting regression equation of the form:

$$\frac{R_t}{\rho g B h^2} = 5{,}2594 + 4{,}35 \frac{V}{\sqrt{gh}} + 1{,}676 \frac{V^2}{gh} + 5{,}4635 \frac{h_s}{h}$$

EQ.: 5.4

where: R_t: total resistance (kN) ; ρ: water mass density
B : maximum beam (m) ; h: ice thickness (m);
g : gravit. acc. (m/s^2) ; V: ship speed (m/s)
h_s: snow thickness (m).

The 39 data points obtained on a 1/48th scale model of the USCGC MACKINAW were analyzed by regression analysis technique, the results of which gave:

$$\frac{R_t}{\rho g B h^2} = 3{,}455 + 4{,}68 \frac{V}{\sqrt{gh}} + 0{,}019 \frac{\sigma}{\rho g h} \qquad \text{EQ.: 5.5}$$

In Figure 5.2, predictions given by EQ.: 4.1 are compared with:

a.: full scale data represented by EQ.: 5.4;
b.: model tests data represented by EQ.: 5.5;
c.: Kashteljan formula;

for mean values of h, h_s, and f, and for a small value of σ, where, as stated by the authors, "measurement error is small compared to that which was encountered in the region of high ($\sigma/\rho g h$)."

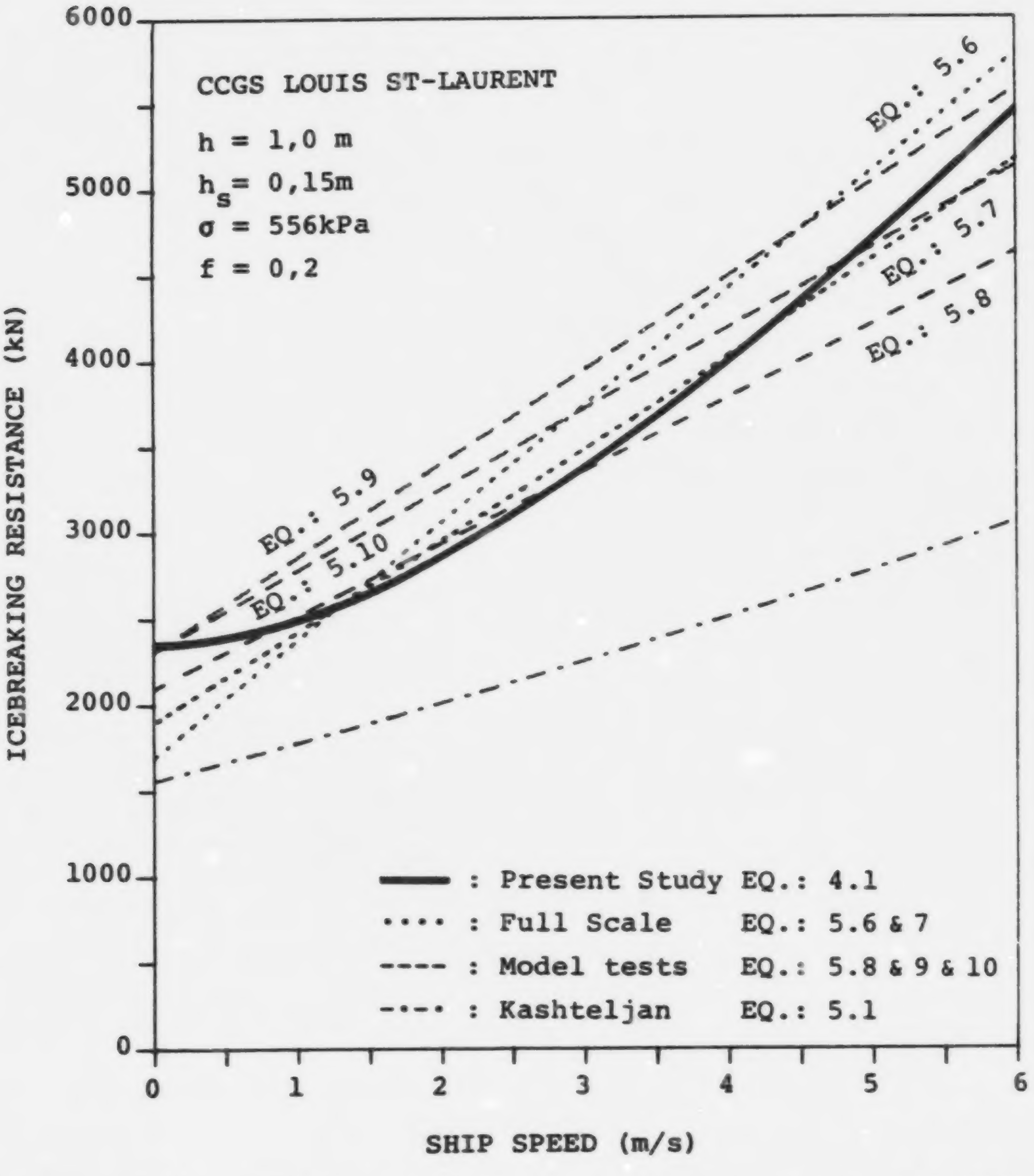

Figure 5.3.: Predicted icebreaking resistance for CCGS LOUIS ST-LAURENT as compared to regression lines from full-scale trials and model tests.

5.3.: CCGS LOUIS ST.LAURENT

Sources of data: German,J.G.,and Lawrence,R.G.A. 1975
Edwards,R.Y.Jr., et alt. 1976

The full-scale data points for the CCGS LOUIS ST.LAURENT have been collected on ramming penetrations under full power. Prediction of the continuous-mode resistance from these ramming tests was made using the deceleration force in addition to the thrust of the propellers to compute the resistance of the ship at the instantaneous velocity. Edwards et alt. (1976) have force-fit all the full-scale data points to an equation containing dimensionless groups previously retained. The resulting regression equation is:

$$\frac{R_t}{\rho g B h^2} = 4{,}242 + 0{,}05033 \frac{\sigma}{\rho g h} + 8{,}948 \frac{V}{\sqrt{gh}} \qquad \text{EQ.: 5.6}$$

Using different variables, Michel (1978) obtained for the ST.LAURENT full-scale data points the following best fit linear regression equation:

$$\frac{R_t}{\rho g B h^2} = 7{,}94 + 6{,}61 \frac{V}{\sqrt{gh}} \qquad \text{EQ.: 5.7}$$

Geometric scale factors of 36 and 48 were used by Edwards et alt. (1976) during their model test program. The best fit regression equation obtained by Edwards et alt. (1976) which represents both models combined may be written for the conditions given in Figure 5.3:

$$\frac{R_t}{\rho g B h^2} = 8{,}77 + 5{,}59 \frac{V}{\sqrt{gh}} \qquad \text{EQ.: 5.8}$$

For the data points collected on the 1/36th scale model, Edwards and Nawwar (1978) suggests the following best fit regression equation:

$$\frac{R_t}{\rho g B h^2} = 9{,}68 + 1{,}92 \frac{V}{\sqrt{gh}} \qquad \text{EQ.: 5.9}$$

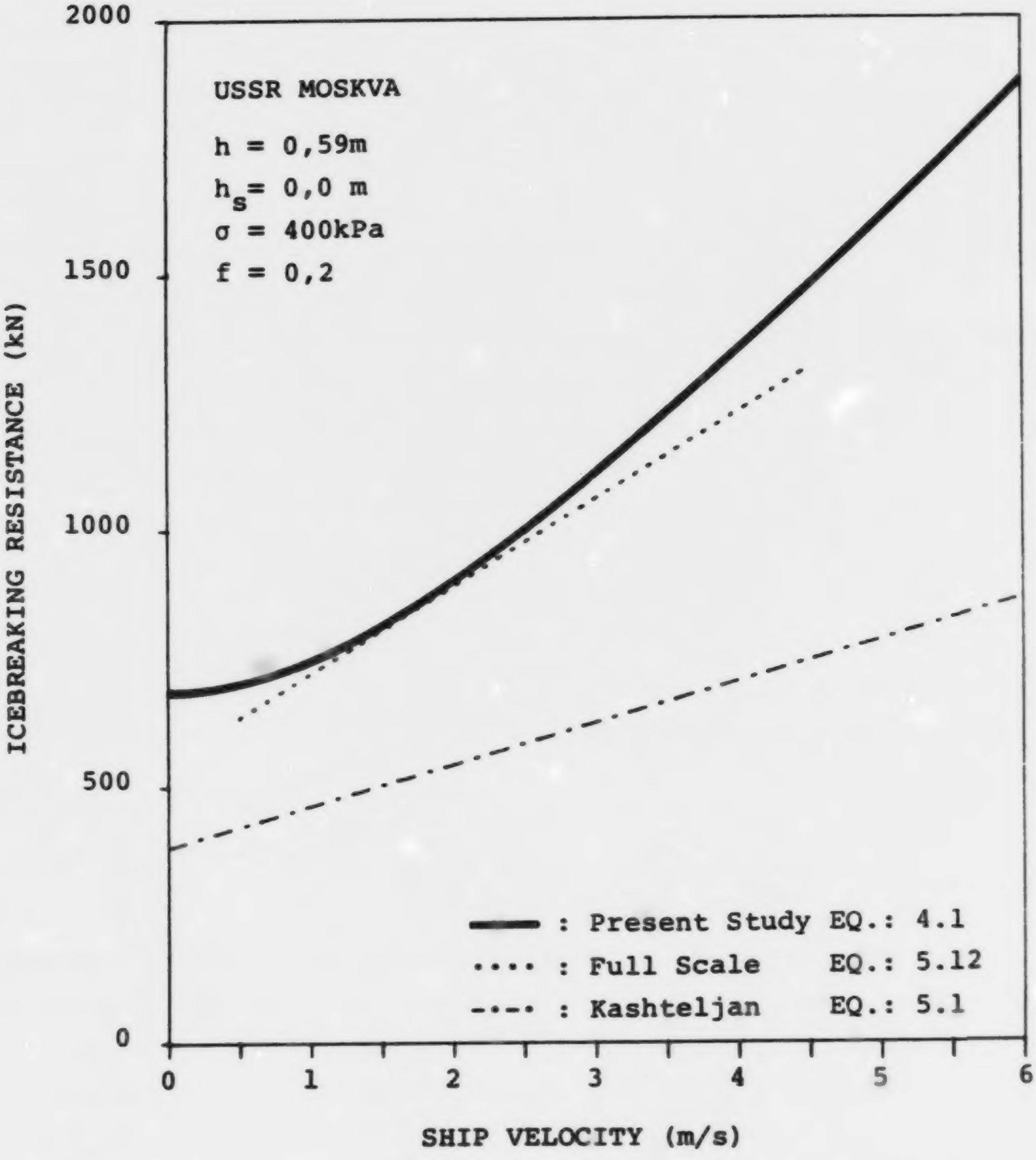

Figure 5.4.: Predicted icebreaking resistance for MOSKVA as compared to regression lines from full scale trials and model tests.

For the data points collected on the 1/48th scale model, Edwards and Nawwar (1978) suggests a slightly different best fitting regression equation:

$$\frac{R_t}{\rho g B h^2} = 9{,}68 + 2{,}28 \frac{V}{gh} \qquad \text{EQ.: 5.10}$$

From the data reproduced by German and Lawrence (1975), it can be seen that the open water resistance for the CCGS LOUIS ST.LAURENT can be closely approximated by the following empirical equation:

$$R_{ow} = 2{,}94\,V + 6{,}43\,V^2 \text{ (kN)} \qquad \text{EQ.: 5.11}$$

In Figure 5.3, our predictor equation (EQ.: 4.1) is compared with EQ.: 5.6 - 10 and the Kashteljan formula (EQ.: 5.1) for the mean values of the conditions prevailing during the full-scale trials of the CCGS LOUIS ST.LAURENT.

5.4.: USSR MOSKVA

Source of data: Enkvist 1972

Enkvist (1972) reported four different data sets obtained on MOSKVA type icebreakers (USSR MOSKVA & USSR VLADIVOSTOCK)

1.: Full-scale tests by Wartsila 1969;
2.: Full-scale tests by Arctic and Antarctic Institute 1964;
3.: Model tests 1:50 by Enkvist 1972;
4.: Model testd 1:25 by Enkvist 1972;

For the conditions prevailing during the full-scale trials, the ice resistance is then given by:

$$R_i = 550 + 170\,V \text{ (kN)} \qquad \text{EQ.: 5.12}$$

The above equation where the open-water resistance is not included is compared to our predictor equation (EQ.: 4.1) and to Kashteljan formula in Figure 5.4.

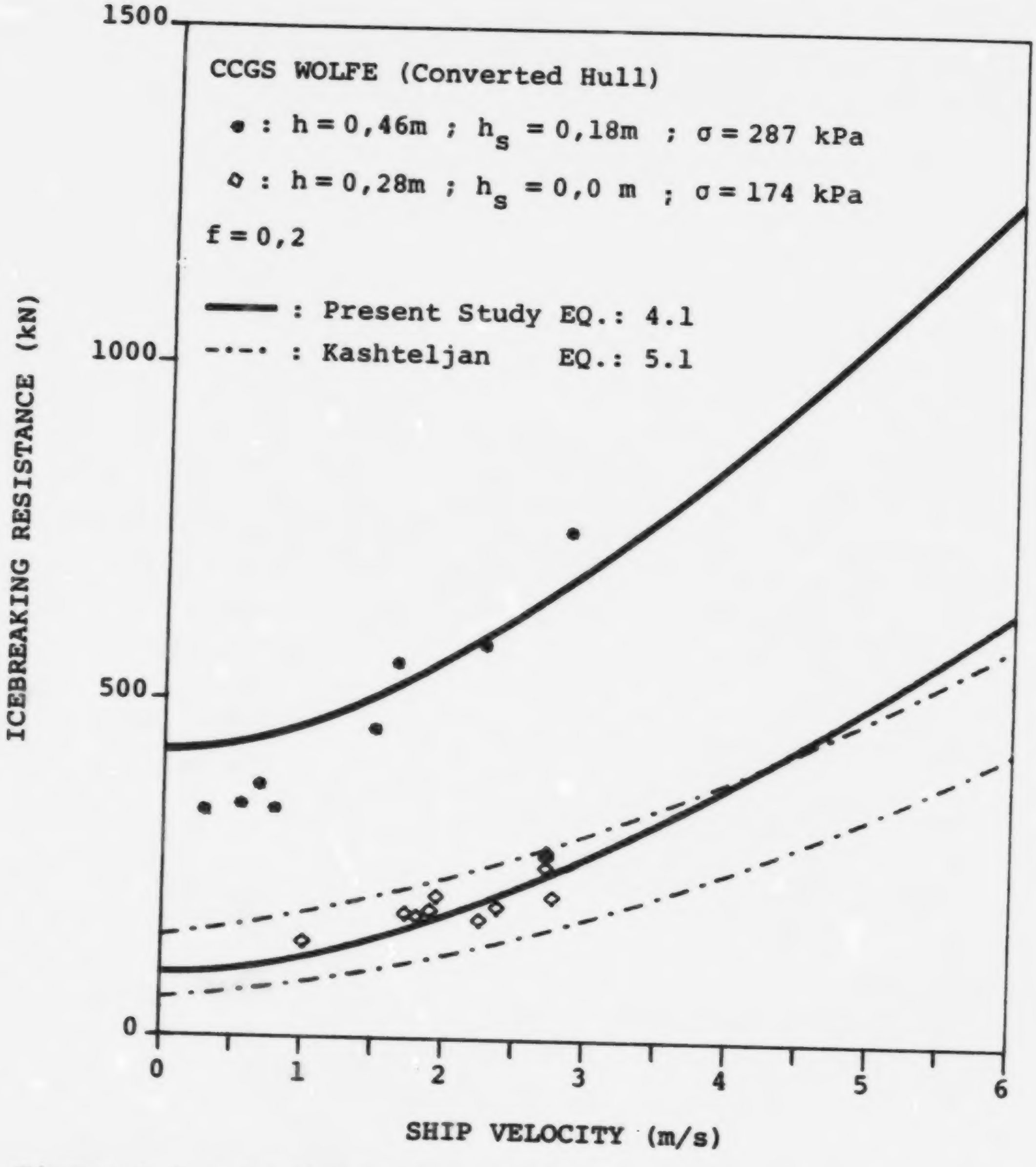

Figure 5.5.: Predicted icebreaking resistance for CCGS WOLFE (converted hull) as compared to measured values in snowless ice cover (0,28m) and in ice cover (0,46m) with snow (0,18m).

5.5.: CCGS WOLFE (Converted Hull)

Source of data: Edwards,R.Y.Jr. and Nawwar,A.M.,1978

The data from full-scale trials on the CCGS WOLFE with the converted hull are reported for 33 trials made in 1976 and 1977 during continuous icebreaking and for 13 trials made in 1976 during ramming tests.

In Figure 5.5, the predictions obtained by EQ.: 4.1 are compared with measured values in snowless ice cover, 0,28m thick, and in snowy ice cover, 0,46m thick. The values predicted by the Kashteljan formula are also shown for the two situations.

In Figure 5.6, the 46 actual measurements obtained by the CCGS WOLFE with the converted hull during full-scale trials under various ice conditions are compared to predictions given by EQ.: 4.1. The predicted values seem to reflect the correct icebreaking resistance.

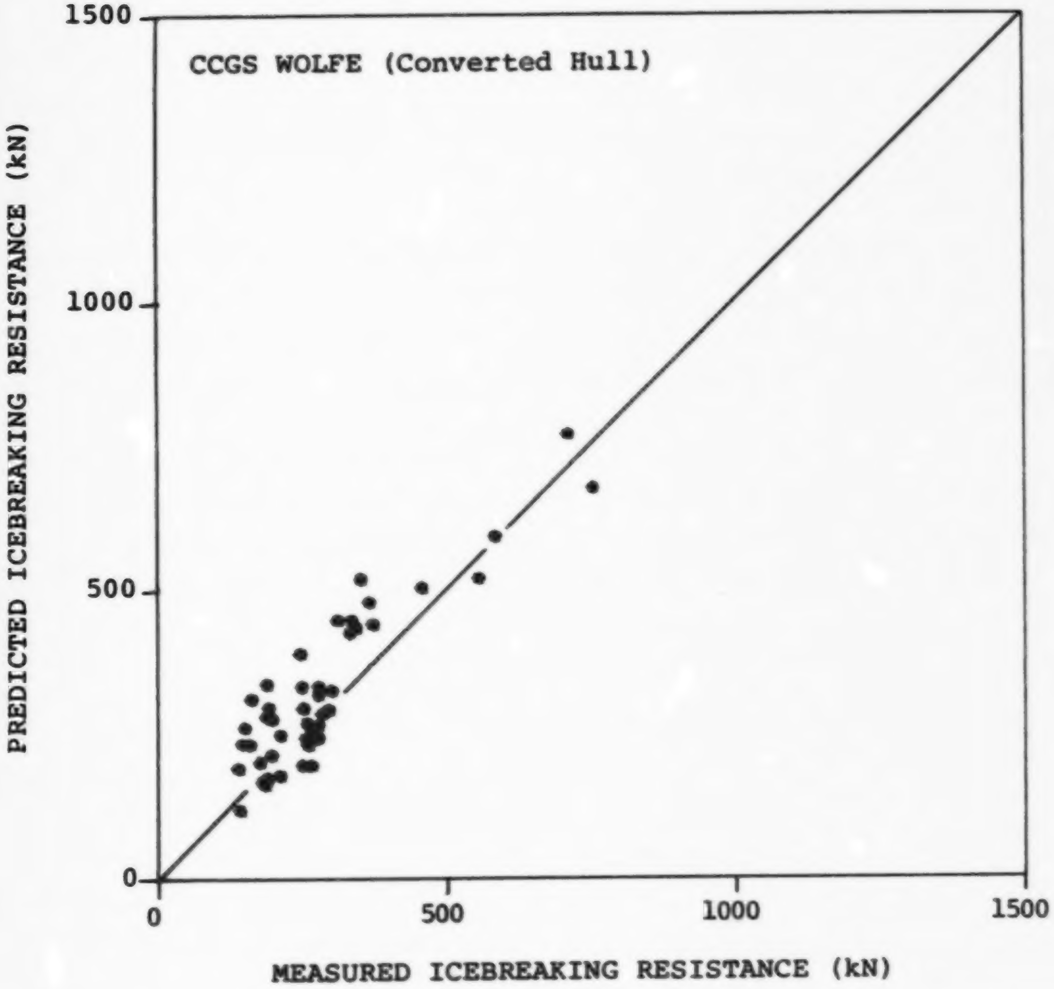

Figure 5.6.: Predicted icebreaking resistance for CCGS WOLFE (converted hull) as compared to actual measurements during full scale trials under various ice conditions.

5.6.: CCGS PIERRE RADISSON

Source of data: Edwards,R.Y.Jr et alt. 1981

Level ice resistance tests were carried out on CCGS PIERRE RADISSON under two dissimilar ice conditions:

1.: Arctic summer ice - weak, thick, melting one-year ice;
2.: Winter fresh and saline ice in the Saguenay River and St.Lawrence River

Icebreaking resistance data points are related to environmental conditions existing at the time the resistance is measured which include:

1.: Meteorological conditions;
2.: Ice properties.

From the experimental data, it was found that the open-water resistance for the CCGS PIERRE RADISSON is closely approximated by:

$$R_{OW} = 16\,V + 0{,}0013\,V^6 \text{ (kN)} \qquad \text{EQ.: 5.12}$$

and the maximum thrust at full power:

$$T = 1245 - 18{,}2\,V - 4{,}5\,V^2 \text{ (kN)} \qquad \text{EQ.: 5.13}$$

where V: ship speed (m/s).

Figure 5.7 shows a comparison between the predictions given by EQ.: 4.1 and the actual values measured under two extreme conditions, thick deteriorated one-year sea ice and thin solid ice. For comparison purpose, the values predicted by the Kashteljan formula are also shown.

In Figure 5.8, all ice resistance data points are compared to predictions given by EQ.: 4.1. The predictive model provides a relatively good estimate.

Figure 5.9 and Figure 5.10 show typical curves readily obtainable from the proposed model for any ship operating under given conditions.

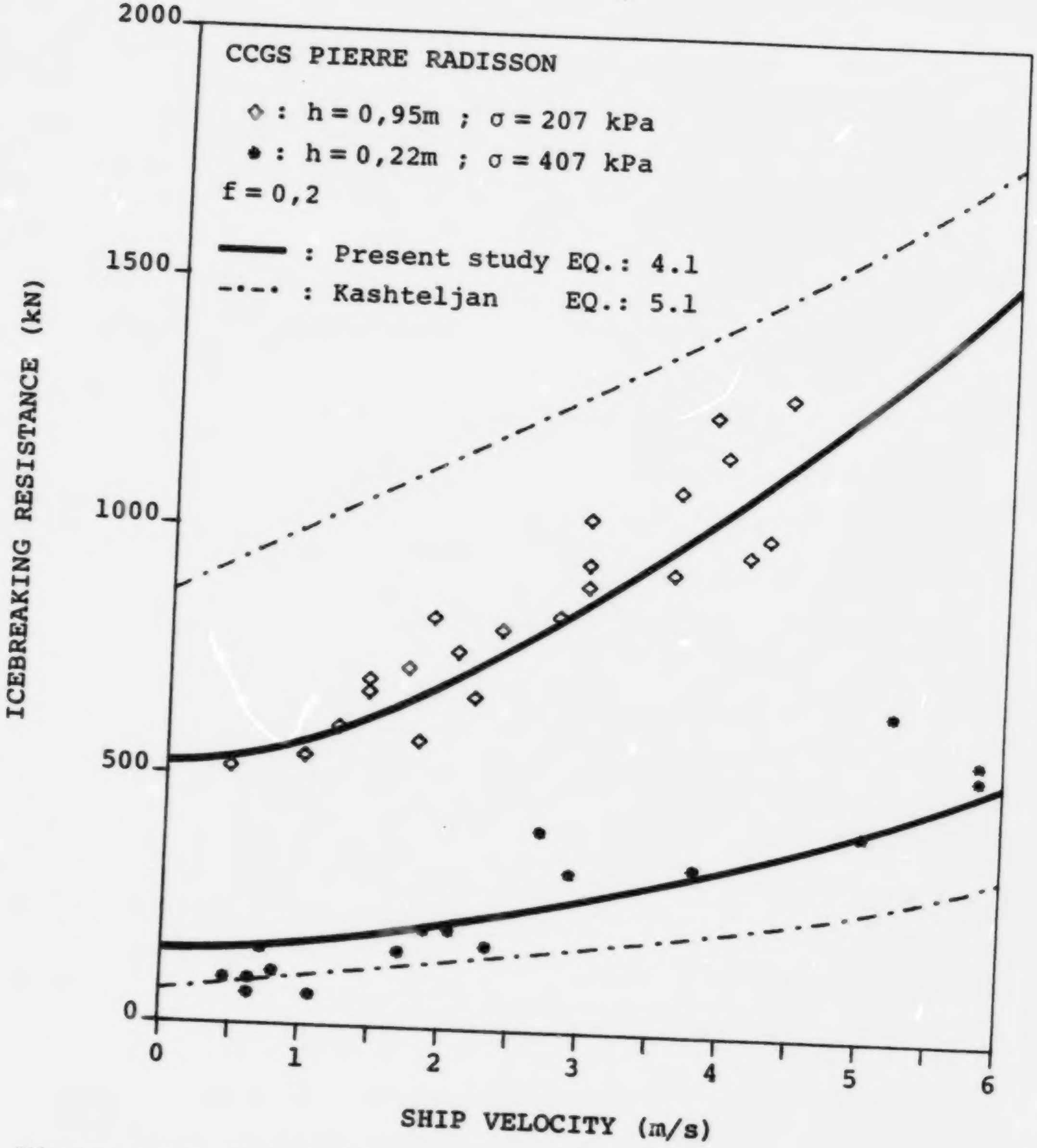

Figure 5.7.: Predicted icebreaking resistance for CCGS PIERRE RADISSON as compared to measured values in deteriorated one year sea ice and in solid fresh and saline ice.

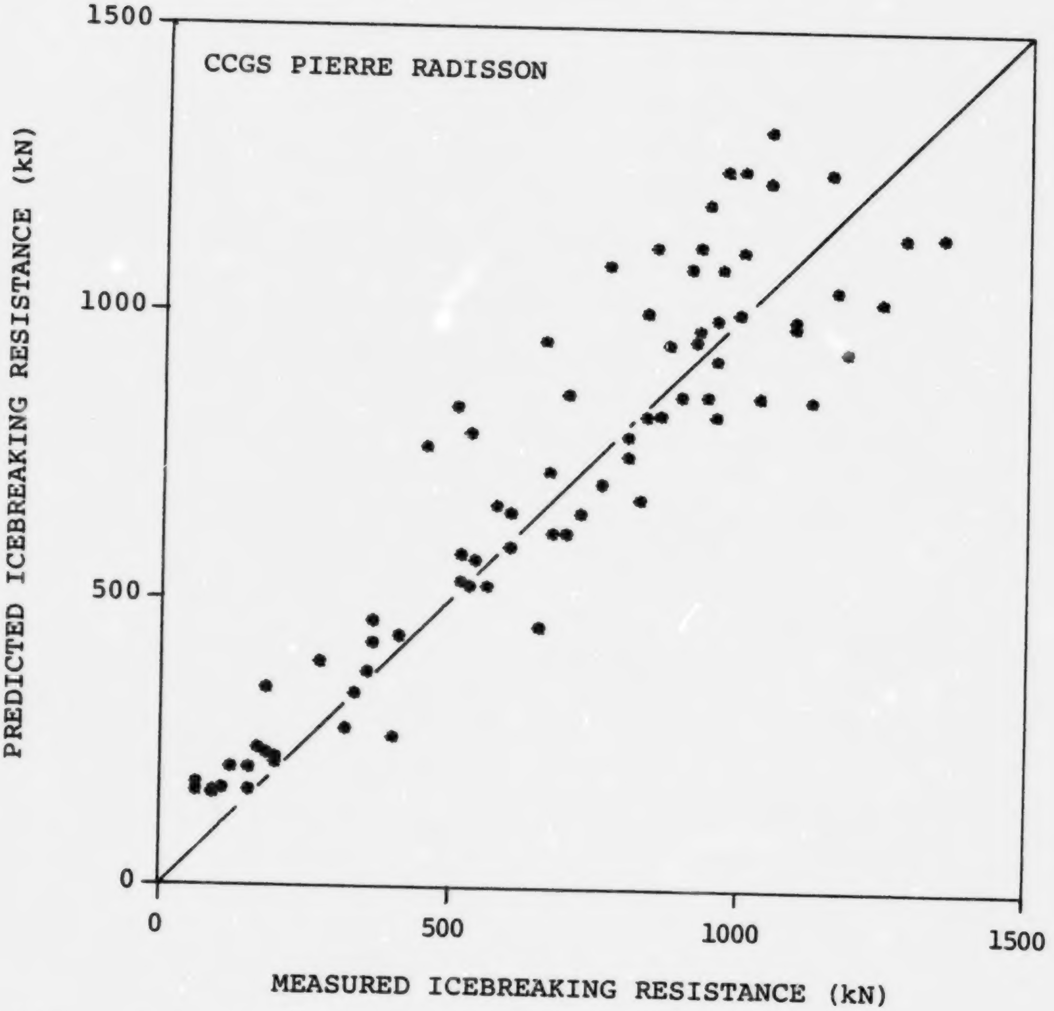

Figure 5.8.: Predicted icebreaking resistance for CCGS PIERRE RADISSON as compared to actual measurements during full scale trials under dissimilar ice conditions.

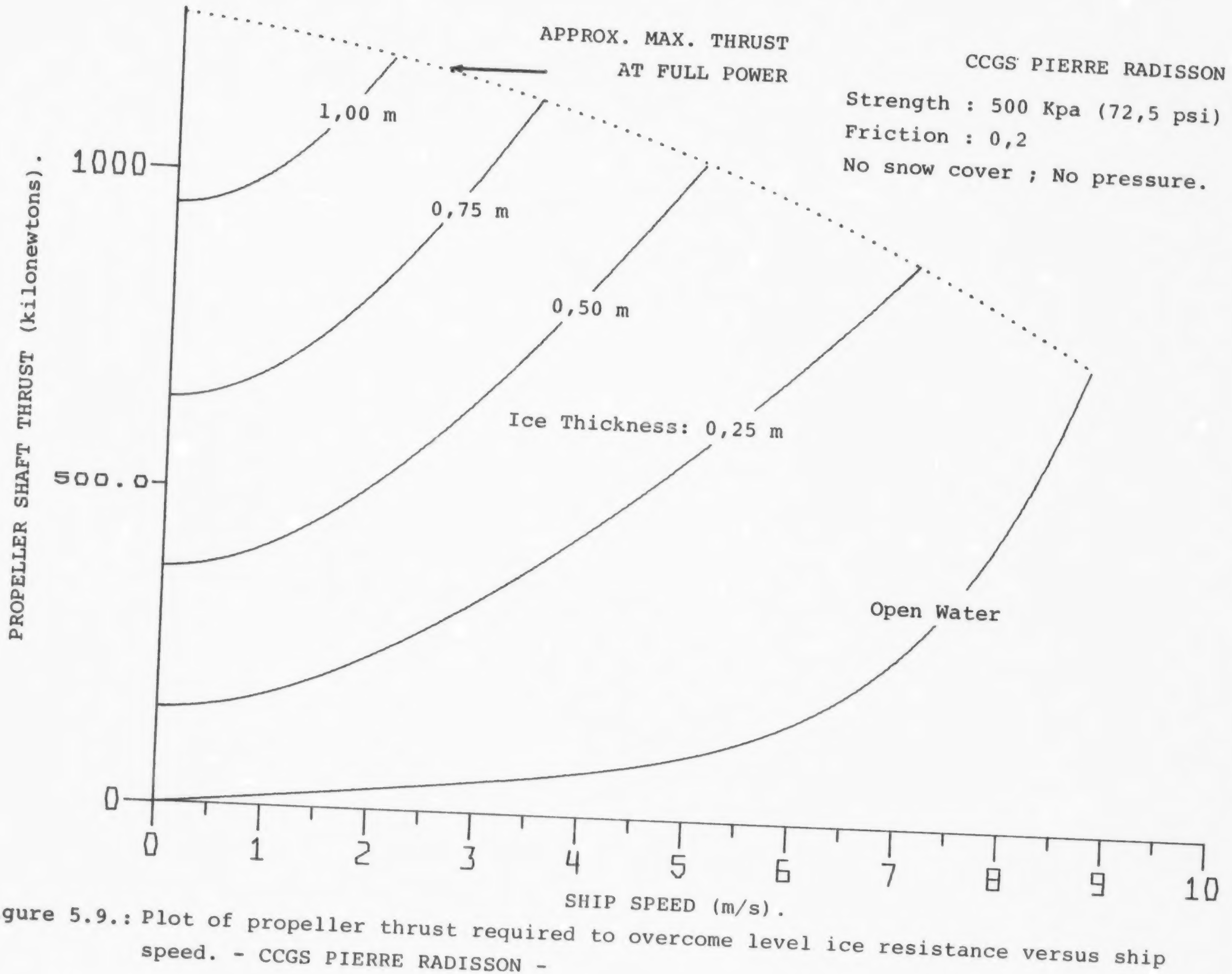

Figure 5.9.: Plot of propeller thrust required to overcome level ice resistance versus ship speed. - CCGS PIERRE RADISSON -

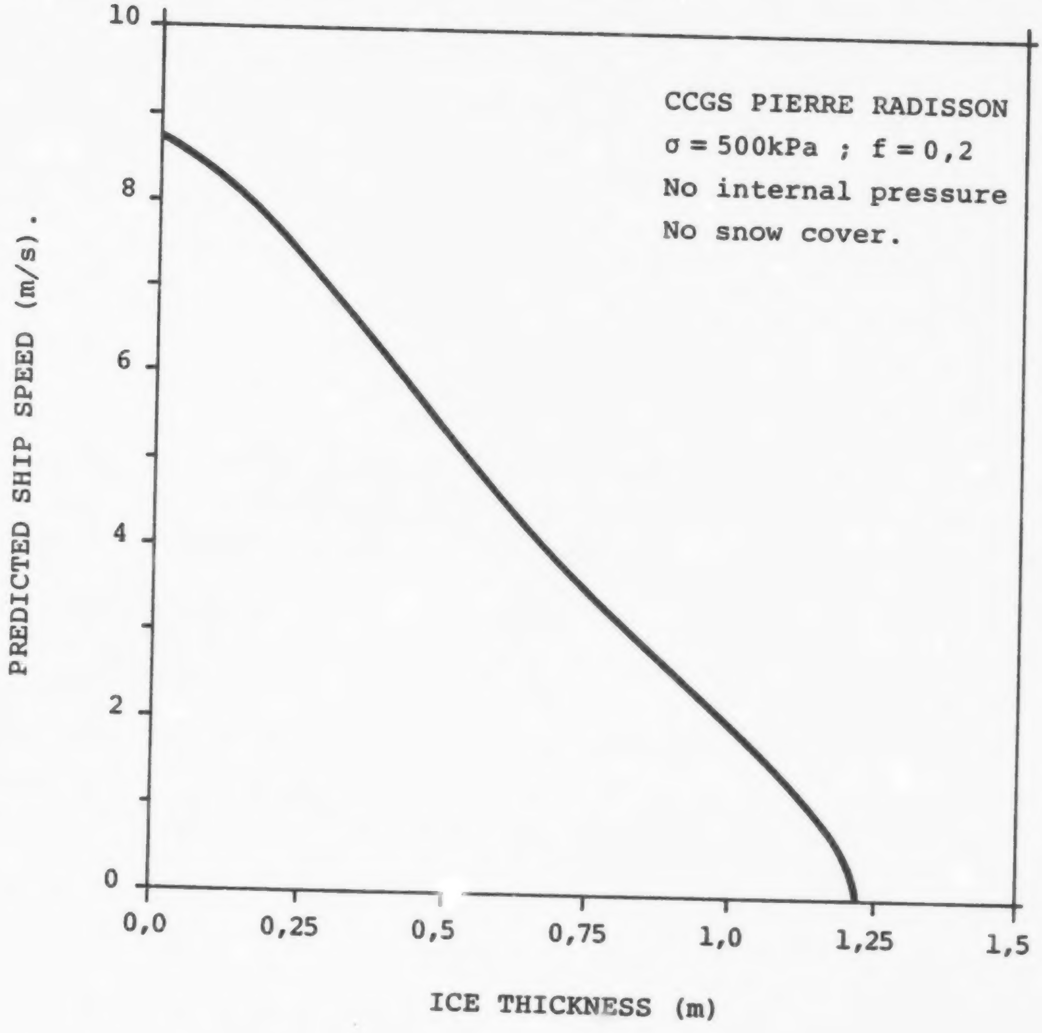

Figure 5,10.: Typical relationship between ice thickness and speed of advance in the continuous icebreaking mode for the CCGS PIERRE RADISSON operating at full power.

5.7.: COMMENTS

Our model assumes that most of the resistance to movement through the icefield is due to breaking the ice and friction forces. Inertial and buoyancy forces were neglected for the reason that, when ships are moving in broken ice the resistance is significantly increased only when the brash ice is constrained from moving and has to be broken.

> "If the concentration of broken ice is low, below 6 or 7 on a base of 10, the broken ice will not represent a significant obstacle to ship motion." (Milano 1973)

> "For low concentrations, ship speed is identical to that in open water obtained at the same power level."
> (Buzuev and Ryvlin 1961)

> "If the concentration is lower than 60%, ship progress is very slightly affected." (Edwards et alt. 1979)

From the above observations, it was concluded that the energy lost in accelerating the ice pieces equals the energy that would be required to accelerate the equivalent weight of water.

Kashteljan (1968), Nogid (1962) and others have shown that the effect of upturning or submerging the ice pieces is small and can be ignored.

The net total energy lost is set, in our study, equal to that absorbed in icebreaking by bending, buckling or crushing.

In our approach, the icebreaking and friction were maximized whereas the inertial and buoyancy forces were neglected. The resulting equation, EQ.: 4.1, has been compared with actual data obtained from full-scale trials and model tests for six (6) different icebreakers. The range of variations of the relevant full-scale parameters was:

Maximum Beam	$14{,}6\text{m} \le B \le 24{,}4\text{m}$
Forebody length	$67{,}1\text{m} \le L^* \le 112{,}4\text{m}$
Bow opening angle	$25° \le \theta \le 45{,}5°$
Stem angle	$16° \le \beta \le 32°$
Flare angle	$0° \le \gamma \le 20°$
Ice thickness	$0{,}09\text{m} \le h \le 1{,}92\text{m}$
Snow thickness	$0{,}00\text{m} \le h_s \le 0{,}30\text{m}$
Flexural strength	$146\text{kPa} \le \sigma \le 1650\text{kPa}$
Friction coefficient	$0{,}08 \le f \le 0{,}48$

Figures 5.1 to 5.8 show a good agreement between the predicted total resistance and the thrust required to overcome level ice resistance, measured during continuous icebreaking and calculated from the deceleration force during ramming tests.

The approach taken which states the problem from the point of view of the ice cover resistance rather than from the point of view of the ship motion does tend to generate resistance results that correlate very well with full scale trials and model tests data.

It is well realized that the proposed model, based upon gross assumptions and simplifications remains greatly perfectible. Nevertheless, it must be recognized that the resistance predictions obtained from EQ.: 4.1 for a wide range of ship parameters and environmental conditions compare favorably with actual data.

CONCLUSIONS AND RECOMMENDATIONS

In our attempt to develop an analytical solution to the determination of the resistance that an uniformly thick ice cover offers to a moving ship, we had to go through the following steps:

1.: Analytical representation of the ship forebody;

2.: Analysis of all possible mechanisms of ice failure and derivation of proper ice failure criteria;

3.: Determination and integration of the incremental ice forces acting all along the waterline;

4.: Comparison of the model predictions with full-scale data available from literatue.

The proposed model takes into account all possible mechanisms of ice failure and dynamics of both ship and ice and, predicts the effects of variations in ice properties and ship characteristics.

The major parameters affecting the ship resistance to continuous motion in level ice have been identified and evaluated.

There seems to be a good correlation between the full-scale data readily available from literature and the predictions of the proposed mathematical model.

It is thought that our very simple model is a promising step towards a better understanding of the icebreaking phenomenom and a further knowledge of the details and mechanisms involved. The analytical solution also appears to be a powerful means of optimizing the ship parameters at a relatively low cost.

Based on the promising results obtained by the use of the approach taken, the following recommendations seem justified:

1.: Development of rigourous ice failure criteria based on theory as well as experiments.

2.: Rigourous analysis to assess the validity of the assumptions and simplifications used in the present model.

It is believed that, with time and continued attention, the limitations of the present model may be improved such that one day a truly reliable analytical model to predict ship resistance to motion through ice will be possible.

REFERENCES

BUZUEV, A. and RYVLIN, A., 1961, "On Calculations of Icebreaker Resistance in Finely Broken Ice" Worskoj Flot 21.

CARTER, D., 1975, "Mathematical Model of the Icebreaking Mechanism under an Air Cushion Vehicle Operating at or near the Critical Velocity" Transport Canada, Transportation Development Agency, Montreal, 62 pages.

EDWARDS, R.Y.Jr., LEWIS, J.W., WHEATON, J.W., COLBURN, J., 1972 "Full Scale and Model Tests of a Great Lakes Icebreaker" Trans. SNAME Vol.80.

EDWARDS, R.Y.Jr., MAJOR, R.A., KIM, J.K., GERMAN, J.G., LEWIS, J.W., and MILLER, D.M., 1976 "Influence of Major Characteristics of Icebreaker Hulls on Their Powering Requierements and Maneuverability in Ice" Paper No. 12, SNAME Annual Meeting, New-York, November 1976.

EDWARDS, R.Y.Jr., and NAWWAR, A.M., 1978 "Compilation and Analysis of Recent Icebreaking Model Test Data of a World-Wide Variety of Hull Forms" Report 1294 prepared for Transport-Canada Research and Development Centre by Arctec Canada Ltd.

EDWARDS, R.Y.Jr., NAWWAR, A.M., NOBLE, P.G., and DUNNE, M., 1979 "Development of a Research Program for Improving Arctic Marine Transportation Technology" Vol. 2, TP 2004, Report prepared for Transport Canada Research and Development Centre, Montreal, by Arctec Canada Ltd.

EDWARDS, R.Y.Jr., DUNNE, M.A., COMFORT, G., BULAT, V., and JOHNSON, B. 1981, "Results of Full Scale Trials in Ice of CCGS PIERRE RADISSON", SNAME Proceedings Spring Meeting /STAR Symposium, Ottawa Ontario, June 17-19, 1981

ENKVIST, E., 1972, "On the Resistance Encountered by Ships Operating in the Continuous Mode of Icebreaking" The Swedish Academy of Engineering Sciences in Finland, Report 24, Helsinky.

GERMAN, J.G., and LAWRENCE, R.G.A., 1975, "Full Scale Testing in Ice of Three Icebreakers", SNAME Ice Tech Symposium, Montreal

KASHTELJAN, V.I., POZNJAK, I.I., and RYVLIN, A.Ja., 1968 "Ice Resistance to Motion of a Ship" Sudostroenie, Leningrad,(Transl.)

LEWIS, J.W., and EDWARDS, R.Y.Jr., 1970 "Methods for Predicting Icebreaking and Ice Resistance Characteristics of Icebreakers" Paper No. 5, SNAME Annual Meeting, New York, 1970.

MICHEL, B., 1978, "Ice Mechanics" Les Presses de l'Université Laval, Québec, 499 pages.

MILANO, V.R., 1973, "Ship Resistance to Continuous Motion in Ice" Paper presented at the Annual Meeting, New York, November 15 -17, 1973, of SNAME.

NEVEL, D., 1961, "The Narrow Infinite Wedge on an Elastic Foundation" Research Report 79, U.S. Snow, Ice and Permafrost Research Establishment.

NOGID, L.M., and DUBROVIN, D.V., 1962, "On Viscous Resistance of Icebreakers" Sudostroyeniye 28, June 1962.

RUNEBERG, R.I., 1890, "On Steam Ships for Winter Navigation and Icebreakers" Proceedings of the Institution of Civil Engineers, Vol.CXL, Session 1899-1900, Part II., Leningrad.

SORENSEN, R.M., 1973, "Water Waves Produced by Ships" Journ. of Waterways, Harbors and Coastal Engineering Division, ASCE, Vol. 99, No. WW2, Proc. Paper 9754, p 245-256.

VANCE, G.P., 1975, " A Scaling System for Vessels Modeled in Ice" Paper H, presented at the SNAME ICE TECH Symposium, Montreal April 9-11, 1975

- APPENDIX A -

- ICE FORCES -

APPENDIX A

TABLE OF CONTENTS

A.1 INTRODUCTION 65

A.2 RADIAL CRACK FORMATION 66

- A.2.1 UNDER VERTICAL LOADS 66
- A.2.2 UNDER HORIZONTAL LOADS 68

A.3 FINAL FAILURE 70

- A.3.1 UNDER VERTICAL LOADS 70
  - A.3.1.1 Complete Wedge 70
  - A.3.1.2 Truncated Wedge 72
- A.3.2 UNDER HORIZONTAL LOADS 74
- A.3.3 UNDER OBLIQUE LOADS 80

A.4 SUMMARY AND CONCLUSIONS 84

- A.4.1 LOADS APPLIED ON THE ICE COVER 84
- A.4.2 LOADS APPLIED AT THE EDGE OF AN ICE COVER 84

BIBLIOGRAPHY 88

APPENDIX A

ICE FORCES

A.1. INTRODUCTION

Observations in the field indicate that ice cover failures often occur in two stages: First, the ice cracks radially from the loaded region and, under increasing load, this is followed by the formation of circumferential cracks that cause final failure.

Most attempts to determine the resistance of floating ice plates are based on the theory of homogeneous and isotropic elastic plates that rest on a liquid.

In actual ice plates, the lower surface is at the freezing temperature while the upper surface is subjected to the air temperature fluctuations. The Young's modulus, E, which is dependent on temperature and type of ice, may obviously vary across the plate thickness. The resulting stress distribution is, therefore, not necessarily linear.

Depending on the stress distribution, the corresponding moments may vary between the two limiting values $\sigma h^2/6$ and $\sigma h^2/4$ where σ is the tensile stress and, h the ice thickness.

Experimental tests conducted by Panfilov (1960) and dicussed by Kerr (1976) indicate that the factor 1,5 takes into consideration not only the effect of the non-linear stress distribution but also the wedge-in moments. The formation of full plastic moment is not observed in the field for loads of short duration.

The area between the envelopes corresponding respectively to the elastic and plastic stress distributions is the region of failure loads. Below the elastic envelope, failure never occurs and, above the plastic envelope failure always occurs.

For engineering purposes, the elastic envelope corresponds to the loads that an ice plate can safely bear and, the plastic envelope to the loads at which the plate must definitely collapse, e.g. for the design of ice breakers.

A.2 RADIAL CRACK FORMATION

A.2.1 UNDER VERTICAL LOADS

The response of a homogeneous and isotropic elastic plate that rests on a liquid and is subjected to a static vertical load, q, is described by the partial differential equation:

$$D\nabla^4\omega + \gamma\omega = q \qquad \text{EQ.: A.1}$$

where ω is the plate deflection, γ is the weight per unit volume of the liquid, and D is the flexural rigidity of the plate defined as:

$$D = \frac{E\,h^3}{12\,(1-\nu^2)} \qquad \text{EQ.: A.2}$$

where E is the Young's modulus of the plate, h is the ice thickness and, ν is the Poisson's ratio for the plate material.

Bernshteyn (1929) by utilizing the solution presented by Hertz (1884) determined the vertical load, V_1, at which an infinite plate cracks radially when subjected to a vertical load concentrated or uniformly distributed over a circular area of radius a. (Figure A.1)

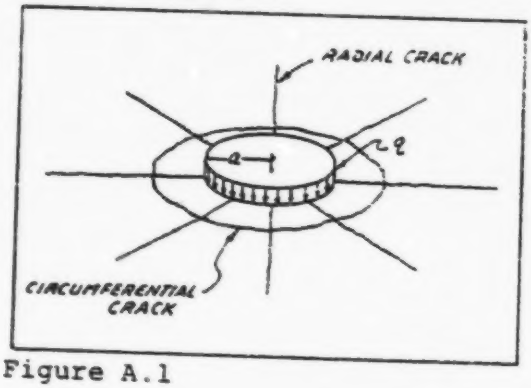

Figure A.1

$$V_1 = \frac{1}{3\,(1+\nu)\,C(\rho)}\,\sigma\,h^2 \qquad \text{EQ.: A.3}$$

where σ is the failure bending stress, h is the ice thickness and, ν is the Poisson's ratio for the ice. The function $C(\rho)$ is given by:

$$C(\rho) = \frac{\mathrm{kei}'\,\rho}{\pi\,\rho} \qquad \text{EQ.: A.4}$$

where $\rho = a/\ell$, a being the radius of the circular area subjected to the uniform load and, ℓ the "characteristic length" of the plate being defined as:

A.2.1 UNDER VERTICAL LOADS (Cont'd)

$$\ell = \left[\frac{D}{\gamma}\right]^{1/4} \qquad \text{EQ.: A.5}$$

Solution for the floating semi-infinite plate with a free edge subjected to vertical loads (Figure A.2) was presented by Shapiro (1943) using Fourier integral methods.

According to Shapiro's results, verified and extended by Nevel (1965), the vertical load at which the first radial cracks occur in a semi-infinite plate becomes:

$$V_2 = S(\rho)\ \sigma h^2 \qquad \text{EQ.: A.6}$$

where, according to Panfilov (1960)

$$S(\rho) = \frac{C(\rho)}{2{,}45} \qquad \text{EQ.: A.7}$$

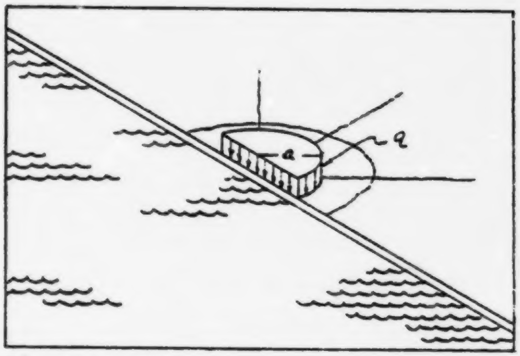

Figure A.2

C(ρ) being the function for the infinite plate given by EQ.: A.4

Figure A.3 shows a comparision between the loads at which the radial cracks occur in infinite (EQ.: A.3) and semi-infinite (EQ.: A.6) ice plates for ν=0,3.

Experimental data show that Bernshteyn's and Shapiro's results closely predict the radial crack formation under vertical loads.

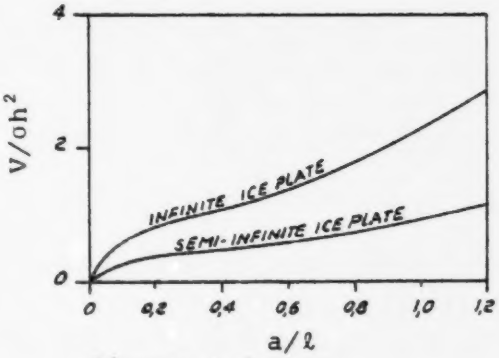

Figure A.3

A.2.2 UNDER HORIZONTAL LOADS

When a floating elastic semi-infinite plate is subjected to a horizontal pressure, p, uniformly distributed on a width, B, as shown in Figure A.4, the largest shear stress occuring at points (0,±B/2) is given by:

$$\tau = \frac{p}{\pi} \qquad \text{EQ.: A.8}$$

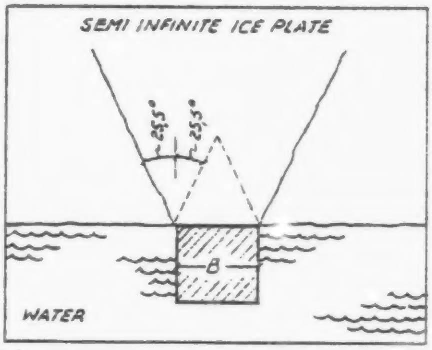

Figure A.4

The direction of the planes of maximum shear stress then makes an angle equal to ±π/4 with the normal to the structure.

It has been shown theoretically by Stroh (1954) and Smith and Barnby (1967) and verified experimentally by Carter (1971) that cracks will be formed when:

$$\tau = \frac{\sigma_1}{2} \qquad \text{EQ.: A.9}$$

where σ_1 is the tensile strength of the ice plate.

Combining EQ.: A.8 & 9, we obtain the pressure intensity which causes the formation of the radial cracks under horizontal loads as:

$$p = \frac{\pi}{2}\sigma_1 \qquad \text{EQ.: A.10}$$

The directions in which the cracks will propagate then make an angle of ≃70.5° with the direction of the planes of maximum shear stress, ±π/4, i.e. ±25.5° with the normal to the structure.

The two limiting cases occur respectively when the two cracks are converging, shown as dashed line, and diverging, shown as full line in Figure A.4.

A.2.2 UNDER HORIZONTAL LOADS (Cont'd)

The interception of the two converging cracks causes the ice plate failure and, the minimum horizontal load, H_{min}, is then obtained from EQ.: A.10 as:

$$\boxed{H_{min} = \frac{\pi}{2} \sigma_I B h} \qquad \text{EQ.: A.11}$$

where σ_I is the tensile strength of the ice, B the structure width and h the ice thickness.

As it will be discussed later, the maximum horizontal force, H_{max}, will be related to either the crushing or buckling failure of a truncated floating wedge formed by the diverging cracks emaning from the loaded region of the ice plate.

A.3 FINAL FAILURE

After the ice plate is radially cracked, the location and magnitude of the stresses that cause the final failure associated to the formation of the circumferential cracks is predicted by the theory of a wedge on an elastic foundation.

A.3.1 UNDER VERTICAL LOADS

The response of a floating infinite wedge subjected to vertical loading is described by an ordinary differential equation with a variable coefficient: (Nevel (1961))

$$\frac{d^4\omega}{d\rho^4} + \frac{2}{\rho}\frac{d^3\omega}{d\rho^3} + \omega = \frac{q}{\gamma} \qquad \text{EQ.: A.11}$$

where ω is the wedge deflection, q the vertical loading, ρ the ratio r/ℓ, and γ the weight of the liquid per unit volume, ℓ the characteristic length is defined by EQ.: A.5.

This equation was solved by Dieudonné (unpublished) using the

A.3.1 UNDER VERTICAL LOADS (Cont'd)

Laplace method of integration and by Nevel (1958) by means of the method of Frobenius. The solution for the unloaded part is:

$$\omega = C_0\ Dn_0(\rho) + C_1\ Dn_1(\rho) + C_2\ Dn_2(\rho) + C_3\ Dn_3(\rho)$$

EQ.: A.12

where C_0, C_1, C_2, C_3, are the four constants of integration depending on the boundary conditions and $Dn_0(\rho)$, $Dn_1(\rho)$, $Dn_2(\rho)$, $Dn_3(\rho)$ are infinite series which were evaluated by Nevel (1961).

A.3.1.1 Complete Wedge

Solution for a wedge on an elastic foundation with a uniformly distributed load for a distance a from its apex was presented by Nevel (1961) (Figure A.5).

Noting that the total load is equal to the sum of the loads on the wedges, Nevel's results may be expressed as follows:

$$\boxed{V_{min} = fn_1(\rho)\ \theta\ \sigma\ h^2}$$

EQ.: A.13

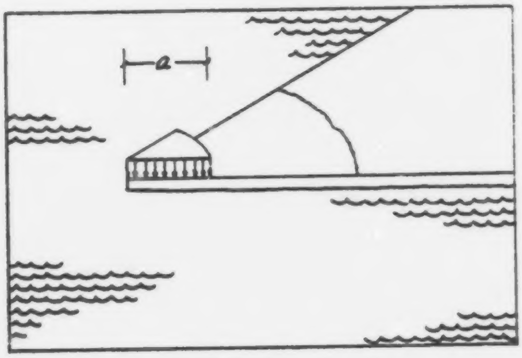

Figure A.5

where V_{min} is the minimum total vertical load required to form the circumferential cracks and θ is the total angle (radians) formed by the sum of the individual wedges. The rather complicated function $fn_1(\rho)$ is shown in Figure A.6. Taking into consideration the effects of the non-linear stress distribution, the inhomogeneity of the plate and the wedge-in moments, the maximum total vertical load is written:

$$\boxed{V_{max} = 1{,}5\ fn_1(\rho)\ \theta\ \sigma\ h^2}$$

EQ.: A.14

A.3.1 UNDER VERTICAL LOADS (Cont'd)

Some authors assuming that the ice plate can, without cracking, resist a full plastic moment, utilized methods based on the yield-line or limit analysis for the determination of the allowable load on an infinite plate (Figure A.1). Typical of that mode of approach, the analysis of Persson (1948) leads to:

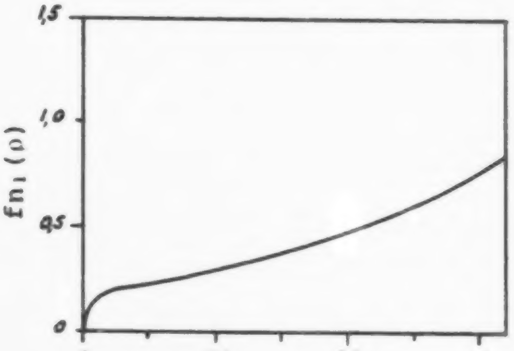

Figure A.6

$$V_{max} = \frac{\pi\,\sigma\,h^2}{(1+\nu)\,(1-0{,}62\rho^{2/3})}$$

EQ.: A.15

Many other investigators (Shulman (1946), Panfilov (1960), etc.) simplified the relation between the allowable loads and ρ by replacing the curve for a given range of ρ with a straight line described by an equation of the form:

$$V = (\,A + B\rho\,)\,\sigma h^2$$

EQ.: A.16

where A and B are constants.

For example, Kerr (1976) represented the upper envelope for the test data obtained by Panfilov (1960) by:

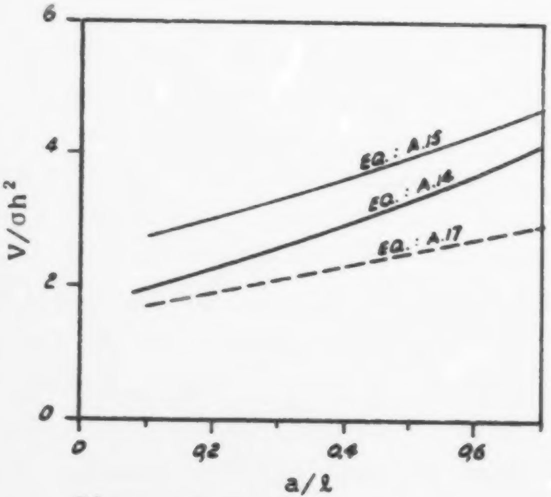

Figure A.7

$$V_{max} = (\,1{,}5 + 1{,}1\,\rho\,)\,\sigma h^2$$

EQ.: A.17

A comparison of EQ.: A.14, 15, 16 is made in Figure A.7 for an infinite plate ($\theta = 2\pi$) .

A.3.1 UNDER VERTICAL LOADS (Cont'd)

Noting that ρ is a function of $1/h^{\frac{3}{4}}$ (EQ.: A.2 & 5), straigth line approximations lead to a relation of the following form:

$$V = (A h^2 + B h^{5/4}) \sigma \qquad \text{EQ.: A.17}$$

where A and B are constants.

Such approximate expressions are valid only for a given range of ρ and should be used very cautiously.

A.3.1.2 Truncated Wedge

The geometry of the problem shown in Figure A.8 corresponds to several engineering applications, namely the design of icebreakers and the determination of vertical ice forces on structures. The exact solution of a truncated wedge subjected to a vertical load along its free edge, b, was obtained by Carter (1981) using EQ.: A.12. The constants of integration were determined from the conditions at the edge. Since Dn_0 and Dn_1 increase rapidly with increasing argument, the consideration that, at an infinite distance from the application of the load, both ω and $d\omega/d\rho$ must vanish leads to $C_0=0$ and $C_1=0$. The constants C_2 and C_3 are determined to fulfill conditions required for moment = 0 and shear = V/b at the edge of the truncated wedge. The total vertical load required to cause the formation of the circumferential cracks in a floating truncated wedge may be expressed as follows:

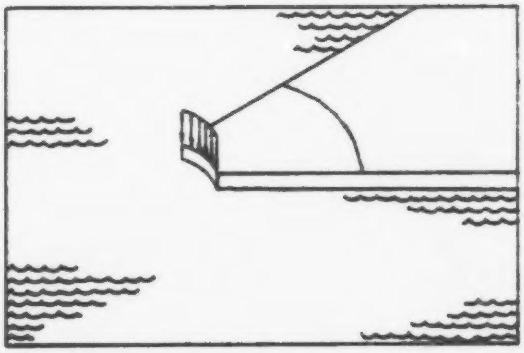

Figure A.8

A.3.1 UNDER VERTICAL LOADS (Cont'd)

$$\boxed{V_{min} = 0,3655 \ (\ 0,5\,\theta + b/\ell \ ) \ \sigma h^2} \qquad \text{EQ.: A.18}$$

and

$$\boxed{V_{max} = 0,5482 \ (\ 0,5\,\theta + b/\ell \ ) \ \sigma h^2} \qquad \text{EQ.: A.19}$$

where θ (radians) is the wedge opening angle at its apex.

Except for small values of b/ℓ, the distance from the load where the circumferential cracks will form is given by:

$$r = \frac{\pi}{4}\,\ell \qquad \text{EQ.: A.20}$$

The region of the vertical failure loads applied at the edge of a semi-infinite ice plate ($\theta = \pi$)is shown in Figure A.9.

Panfilov (1960) who has conducted 50 tests on semi-infinite ice plate subjected to vertical edge loads has proposed the following empirical relation, shown as dashed line in Figure A.9

$$V = (\ 0,45 + 0,38\,b/\ell \ ) \ \sigma h^2 \qquad \text{EQ.: A.21}$$

The agreement between the experimental results and our analytical approach is very close.

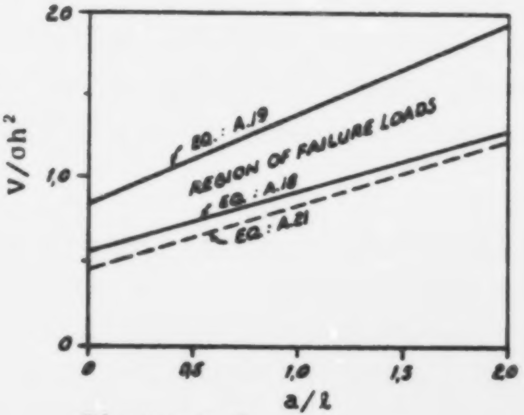

Figure A.9

A.3.2 UNDER HORIZONTAL LOADS

When a horizontal force is applied at the edge of an ice sheet, failure may occur in either the crushing mode or the buckling mode, whichever requires less force.

When failure occurs by crushing, the largest force an ice cover may exert or sustain is given by:

$$\boxed{H_{max} = \sigma_2 B h} \qquad \text{EQ.: A.22}$$

where σ_2 is the compressive strength of the ice; B the width of the contact area; and h the ice thickness.

When failure occurs by buckling, the largest force corresponds to the buckling load of the truncated wedge formed by the cracks emaning from the loaded region. Referring to the geometry of the tapered beam shown in Figure A.10(a), the differential equation governing the buckling of such a beam may be written as: (Kerr, 1978), (Nevel, 1979), `(Sodhi, 1979), (Sodhi and Nevel 1980)

$$\frac{d^2}{d\rho^2}\left[E I_0 \rho \frac{d^2\omega}{d\rho^2}\right] + H \frac{d\omega^2}{d\rho^2} + \gamma b_0 \rho \omega = 0 \qquad \text{EQ.: A.23}$$

where I_0 and b_0 are respectively the moment of inertia and the width of the wedge at $\rho = x/\ell = 1$ from its apex, ℓ being the characteristic length of the ice wedge (EQ.:A.5); ω is the transverse deflection of the tapered beam, E the Young's modulus, H the horizontal load, and γ the specific weight of water.

An analytical relation, showing the dependence of the buckling load on the various geometrical and material parameters of the floating ice wedge, was obtained by Carter (1981) for the different boundary conditions imposed at the contact area, either frictionless, hinged, or fixed.

A.3.2 UNDER HORIZONTAL LOADS (Cont'd)

The results are given along with the approximate buckling load obtained by Kerr (1978) for a simply supported edge and a clamped end:

a.: for a free end

$$H_{min} = (0{,}5\,\theta + b/\ell)\,\gamma\,\ell^3 \qquad \text{EQ.:A.24}$$

$$H_{max} = 1{,}5\,(0{,}5\,\theta + b/\ell)\,\gamma\,\ell^3 \qquad \text{EQ.:A.25}$$

b.: for a hinged end

$$H_{min} = (2\,\theta + 2\,b/\ell)\,\gamma\,\ell^3 \qquad \text{EQ.:A.24(b)}$$

$$H_{max} = 1{,}5\,(2\,\theta + 2\,b/\ell)\,\gamma\,\ell^3 \qquad \text{EQ.:A.25(b)}$$

Kerr (1978) Eq. 26 $\quad H = (3{,}75\,\theta + 2{,}65\,b/\ell)\,\gamma\,\ell^3$

Kerr (1978) Eq. 35 $\quad H = (2{,}48\,\theta + 6{,}48\,b/\ell)\,\gamma\,\ell^3$

c.: for a clamped end

$$H_{min} = (4\,\theta + 2\,b/\ell)\,\gamma\,\ell^3 \qquad \text{EQ.:A.24(c)}$$

$$H_{max} = 1{,}5\,(4\,\theta + 2\,b/\ell)\,\gamma\,\ell^3 \qquad \text{EQ.:A.25(c)}$$

Kerr (1978) Eq. 27 $\quad H = (5{,}65\,\theta + 8\,b/\ell)\,\gamma\,\ell^3$

For a direct comparison with the results obtained by Nevel (1979) from an analytical solution and by Sodhi (1979) from a finite element analysis, the above equations may be expressed in the form of a non-dimensional buckling pressure. For example, noting that $b = r\,\theta$, EQ.A.24 yields:

$$\frac{H_{min}}{b\gamma\ell^2} = 1 + \frac{0{,}5}{r/\ell}$$

In Figure A.10, the above equations are plotted along with the nondimensional buckling pressure obtained by Sodhi and Nevel (1980) (page 135) for the different boundary conditions.

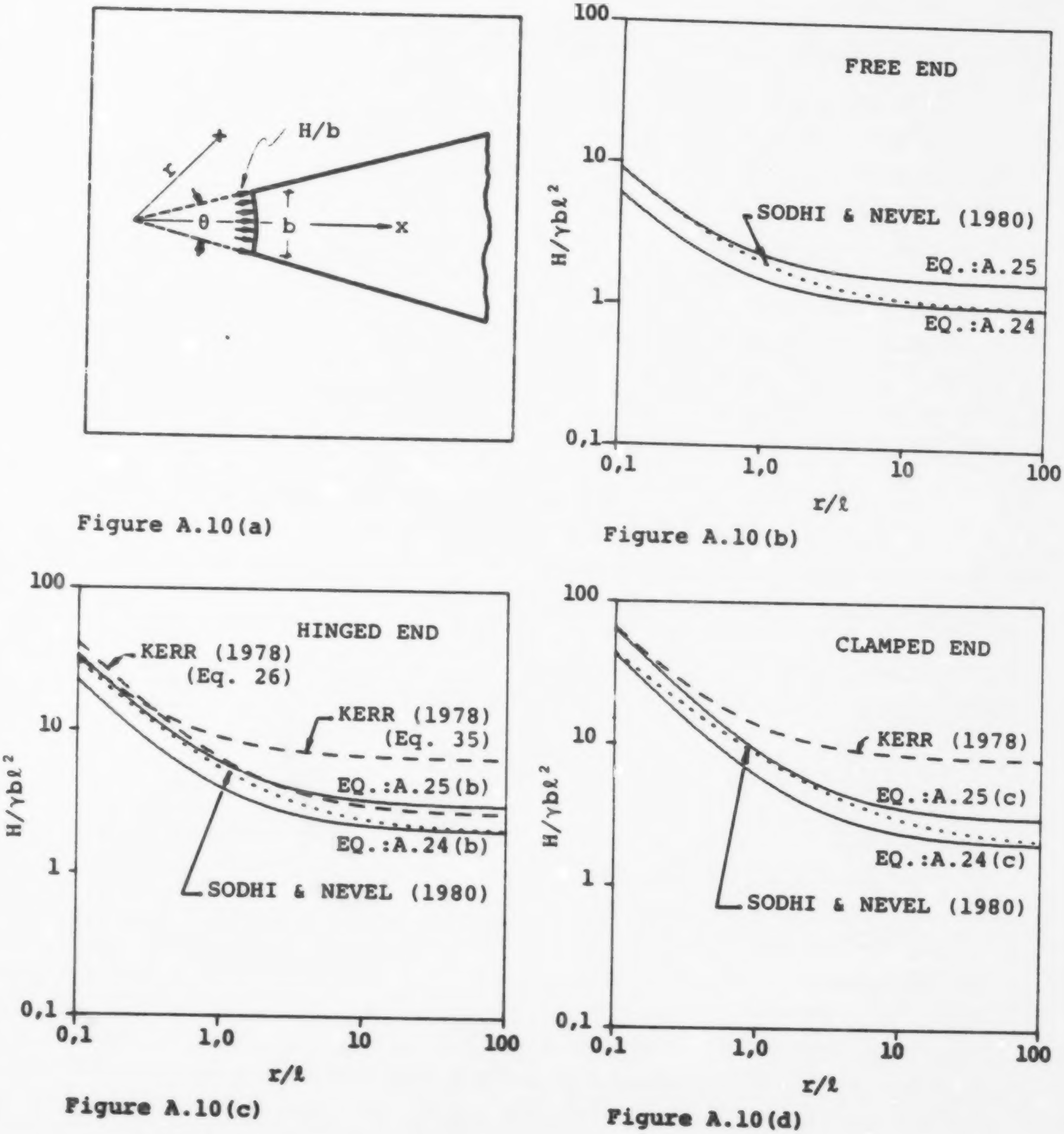

Figure A.10(a)

Figure A.10(b)

Figure A.10(c)

Figure A.10(d)

Figure A.10 (a) Geometry of a tapered beam and (b) (c) (d) nondimensinal buckling pressure for different boundary conditions.

A.3.2 UNDER HORIZONTAL LOADS (Cont'd)

From Figure A.10 (b), (c), (d), it can be seen that, for large ratios r/ℓ, EQ.:A.24; A.24(b); A.24(c) as well as the results obtained by Sodhi and Nevel (1980) approach the values of buckling pressure associated with infinite beams having the same boundary conditions as wedge-shaped ice sheets.

For small ratios r/ℓ, EQ.:A.24; A.24(b); A.24(c) predict values smaller than the results obtained by Sodhi and Nevel (1980). However, Sodhi and Nevel (1980)(page 142) pointed out that their "theoretical values of buckling pressure are generally higher than the experimental values."

Therefore, till systematic experiments are conducted to verify the theoretical results, we suggest the use of the very simple relations given by EQ.:A.24; A.24(b); A.24(c) to estimate the minimum buckling load of wedge-shaped ice sheets.

Comparing EQ.:A.24 and EQ.:A.22, it follows that the ice wedge with a free end will fail by buckling when:

$$\frac{\gamma \ell^3 \, (0,5 \, \theta + b/\ell)}{\sigma_2 \, B \, h} \le 1 \qquad \text{EQ.: A.26}$$

As discussed previously, when a semi-infinite plate is pressing against a structure, cracks will be formed at both ends of the contact area. The upper limiting case occurs when the two cracks are diverging, making an angle of 25,5° with the normal to the structure.

From EQ.: A.26, it can be seen that the transition from failure by crushing to failure by buckling depends on ℓ and σ_2 related to the ice characteristics, and, on b, B, θ, associated to the shape of the structure.

For the three shapes of practical interest, shown in Figure A. 11, the maximum relative values of b, B, and θ are as follows:

A.3.2 UNDER HORIZONTAL LOADS (Cont'd)

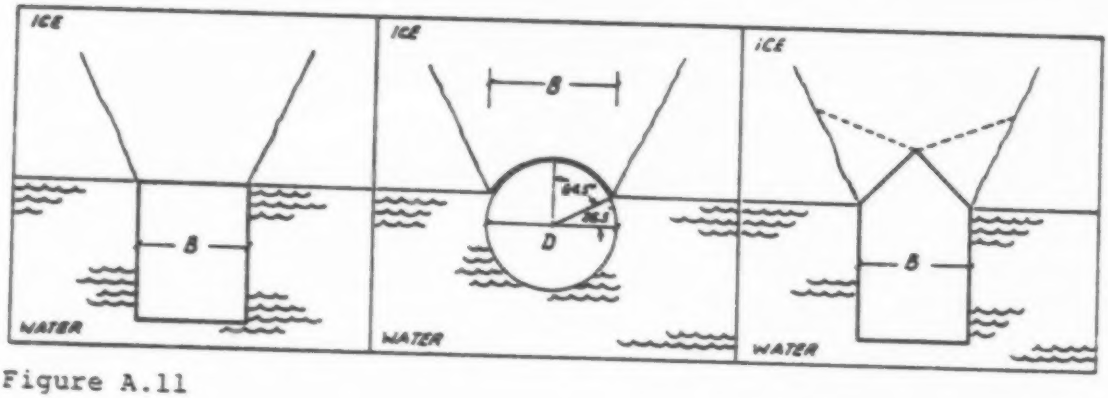

Figure A.11

a) rectangular

$b = B \qquad \theta = 0{,}9\ (\text{rad})$

b) circular (D : diameter)

$B = 0{,}9\,D \quad b = 1{,}1\,D \qquad \theta = 0{,}9\ (\text{rad})$

c) angular

$$b = \frac{B}{\sin \beta} \qquad \theta = 0{,}9\ (\text{rad})$$

From Figure A.11, it can be seen that, when a semi-infinite ice cover is pressing against an angular structure, failure by buckling will not occur. Cracks emaning from the summit (dashed line) will cause failure by splitting at a lower stress level. The largest horizontal force against a vertical angular structure is then given by EQ.: A.11.

For rectangular and circular structures, the transition predicted by EQ.: A.26 is in very good agreement with the observations made by Nevel et alt. (1972).

A.3.3 UNDER OBLIQUE LOADS

When an oblique force is applied at the edge of a semi-infinite ice plate (Figure A.12), failure may occur by crushing or splitting and by the combined effects of buckling and bending.

When failure occurs by crushing or splitting, the limiting values of the oblique load, P, are obtained from EQ.: A.11 & 22 as:

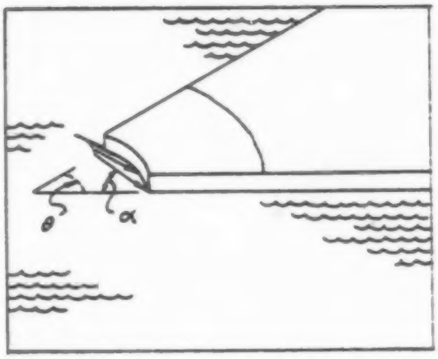

Figure A.12

$$\boxed{P_{min} = \frac{\pi}{2} \frac{\sigma_1 B h}{\cos \alpha}}$$

and EQ.: A.27

$$\boxed{P_{max} = \frac{\sigma_2 B h}{\cos \alpha}}$$ EQ.: A.28

where σ_1 and σ_2 are respectively the tensile and compressive strength of the ice; B is the width of the contact area; h is the ice thickness; α is the angle between the direction of the load and the horizontal.

When the failure occurs by the combined effect of the bending and buckling, by putting the critical moment equal to the sum of the moments due to the vertical and horizontal components of the oblique load, P, then we obtain:

$$X = H \cos \alpha \quad \text{and} \quad Y = V \sin \alpha$$ EQ.: A.29

where X and Y are respectively the horizontal and vertical components of the force P; H and V are the horizontal and vertical forces required to cause failure by buckling and bending.

A.3.3. UNDER OBLIQUE LOADS (Cont'd)

From EQ.: A.29, we obtain:

$$\frac{X^2}{H^2} + \frac{Y^2}{V^2} = 1 \qquad \text{EQ.: A.30}$$

which is the equation of an ellipse with semi-axes H and V.

The magnitude of the oblique force P required to cause failure by the combined effects of buckling and bending is then equal to:

$$P_{max} = \left[\frac{H^2_{max} \; V^2_{max}}{H^2_{max}\sin^2\alpha + V^2_{max}\cos^2\alpha} \right]^{\frac{1}{2}} \qquad \text{EQ.: A.31}$$

$$P_{min} = \left[\frac{H^2_{min} \; V^2_{min}}{H^2_{min}\sin^2\alpha + V^2_{min}\cos^2\alpha} \right]^{\frac{1}{2}} \qquad \text{EQ.: A.32}$$

where H_{min} and H_{max} are respectively given by EQ.: A.24 & 25;

V_{min} and V_{max} are respectively given by EQ.: A.18 & 19.

Nevel (1979) has presented a theoretical analysis of the bending of a wedge-shaped ice sheet under an oblique load. His results show a rather complicated relation between the stress on the top and bottom surface of the ice wedge and the material and geometrical characteristics.

Typical results for his analysis are given (Nevel 1979 page 288) for $\alpha = 26{,}5°$; $h/\ell = 0{,}1$; $b/\theta\ell = 0{,}2$ when the oblique force is applied at the neutral axis or at the top edge of the ice sheet.

A.3.3. UNDER OBLIQUE LOADS (Cont'd)

Figure A.13 shows Nevel's theoretical relation between the vertical and horizontal components of the oblique force required to induce the maximum tensile stress in the ice wedge. It seems surprising to see that, when an horizontal component equal to 0 is applied either at the neutral axis or at the top edge of the ice sheet, different vertical components are required to produce failure.

Along with Nevel's results is also plotted the relation obtained by the use of EQ.:A.31. In agreement with experimental values, (Sodhi and Nevel 1980 (page 142)), EQ.:A.31 predicts smaller values for the buckling load than Nevel's results.

Noting that the representation of the bending and buckling of a cracked ice cover by the bending and buckling of a perfect wedge is, at best, an approximation, it seems that the direct relation given by EQ.:A.31 may be used till systematic experiments are conducted to systematically assess the applicability of the theoretical results.

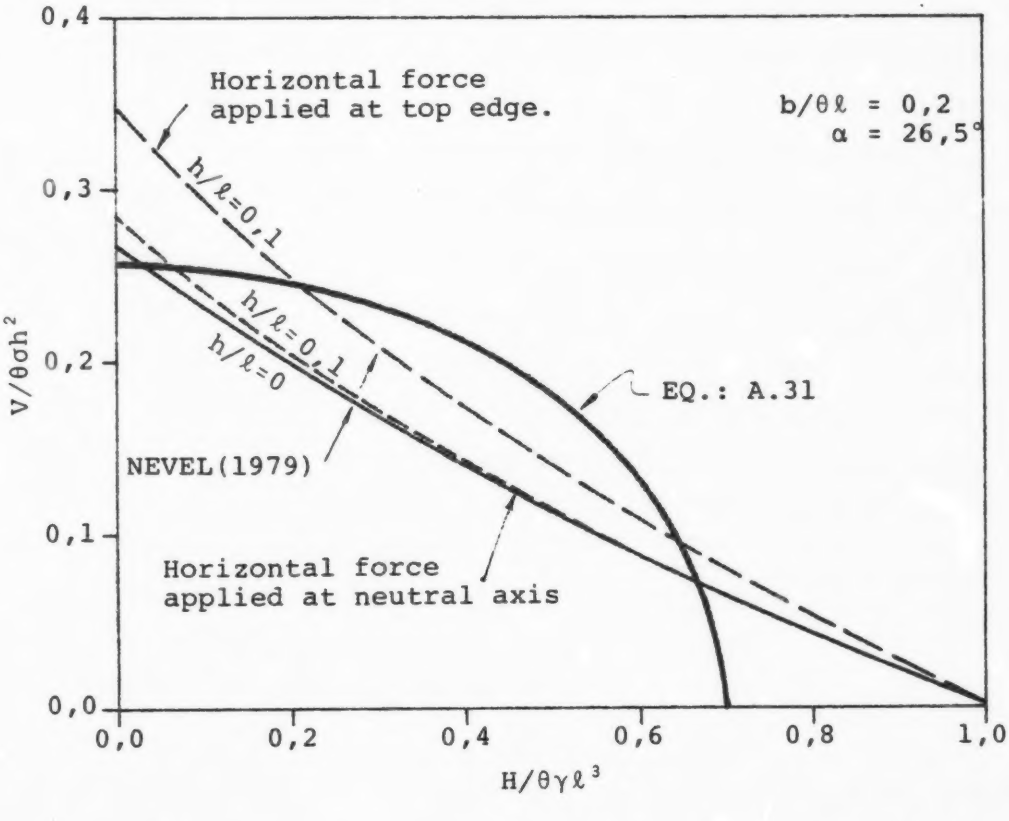

Figure A.13.: Relation between the vertical and horizontal components of an oblique force required to induce failure as obtained by Nevel (1979) and as given by EQ.:A.31, for a typical example. (Nevel 1979 page 288)

A.4 SUMMARY AND CONCLUSIONS

Our review of relevant analyses and tests has shown a marked distinction between the two situations of prime interest for engineering purposes:

a) loads applied on the ice cover;
b) loads applied at the edge of the ice cover.

A.4.1 LOADS APPLIED ON THE ICE COVER

The problem of *bearing capacity* of ice plates related to the failure of a complete wedge on an elastic foundation has been extensively studied both analytically and experimentally.

From Nevel's results the vertical loads required to cause failure may be expressed as follows: (EQ.: A.13 & 14)

$V_{min} = fn_1(\rho)\ \theta\ \sigma_1\ h^2$
$V_{max}\quad 1,5\ fn_1(\rho)\ \theta\ \sigma_1\ h^2$

where θ is the total angle (radians) formed by the wedges; σ_1 the tensile strength of ice; h the ice thickness; and, $fn_1(\rho)$ a function of a/ℓ shown in Figure A.6.

A.4.2 LOADS APPLIED AT THE EDGE OF AN ICE COVER

No exact solution was available from the litterature for the determination of *the largest force* an ice cover may exert on a structure or a ship hull. This problem is related to the failure of a truncated wedge on an elastic foundation.

Our analytical approach, in agreement with observations in the field, has shown that, depending on the ice characteristics and structure shapes, the failure of a floating truncated wedge

A.4.2 LOADS APPLIED AT THE EDGE OF AN ICE COVER(Cont'd)

formed by the cracks emaning from the loaded region may occur in the following modes:

a) by splitting or crushing;
b) by the combined effect of bending and buckling.

When failure occurs by splitting or crushing, the criteria are given by EQ. A.27 & 28:

$$\boxed{\begin{array}{l} P_{min} = \frac{\pi}{2} \frac{\sigma_1 B h}{\cos \alpha} \\ \hline P_{max} = \frac{\sigma_2 B h}{\cos \alpha} \end{array}}$$

When failure occurs by the combined effects of buckling and bending the criteria are given by EQ.: A.31 & 32:

$$\boxed{\begin{array}{l} P_{min} = \left[\frac{H^2_{min} V^2_{min}}{H^2_{min} \sin^2\alpha + V^2_{min} \cos^2 \alpha} \right]^{\frac{1}{2}} \\ \hline P_{max} = \left[\frac{H^2_{max} V^2_{max}}{H^2_{max} \sin^2\alpha + V^2_{max} \cos^2 \alpha} \right]^{\frac{1}{2}} \end{array}}$$

where σ_1 and σ_2 are respectively the tensile and compressive strength of the ice; B the width of the contact area; h the ice thickness; α the angle between the direction of application of the load and the horizontal; H_{min} and H_{max} are given by EQ.: A.24 & 25; V_{min} and V_{max} are given by EQ.: A.18 & 19.

A.4.2 LOADS APPLIED AT THE EDGE OF AN ICE COVER(Cont'd)

It is very convenient to represent graphically the failure criteria for loads applied at the edge of an ice cover by superimposing the four (4) above equations. Figure A.14(a) shows typical failure criteria for small B/ℓ, i.e. thick ice cover or narrow structures. The crushing load is then, according to EQ.: A.26, less than the buckling load. Figure A.14(b) shows typical failure criteria for large B/ℓ, i.e. thin ice cover or wide structures. The buckling load is then, according to EQ.: A.26, less than the crushing load. As shown in Figure A.14(a), the transition from failure by crushing to failure by the combined effects of bending and buckling is also a function of the angle of application of the load to the horizontal.

Although the proposed failure criteria for loads applied at the edge of an ice cover seem in good agreement with the very limited experimental results presently available, it is well recognized that systematic experiments to assess their applicability are very desirable.

A.4.2 LOADS APPLIED AT THE EDGE OF AN ICE COVER (Cont'd)

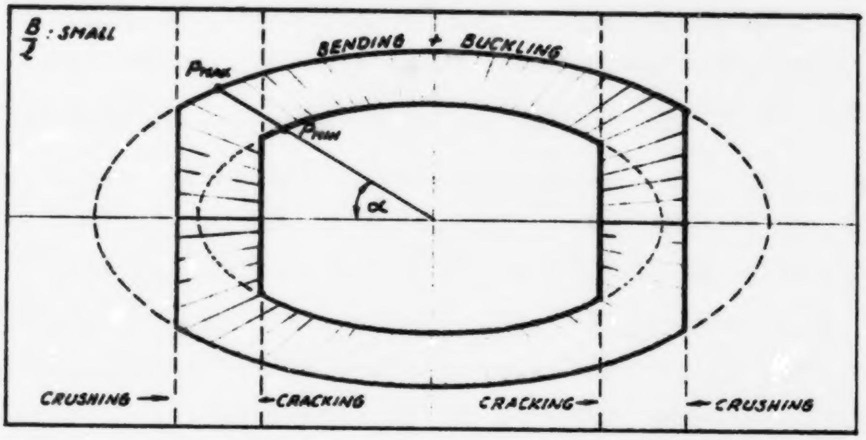
B/ℓ : SMALL
BENDING + BUCKLING
P_{MAX}
P_{MIN}
α
CRUSHING →
← CRACKING
CRACKING →
← CRUSHING

Figure A.14(a) Failure criteria for small B/ℓ.

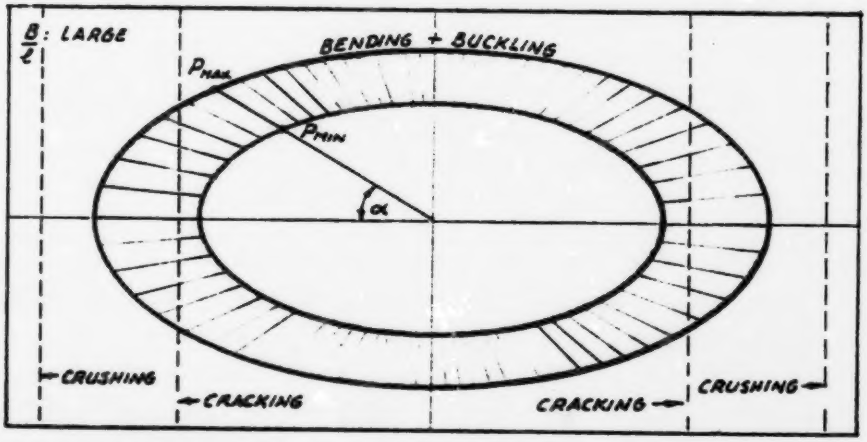
B/ℓ : LARGE
BENDING + BUCKLING
P_{MAX}
P_{MIN}
α
← CRUSHING
← CRACKING
CRACKING →
CRUSHING →

Figure A.14(b) Failure criteria for large B/ℓ.

BIBLIOGRAPHY

Bernshteyn, S., 1929 Ledyaanaya zheleznodorozhnaya pereprava (The railway ice crossing), Trudy Nauchno-Tekhnichesko-go Komiteta Narodnoge Komissariata Putei Soobshcheniya, Tom 84, p. 36-82

Carter, D., 1971 Lois et Mécanismes de l'apparente fracture fragile de la glace de rivière et de lac, Thèse de doctorat, Départ. Génie Civil, Univ. Laval, Québec, Canada

Carter, D., 1981 Ice Forces on Structures (To be published)

Hertz, H., 1884 On the equilibrium of floating elastic plates, in Miscellaneous papers by H. Hertz. London, MacMillan 1896, p. 266-72

Kerr, A. D., 1976 The bearing capacity of floating ice plates subjected to static or quasi-static loads, Journ. of Glaciology, Vol. 17, No. 76, p.229-68

Kerr, A. D., 1978 On the determination of horizontal forces a floating ice plate exerts on a structure, Journ. of Glaciology, Vol. 20, No. 82, p.123-34

Nevel, D. E. 1958 The theory of a narrow infinite wedge on an elastic foundation, Trans. of the Engineering Institute of Canada, Vol. 2, No. 3, p. 132-40.

Nevel, D. E. 1961 The narrow infinite wedge on an elastic foundation, U.S. Snow, Ice and Permafrost Research Establishment. Research Report 79.

Nevel, D. E. et alt. 1972 Ice forces on vertical piles, by D.E. Nevel, R. E. Perham and G. B. Hogue, Proceed. of the 1972 Army Science Conference, U.S. Military Academy, West Point, N.Y. Washington, D.C., Army Research Office, Vol. 3 p. 104-14.

Nevel, D. E. 1965 A semi-infinite plate on an elastic foundation, U.S. Army, CRREL Research Report 136

Nevel, D. E. 1979 Bending and Buckling of a Wedge on an Elastic Foundation, I U T A M Symposium on the Physics and Mechanics of Ice, Technical University of Denmark, Copenhagen, August 1979.

Panfilov, D. F. 1960 (Experimental investigation of the carrying capacity of a floating ice plate), Izvestiya Vsesoyuznogo Nauchno-Issledovatel'skogo Inst. Gidrotekhniki, Tom. 64, p. 101-15

Persson, B. O. E. 1948 Bestandighet och barighet hos ett istacke, Svenska Vagforeningens Tidskrift,Vol. 35, No.10, p. 406 417.

Shapiro, G. S. 1943 (Deflection of a semi-infinite plate on an elastic foundation) Prikladnaya Matematika i Mekhanika, Tom 7, No. 4, p. 316-20

Shulman, A. R. 1946 (Calculation of the load-carrying capacity of ice crossing on the basis of the theory of central flexure of an elastic plate placed on an elastic foundation) Trudy Nauchno-Issledovatel'skikh Uchrezhdenii, Ser. 5, Vyp. 20, p. 30-38

Smith, E. and Barnby, J. T. 1967 Metal Science Journ. Vol. 1, p. 56-64.

Sodhi, D. S. 1979 Buckling Analysis of wedge-shaped floating ice sheet. 5th Int. Conf. on Port and Ocean Engineering under Arctic Conditions, P O A C 79, NTH, Trondheim

Sodhi, D. S., and Nevel, D. E., 1980 A Review of Buckling Analyses of ice sheets. In working group on ice forces on Structures, A state-of-the-Art Report edited by T. Carstens, Special Report 80-26, U.S.Army C R R E L, June 1980

Stroh, A. N., 1957 Adv. Physics, Vol. 6, p. 418

- APPENDIX B -

- APL PROGRAMS -

COMPUTER PROGRAM TO DETERMINE THE FOREBODY CHARACTERISTICS

```
     ∇ ELLIP
[1]    RAD←○(÷180)
[2]    PAO← 0 0
[3]    PBO← 0 0
[4]    GL←L,L+(2÷(3○(BETA×RAD)))
[5]    GB←B,B+(2×(3○(GAMMA×RAD)))
[6]    M←3○(TETA×RAD)
[7]    I←1
[8]   S10:PBO[I]←(GB[I]×((M×GL[I])-GB[I]))÷(2×((M×GL[I])-(2×GB[I])))
[9]    PAO[I]←(((GL[I]÷2)*2)÷(1-(((PBO[I]-(GB[I]÷2))÷PBO[I])*2)))*0.5
[10]   →(2≥I←I+1)/S10
[11]   X←0,(L÷(NDIV×2))×⍳NDIV
[12]   PHI1←¯2○(X÷PAO[1])
[13]   PHI2←¯2○(X+PAO[2])
[14]   PHI←¯2○(GL[2]÷PAO[2]×2)
[15]   Y←PBO[2]×(1○PHI)
[16]   Y1←PBO[1]×(1○PHI1)
[17]   Y2←PBO[2]×(1○PHI2)
[18]   Y2←Y2-Y
[19]   Y1←Y1-Y1[⍴X]
[20]   PHI3←¯1○((Y1+Y)÷PBO[2])
[21]   GAMM←(¯3○(Y2-Y1))
[22]   X2←PAO[2]×(2○PHI3)
[23]   BET←(¯3○(X2-X))
[24]   R←(¯3○((PAO[1]÷PBO[1])×(3○PHI1)))
[25]   S←¯3○(((3○GAMM)×(1○R))+((3○BET)×(2○R)))
[26]   T←¯2○((2○R)×(2○S))
[27]   MAT←(8,(⍴X))⍴X,Y1,(GAMM÷RAD),(BET÷RAD),(PHI1÷RAD),(R÷RAD),(S÷RAD),(T÷RAD)
[28]   ' '
[29]   '    X          Y             FLARE       BETA        PHI          R          S           T'
[30]   ' '
[31]   ⍉MAT
     ∇
```

EXAMPLE

```
B←24.4        ( maximum beam)
L←106.2       ( distance from stem back to maximum beam section × 2)
TETA←36       ( bow opening angle)
BETA←32       ( stem angle)
GAMMA←6.5     ( flare angle at midship)
NDIV←10       ( number of divisions)

ELLIP

 X        Y         FLARE      BETA      PHI       R        S        T

 0       12.2        6.5       80.8      90        90        6.5     90
  5.31   12.11       6.792     71.15     84.91     88.07    12.29    88.11
10.62    11.84       7.677     62.45     79.79     86.09    14.85    86.22
15.93    11.38       9.185     57.35     74.57     84.03    17.91    84.32
21.24    10.72      11.37      55.1      69.23     81.82    21.95    82.42
26.55     9.848     14.31      54.56     63.68     79.38    27       80.55
31.86     8.722     18.11      54.95     57.86     76.61    32.96    78.79
37.17     7.3       22.95      55.78     51.64     73.3     39.63    77.21
42.48     5.502     29.06      56.74     44.82     69.13    46.74    75.87
47.79     3.183     36.87      57.59     37.06     63.35    54.01    74.72
53.1      0         47.38      58        27.55     54       61.21    73.56
```

COMPUTER PROGRAM TO EVALUATE THE SHIP RESISTANCE TO CONTINUOUS MOTION IN LEVEL ICE

```
     ∇ ICE
[1]    RAD←○(÷180)
[2]    YOUNG←5000×TENS
[3]    LG←0.3117×((YOUNG×(THICK*3))*0.25)
[4]    LSB←L÷B
[5]    TET←TETA×RAD
[6]    BET←BETA×RAD
[7]    GAMM←GAMMA×RAD
[8]    R1←0.55×TENS×(THICK*2)×((○0.5)-TET)
[9]    R1←R1×(((1○TET)×(1○BET))+FRICT×2○BET)
[10]   R1←R1÷(((1○TET)×(2○BET))-FRICT×1○BET)
[11]   R2←(3○BET)+FRICT×((LSB×2×(÷(1+2×2○BET)))+(1.732×3○BET))
[12]   R2←R2÷(((1○TET)+(2○TET))×(1+2×1○GAMM))
[13]   R2←R2×0.75×TENS×(THICK*2)×(B÷LG)×(1+2×2○BET)
[14]   RIS←R1+R2
[15]   RI←RIS×(1+(0.4×(VEL*2)×(LG*2)÷(TENS×(THICK*2))))*0.5
[16]   SIGMAO←INTPRES×(1○ALPHA×RAD)*2
[17]   RI←RI×(TENS+SIGMAO)÷TENS
[18]   RI←RI+(FRICT×SIGMAO×THICK×((2×SL)-L))
[19]   RI←RI+(900×SNOW)
[20]   RI←RI+(C1×VEL)+(C2×VEL*2)
[21]   MAT←(2,(⍴VEL))⍴VEL,RI
[22]   ' '
[23]   'VELOCITY  RESISTANCE'
[24]   ⍉MAT
     ∇
```

EXAMPLE

```
B←24.4                ( maximum beam)
L←106.2               ( distance from stem back to maximum beam section × 2)
TETA←36               ( bow opening angle)
BETA←32               ( stem angle)
GAMMA←6.5             ( flare angle at midship)
SL←111.7              ( Ship total Length)
THICK←1               ( ice cover THICKness)
TENS←556              ( ice TENSile strength)
FRICT←0.2             ( FRICTion coefficient)
INTPRES←100           ( INTernal PRESsure in the ice field)
ALPHA←45              ( angle between the directions of ship motion and ice compression)
SNOW←0.25             ( SNOW cover thickness)
C1←2.94               ( Coefficient to evaluate the open water resistance)
C2←6.43               ( Coefficient to evaluate the open water resistance)
VEL←0 1 2 3 4 5 6     ( ship VELocity m/s)

    ICE

VELOCITY  RESISTANCE
    0         3821
    1         3968
    2         4364
    3         4934
    4         5615
    5         6368
    6         7172
```

- APPENDIX C -

LOAD DISTRIBUTION CORRESPONDING TO THE LARGEST ICE RESISTANCE TO SHIP MOTION

It should be noted that higher ice impact pressures may be experienced locally at any point of the ship's forebody when local crushing occurs.

The critical load distribution is estimated by the use of EQ.: 3.9 and EQ.: 3.8 for ice thicknes = 1 m and flexural strength = 500 kPa. For other values of h and σ, multiply the pressure given in the following graphs by $\approx h^{1.25}$ and $\sigma/500$. The largest force that an ice cover may exert on a ship hull is the crushing load.

To take into account the effect of the ship's velocity, the pressure given in the following graphs should be multiplied by the appropriate factor taken from Figure 3.9.

SHIP'S NAME :

CCGS LOUIS S. ST.LAURENT

RELEVANT SHIP'S CHARACTERISTICS:

Beam.................: $B = 24,4$ m
Forebody length × 2...: $L = 106,2$ m
Bow opening angle....: $\theta = 36°$
Stem angle...........: $\beta = 32°$
Flare angle..........: $\gamma = 6,5°$

ENVIRONMENTAL CONDITIONS:

Ice thickness........: $h = 1$ m
Flexural strength....: $\sigma = 500$ kPa
Friction factor......: $f = 0,2$

The three following graphs show respectively:

a.: the normal force per unit length;
b.: the tangential force per unit length;
c.: the axial component per unit length.

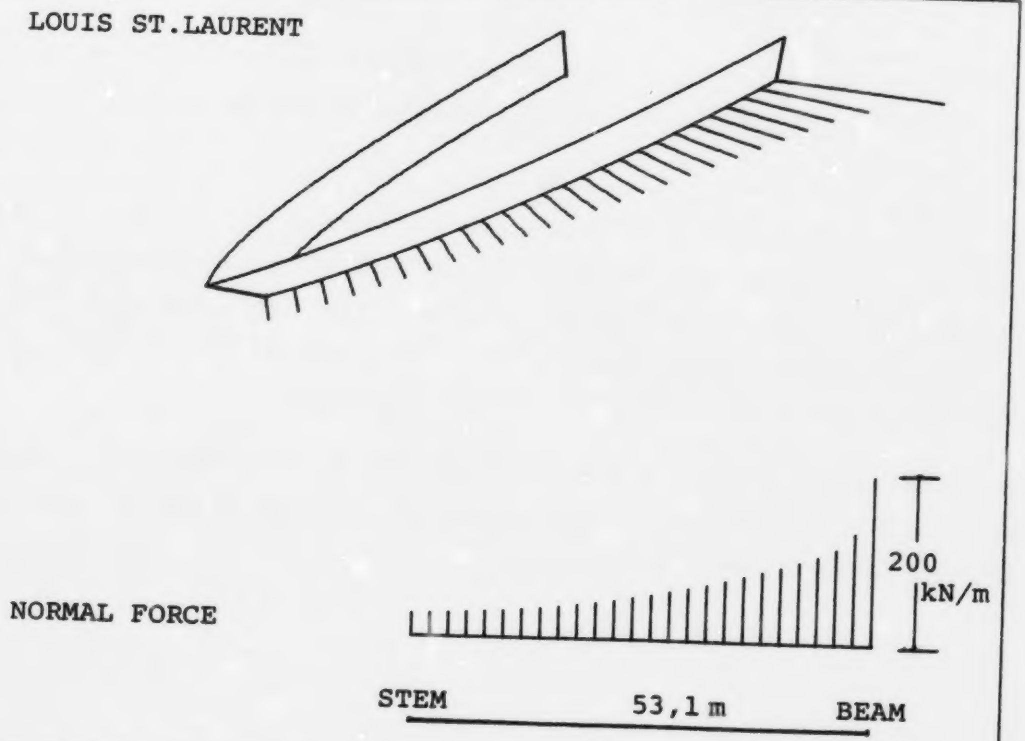
LOUIS ST.LAURENT
NORMAL FORCE
200 kN/m
STEM
53,1 m
BEAM

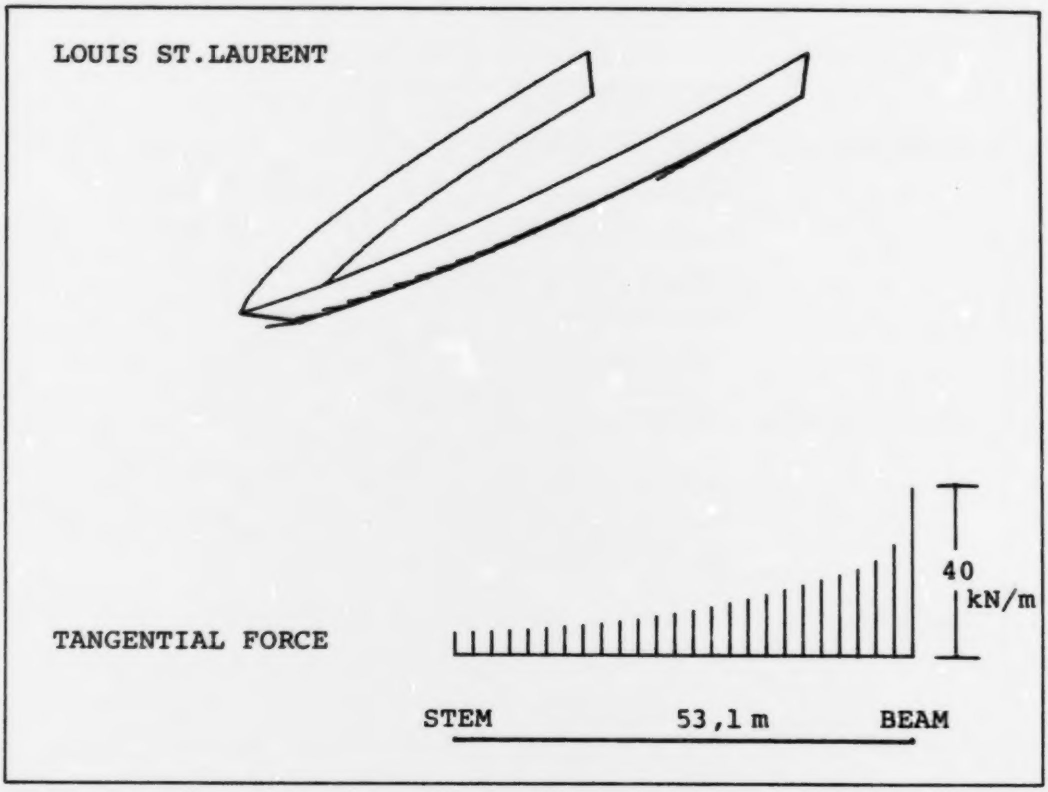
LOUIS ST.LAURENT
TANGENTIAL FORCE
40
kN/m
STEM
53,1 m
BEAM

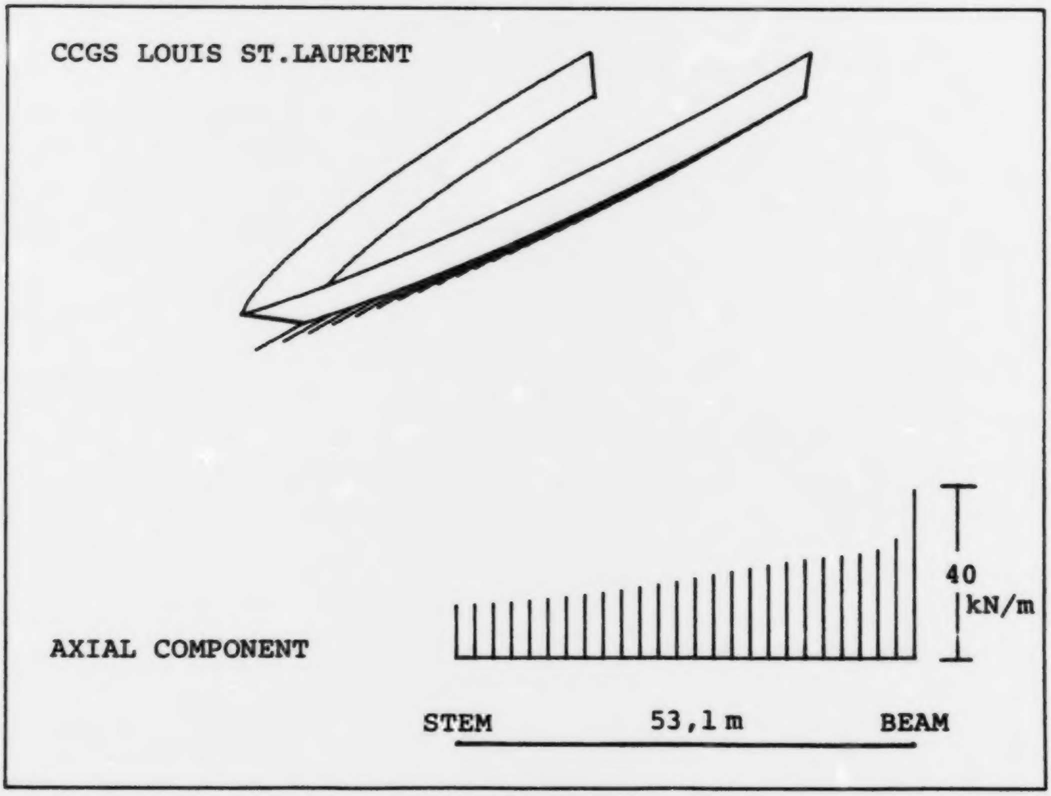
CCGS LOUIS ST.LAURENT
AXIAL COMPONENT
40
kN/m
STEM
53,1 m
BEAM

SHIP'S NAME :

CCGS PIERRE RADISSON

RELEVANT SHIP'S CHARACTERISTICS :

Beam..................: $B = 19,2$ m
Forebody length × 2....: $L = 68,9$ m
Bow opening angle.....: $\theta = 44,5°$
Stem angle............: $\beta = 18°$
Flare angle...........: $\gamma = 5,5°$

ENVIRONMENTAL CONDITIONS

Ice thickness.........: $h = 1$ m
Flexural strength.....: $\sigma = 500$ kPa
Friction factor.......: $f = 0,2$

The three following graphs show respectively:

a.: the normal force per unit length;
b.: the tangential force per unit length;
c.: the axial component per unit length.

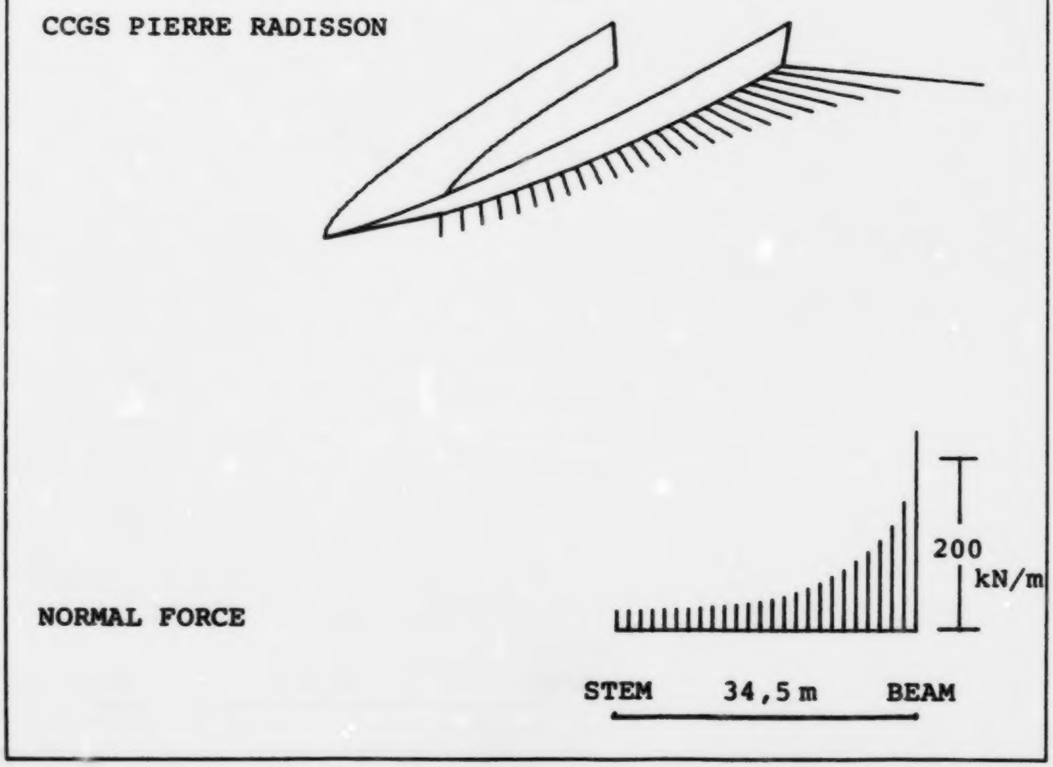

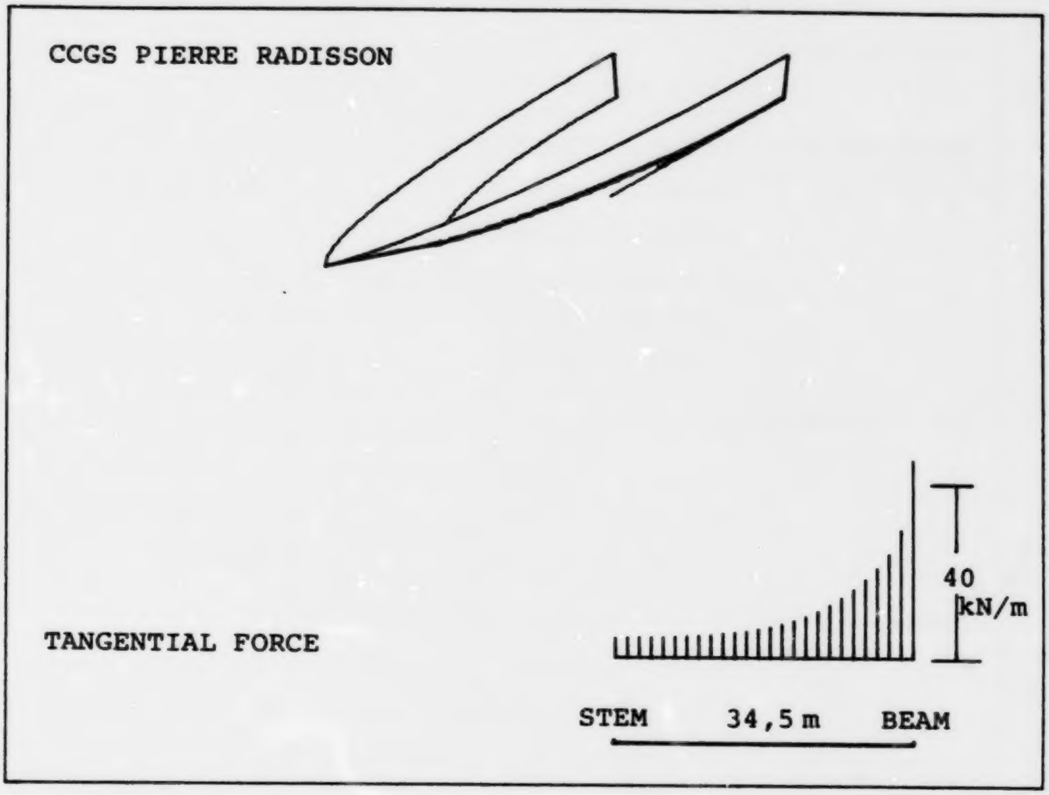
CCGS PIERRE RADISSON
TANGENTIAL FORCE
40
kN/m
STEM
34,5 m
BEAM

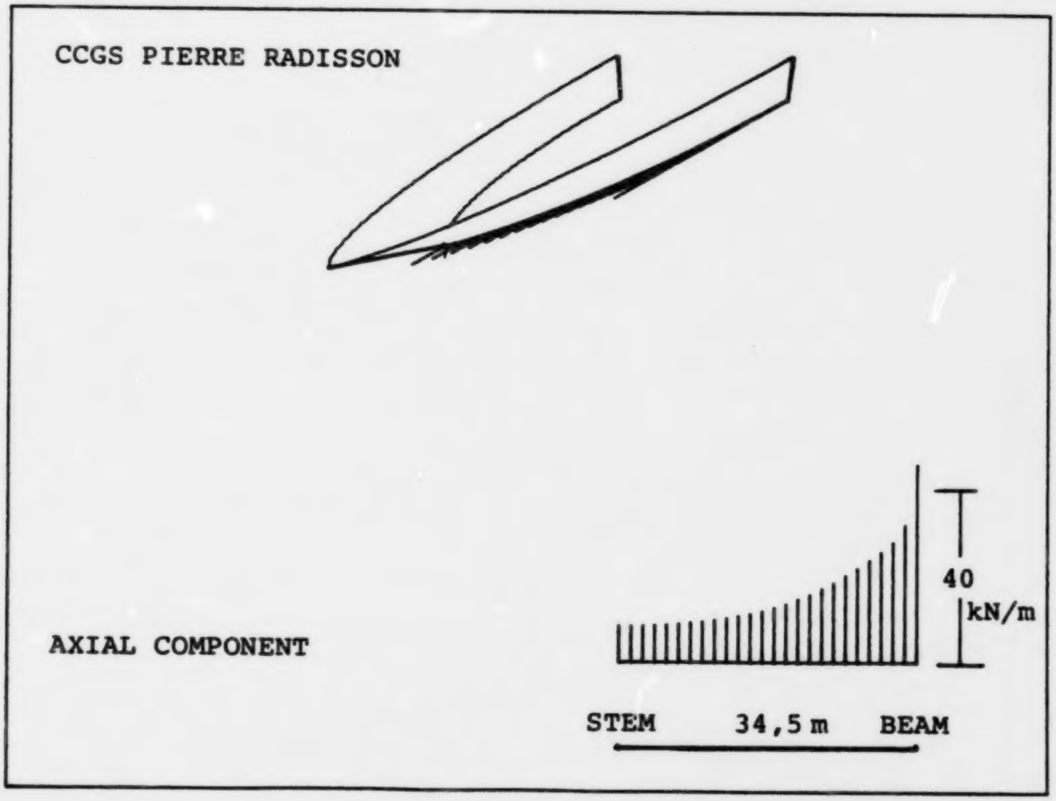
CCGS PIERRE RADISSON
AXIAL COMPONENT
40
kN/m
STEM
34,5 m
BEAM

SHIP'S NAME :

CCGS WOLFE (Converted Hull)

RELEVANT SHIP'S CHARACTERISTICS :

Beam..................: $B = 14{,}6$ m
Forebody length × 2....: $L = 67{,}1$ m
Bow opening angle.....: $\theta = 31°$
Stem angle............: $\beta = 16°$
Flare angle...........: $\gamma = 0°$

ENVIRONMENTAL CONDITIONS :

Ice thickness.........: $h = 1$ m
Flexural strength.....: $\sigma = 500$ kPa
Friction factor.......: $f = 0{,}2$

The three foolowing graphs show respectively:

a.: the normal force per unit length;
b.: the tangential force per unit length;
c.: the axial component per unit length.

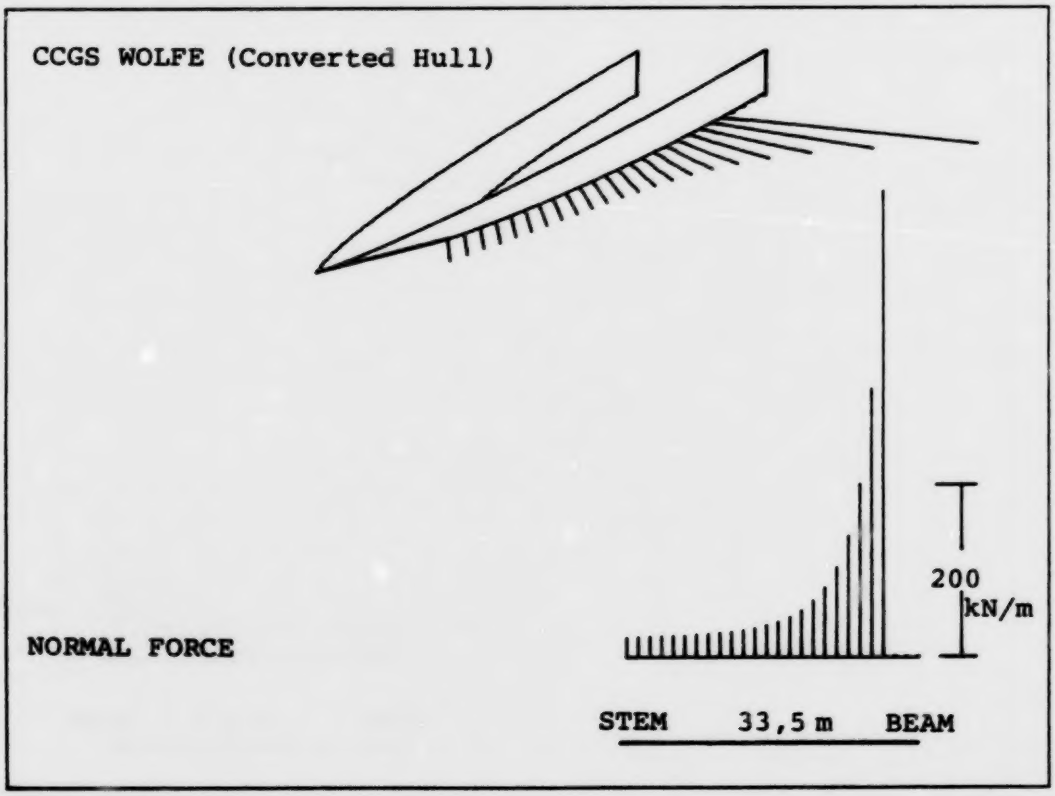

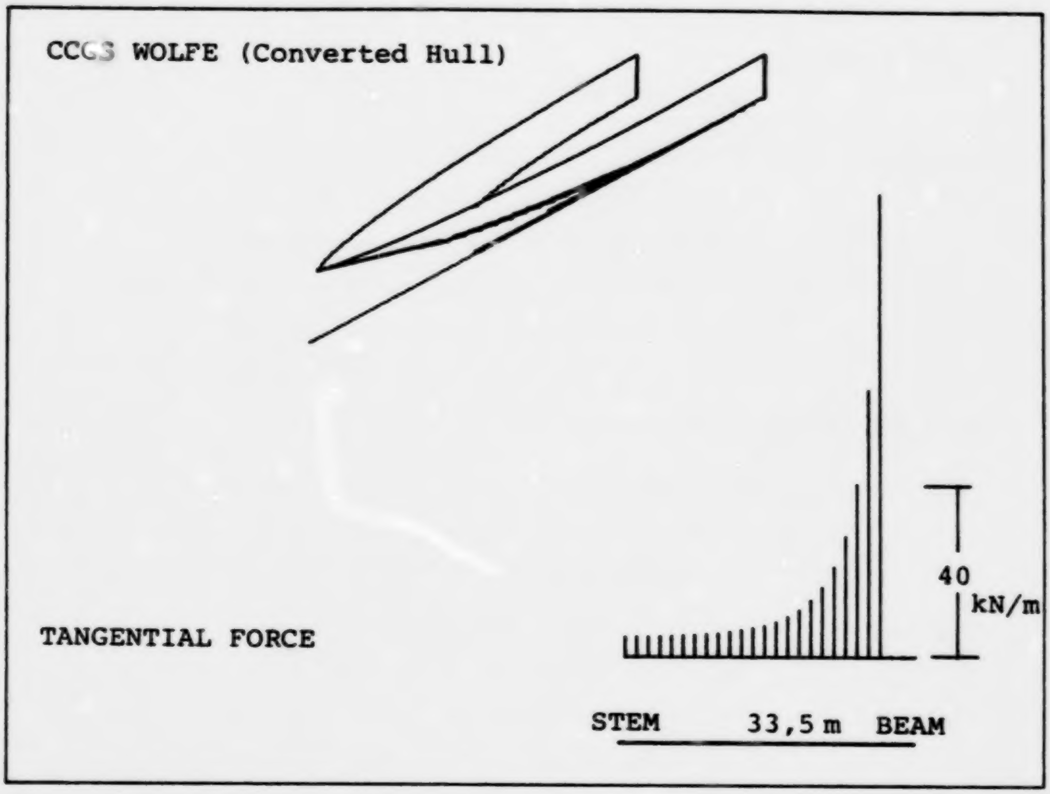
CCGS WOLFE (Converted Hull)
40
kN/m
TANGENTIAL FORCE
STEM
33,5 m
BEAM

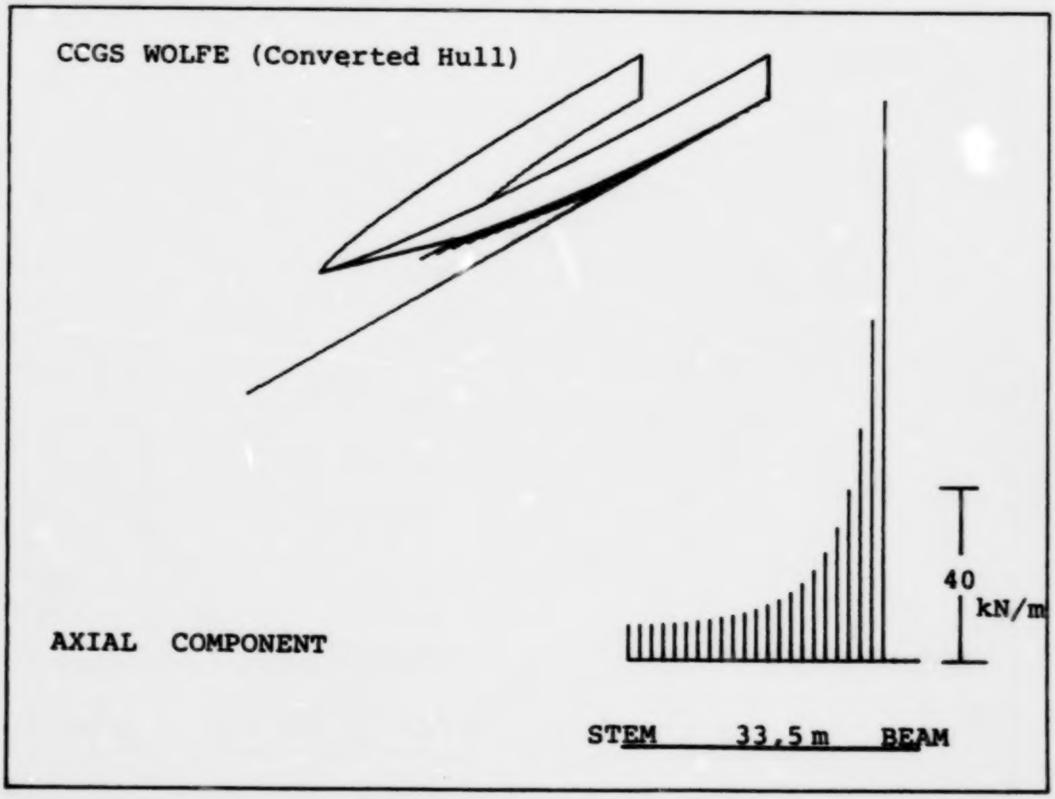
CCGS WOLFE (Converted Hull)
40
kN/m
AXIAL COMPONENT
STEM
33,5 m
BEAM

SHIP'S NAME :

M.V. ARCTIC

RELEVANT SHIP'S CHARACTERISTICS :

Beam..................: $B = 22{,}9$ m
Forebody length × 2....: $L = 76{,}3$ m
Bow opening angle.....: $\theta = 32{,}8°$
Stem angle............: $\beta = 30°$
Flare angle...........: $\gamma = 0°$

ENVIRONMENTAL CONDITIONS :

Ice thickness.........: $h = 1$ m
Flexural strength.....: $\sigma = 500$ kPa
Friction factor.......: $f = 0{,}2$

The three following graphs show respectively:

a.: the normal force per unit length;
b.: the tangential force per unit length;
c.: the axial component per unit length.

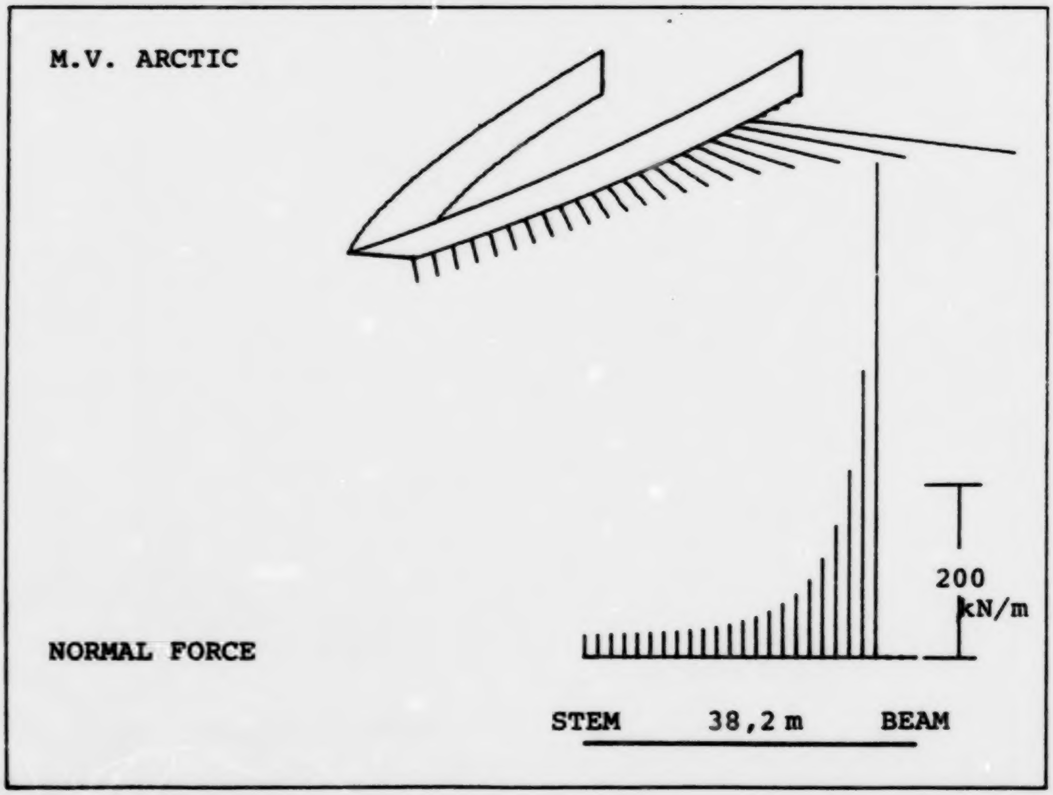

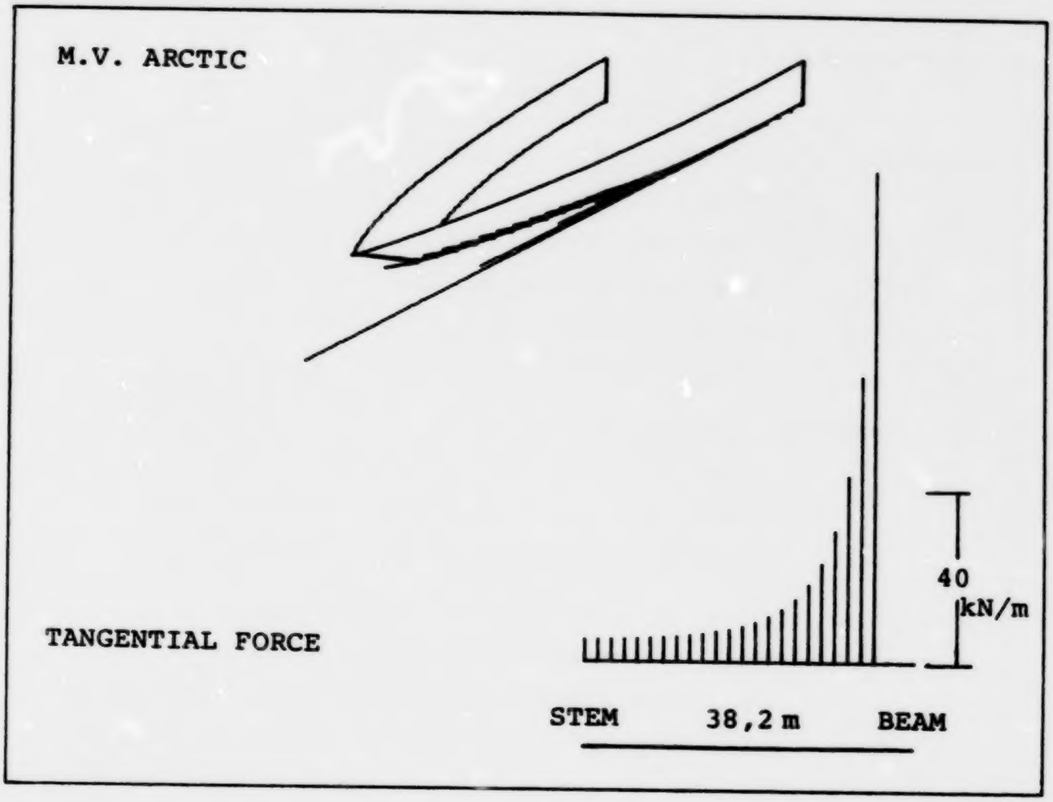
M.V. ARCTIC
TANGENTIAL FORCE
40
kN/m
STEM
38,2 m
BEAM

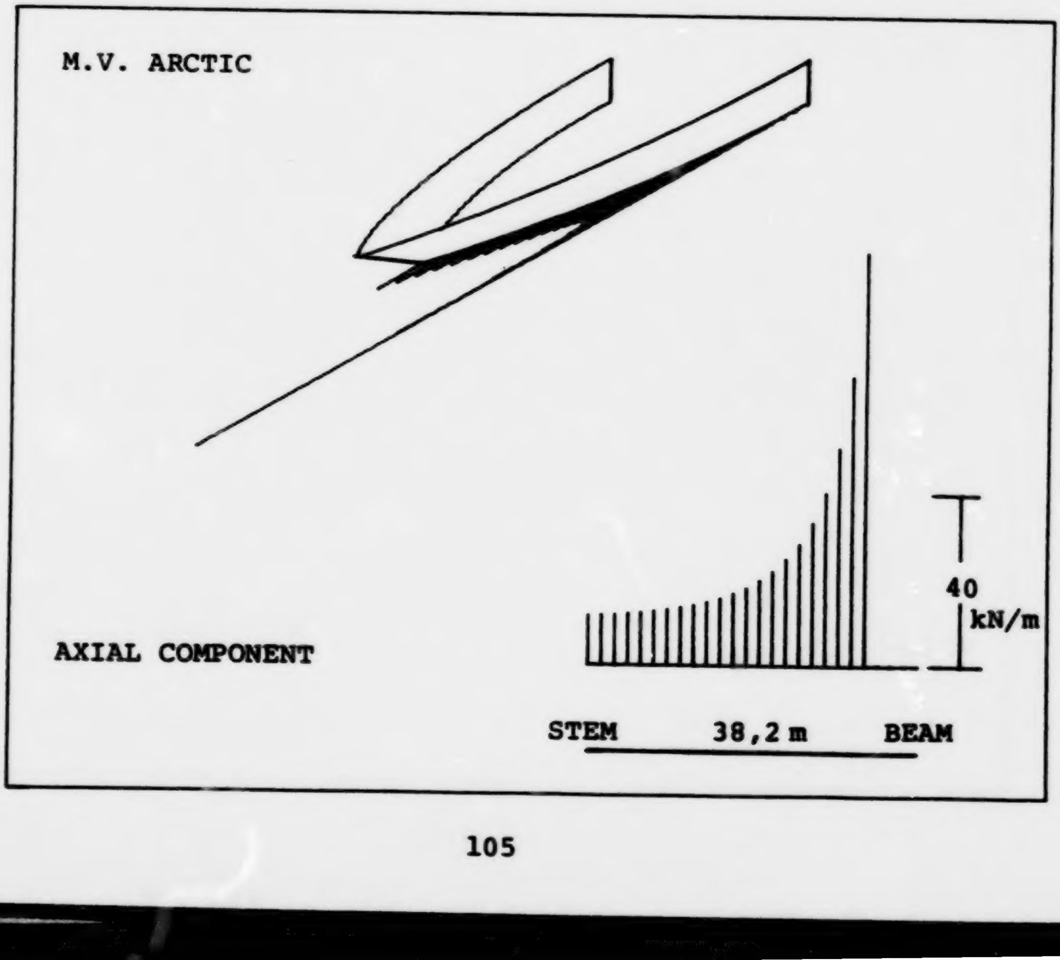
M.V. ARCTIC
AXIAL COMPONENT
40
kN/m
STEM
38,2 m
BEAM

SHIP'S NAME :

CCGS ALEXANDER HENRY

RELEVANT SHIP'S CHARACTERISTICS :

Beam....................: $B = 13{,}3$ m
Forebody length × 2.....: $L = 46{,}3$ m
Bow opening angle......: $\theta = 31°$
Stem angle.............: $\beta = 42°$
Flare angle............: $\gamma = 0°$

ENVIRONMENTAL CONDITIONS :

Ice thickness..........: $h = 1$ m
Flexural strength......: $\sigma = 500$ kPa
Friction factor........: $f = 0{,}2$

The three following graphs show respectively:

a.: the normal force per unit length;
b.: the tangential force per unit length;
c.: the axial component per unit length.

CCGS ALEXANDER HENRY

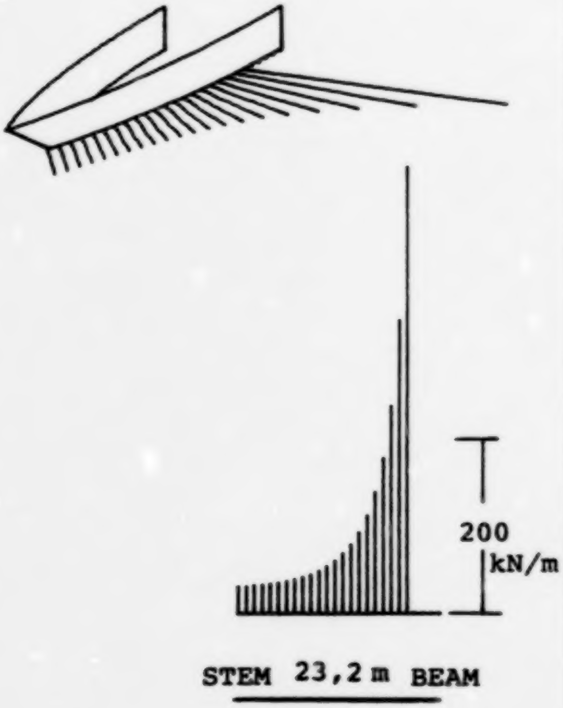

NORMAL FORCE

STEM 23,2 m BEAM

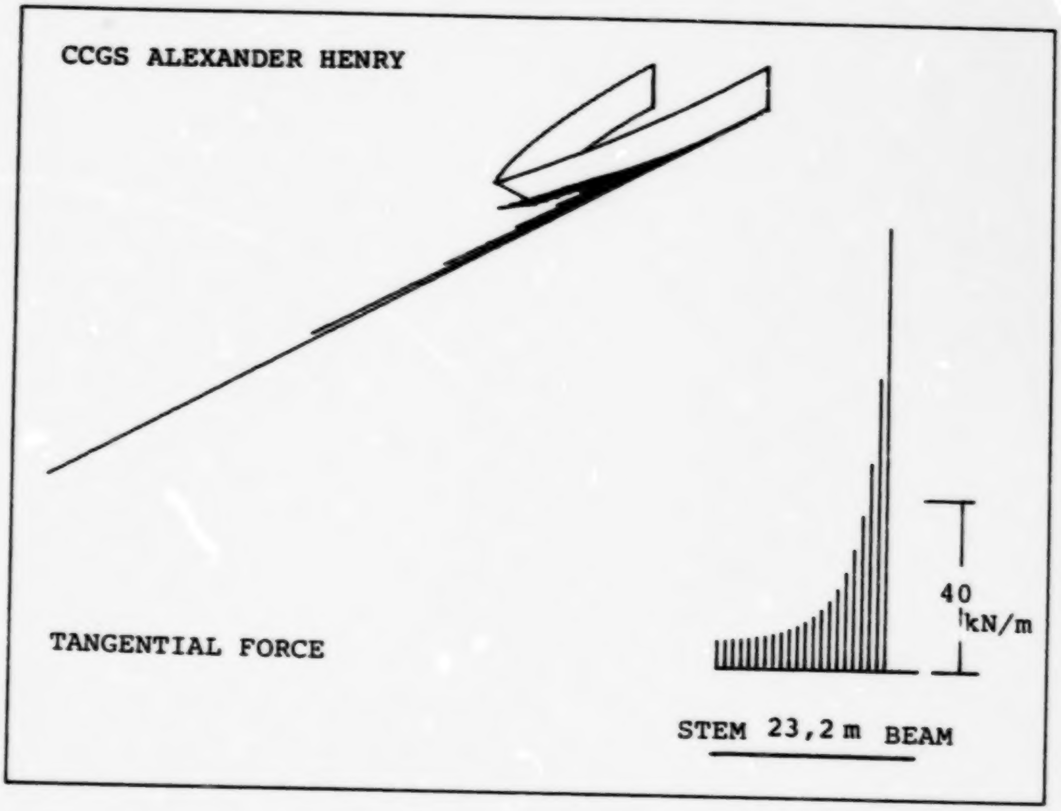

CCGS ALEXANDER HENRY
TANGENTIAL FORCE
40
kN/m
STEM 23,2 m BEAM

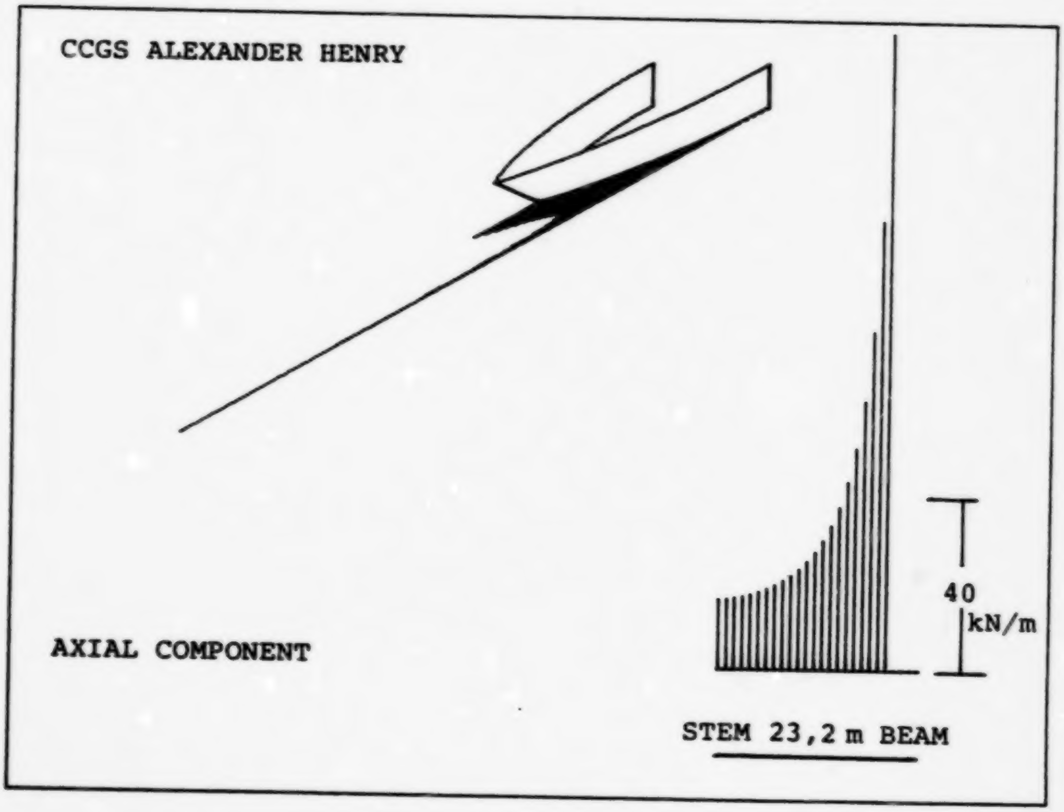

CCGS ALEXANDER HENRY
AXIAL COMPONENT
40
kN/m
STEM 23,2 m BEAM

- APPENDIX D -

FURTHER COMPARISONS WITH DATA FROM FULL-SCALE TRIALS

In this appendix, it is intended to further examine the prediction ability of EQ.: 4.1. When the present report was ready for publication, a study which assembles and documents thoroughly data from full scale trials on twelve (12) international icebreakers became available to us:

Lewis,J.W., Bulat,V., Glen,I.F. and Kotras,T., 1982 "Development of a Semi-Empirical Model for Predicting Resistance and Determining Thrust Requirements For Ships in Level Ice" Report prepared for Transport-Canada, Transportation Development Centre and U S MARAD by ARCTEC CANADA Ltd and ARCTEC Inc., July 31, 1982, 112 pages, 5 appendixes.

Among the twelve full-scale data sets reported in the above study, six (6) have already been considered in Chapter 5. We were asked by the Scientific Authority to compare for the six remaining ships the measured values with the predictions obtained by the use of EQ.: 4.1. Main particulars of these ships are provided in Table D.1.

To obtain an overall assessment of the predictions, the predicted resistance was plotted against the observed in Figures D.1, 3, 5, 7, 9, and 11. Very good overall agreement between full scale and math model data is evident.

The influence of speed and ice thickness on the resistance predictions is shown in Figures D.2, 4, 6, 8, 10 and 12.

TABLE D.1	MANHATTAN	M.V. ARCTIC	KATMAI BAY	ALEXANDER HENRY	FINNCARRIER	JELPPARI
SHIP PARAMETERS						
Beam B(m):B	44,78	22,86	10,40	13,26	23,66	5,08
Forebody length×2 L*(m):L	108,75	76,34	39,62	46,32	130,00	15,00
Ship length L (m):SL	274,38	196,60	42,70	57,91	130,00	15,00
Displacement (m^3):DISPL	152861	37302	660	3196	9848	64
Bow opening angle θ(°):TETA	29,0	32,8	27,5	31,0	17,0	32,0
Stem angle β(°):BETA	15,0	30,0	27,5	42,0	19,0	26,0
Flare angle γ(°):GAMMA	15,0	0,0	19,0	0,0	8,0	19,0
Coefficient μ_0:MU0	1,77	1,65	1,82	2,06	1,36	1,46
Coefficient η_2:ETA2	2,08	2,62	2,44	2,34	4,38	2,27
ENVIRONMENTAL CONDITIONS	PROPRIETARY DATA !					
Ice thickness h(m):THICK		0,34 0,45 0,50	0,28 0,39 0,68	0,23 0,26 0,28	- 0,59 -	0,15 0,17 0,25
Snow thickness h_s(m):SNOW		0,02 0,03 0,04	- 0,00 -	- 0,00 -	- 0,00 -	- 0,00 -
Flexural strength σ(kPa):TENS		- 380 -	580 660 750	- 520 -	- 400 -	560 600 610
Friction coefficient f:FRICT		0,2	0,015	0,1	0,050 0,075 0,100	0,050 0,075 0,100
Ship velocity V(m/s):VEL		0,97 2,33 4,24	0,49 2,95 5,42	0,82 1,28 1,83	0,93 2,03 2,80	0,65 1,32 2,61

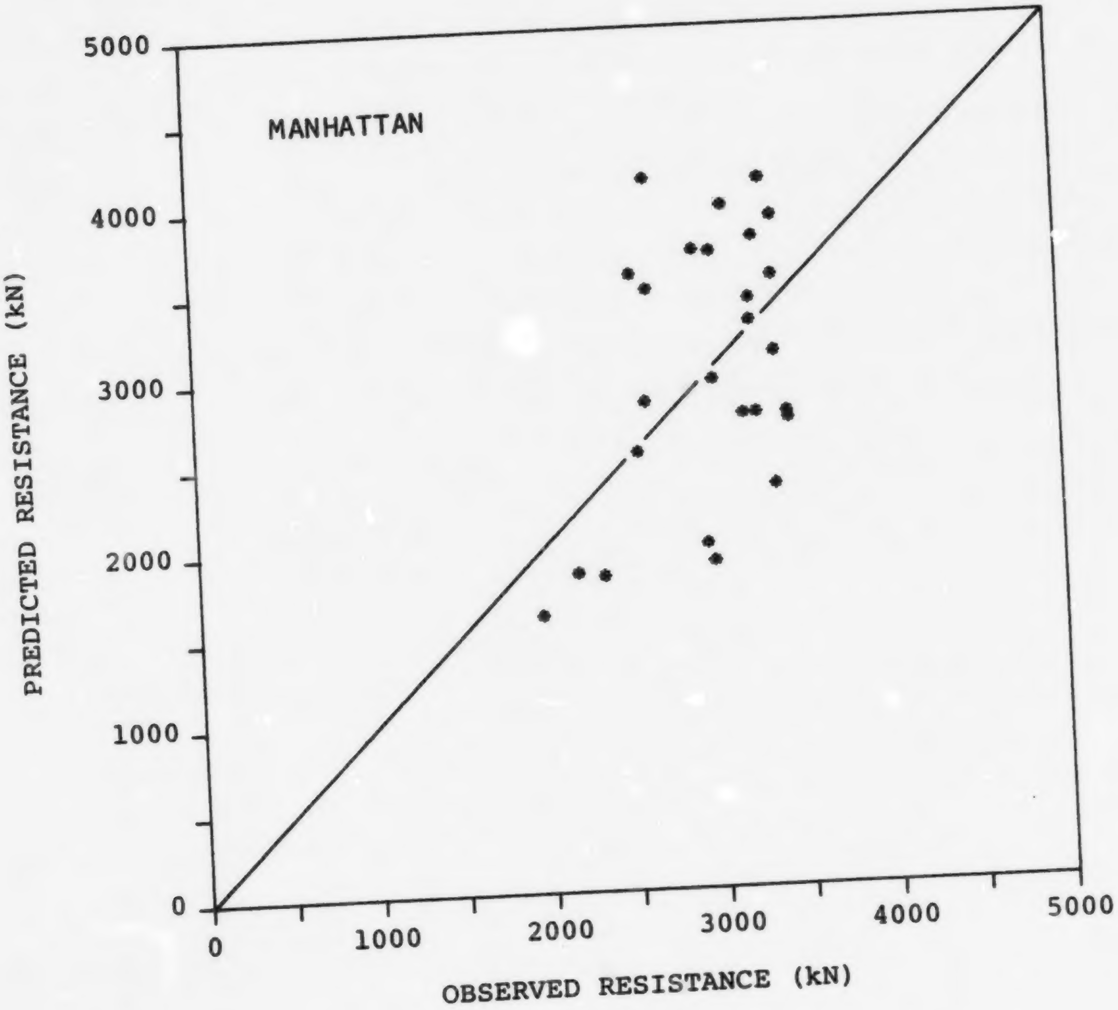

Figure D.1.: Plot of predicted versus observed resistance. Predicted resistance obtained by using EQ.: 4.1.

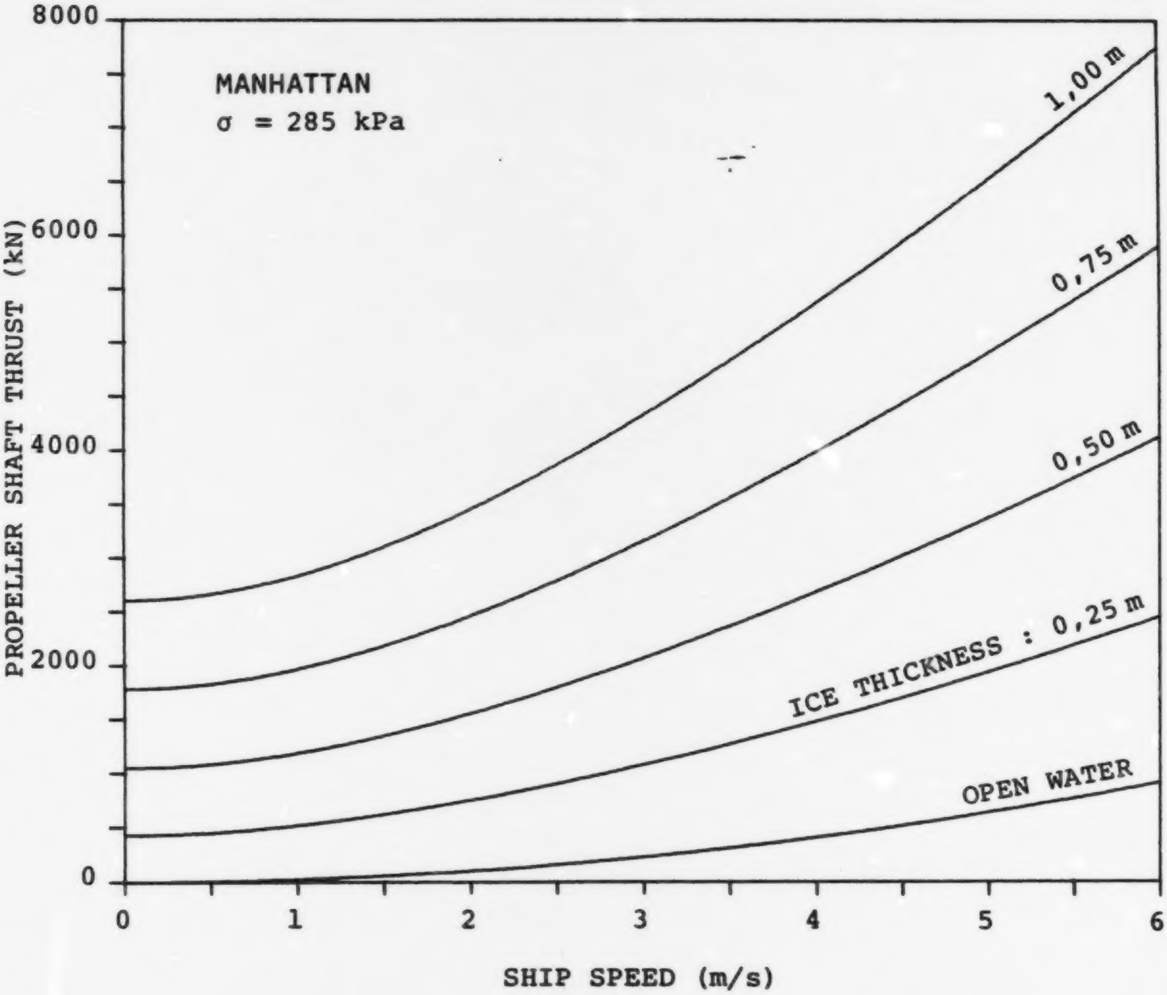

Figure D.2.: Plot of predicted thrust required to overcome level ice resistance versus ship speed. Predicted thrust obtained by using EQ.: 4.1.

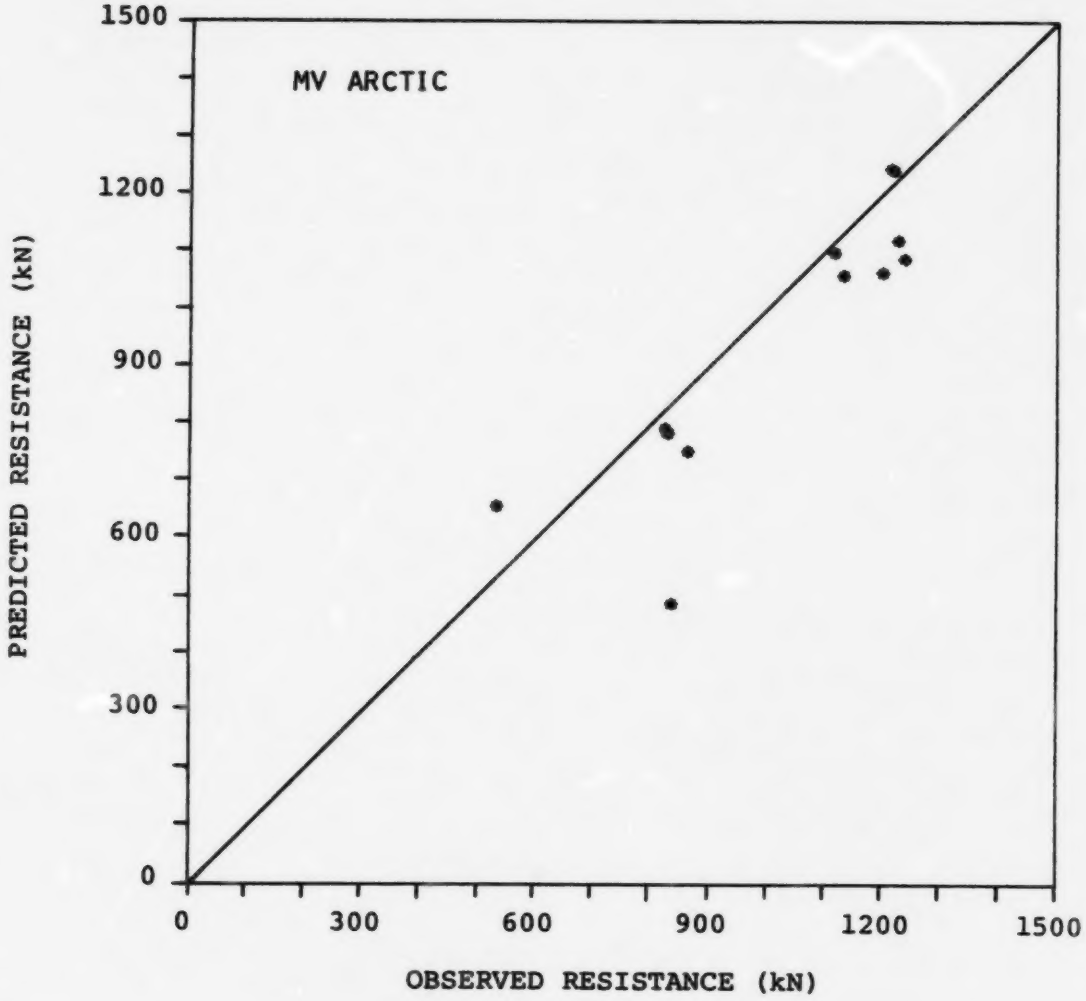

Figure D.3.: Plot of predicted versus observed resistance. Predicted resistance obtained by using EQ.: 4.1.

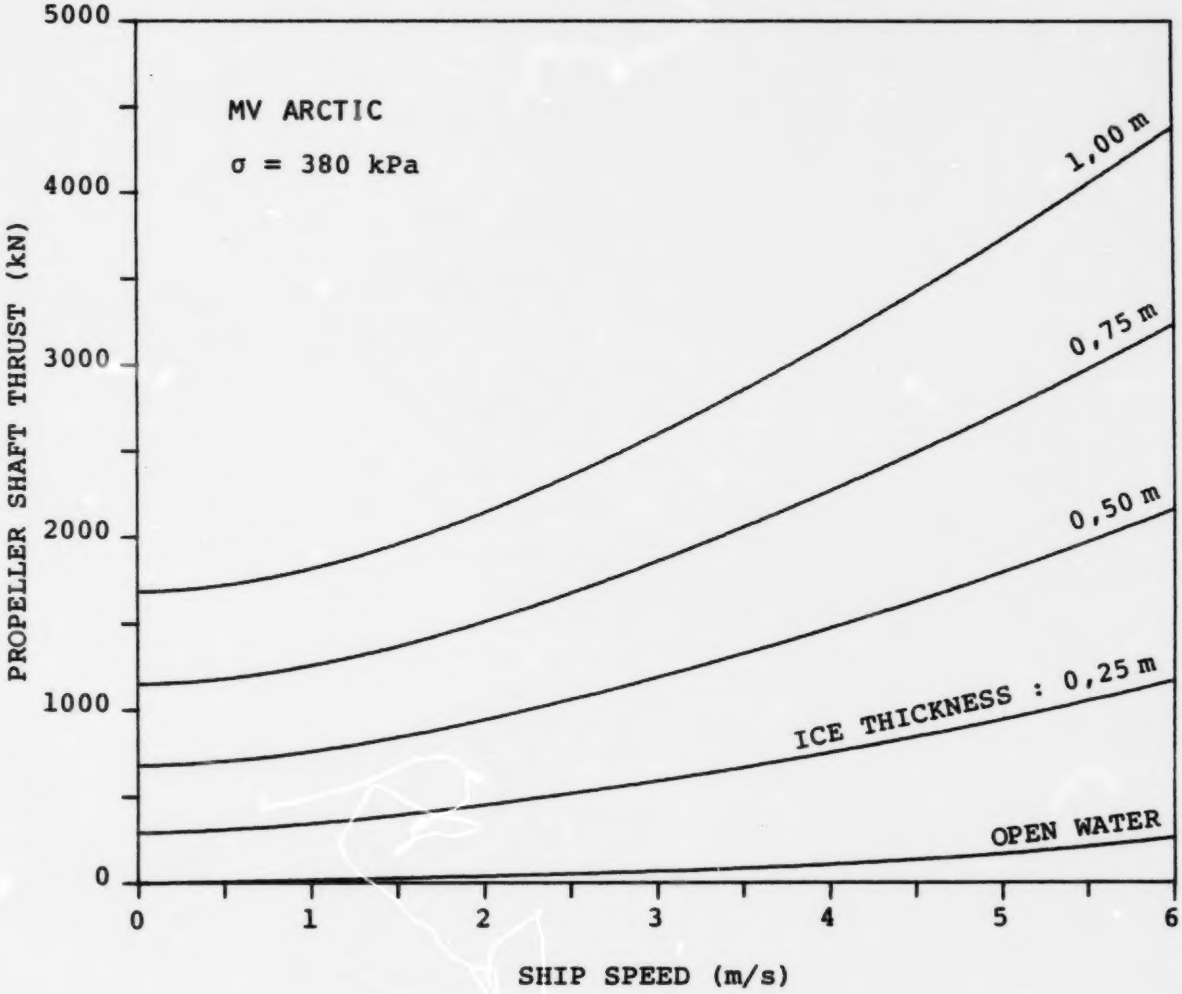

Figure D.4.: Plot of predicted thrust required to overcome level ice resistance versus ship speed. Predicted thrust obtained by using EQ.: 4.1.

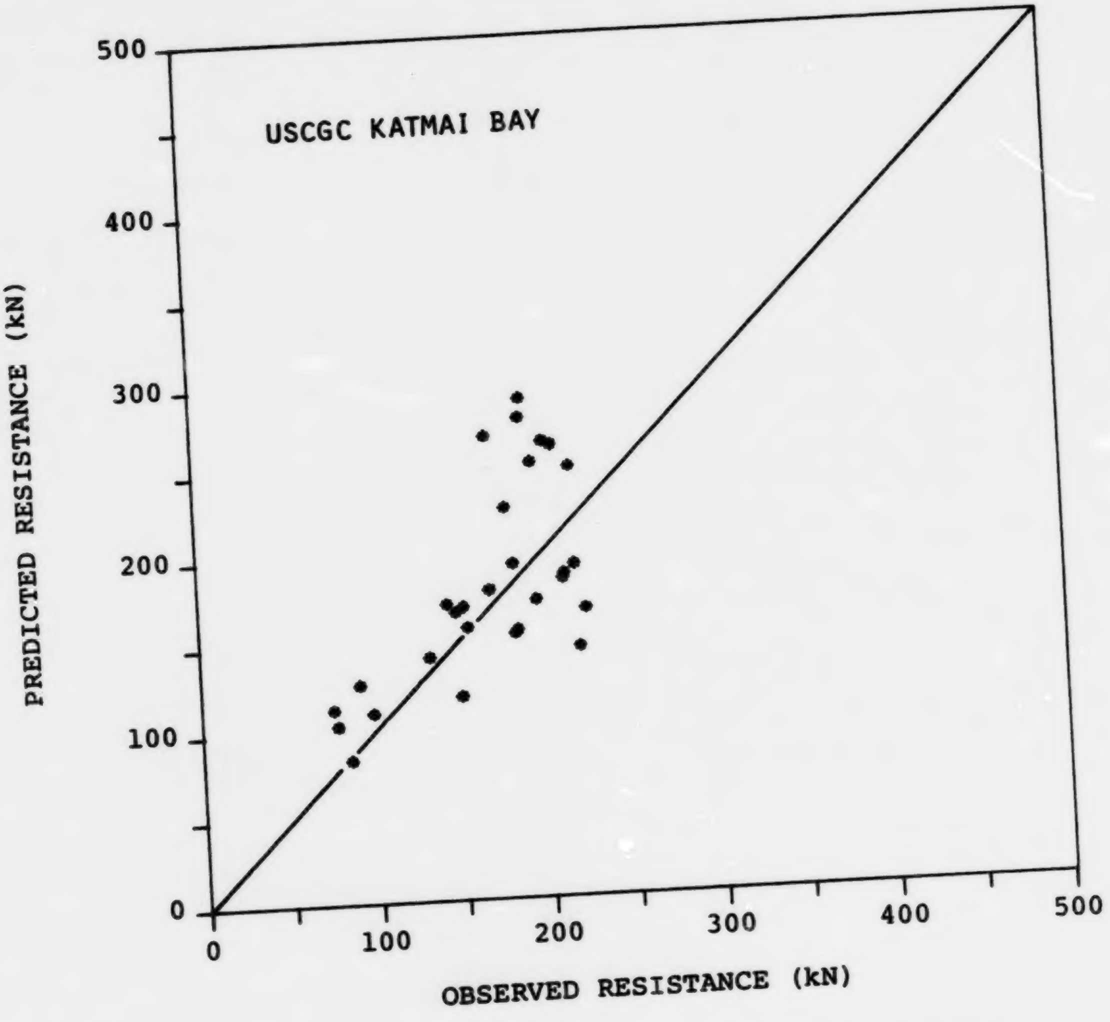

Figure D.5.: Plot of predicted versus observed resistance. Predicted resistance obtained by using EQ.: 4.1.

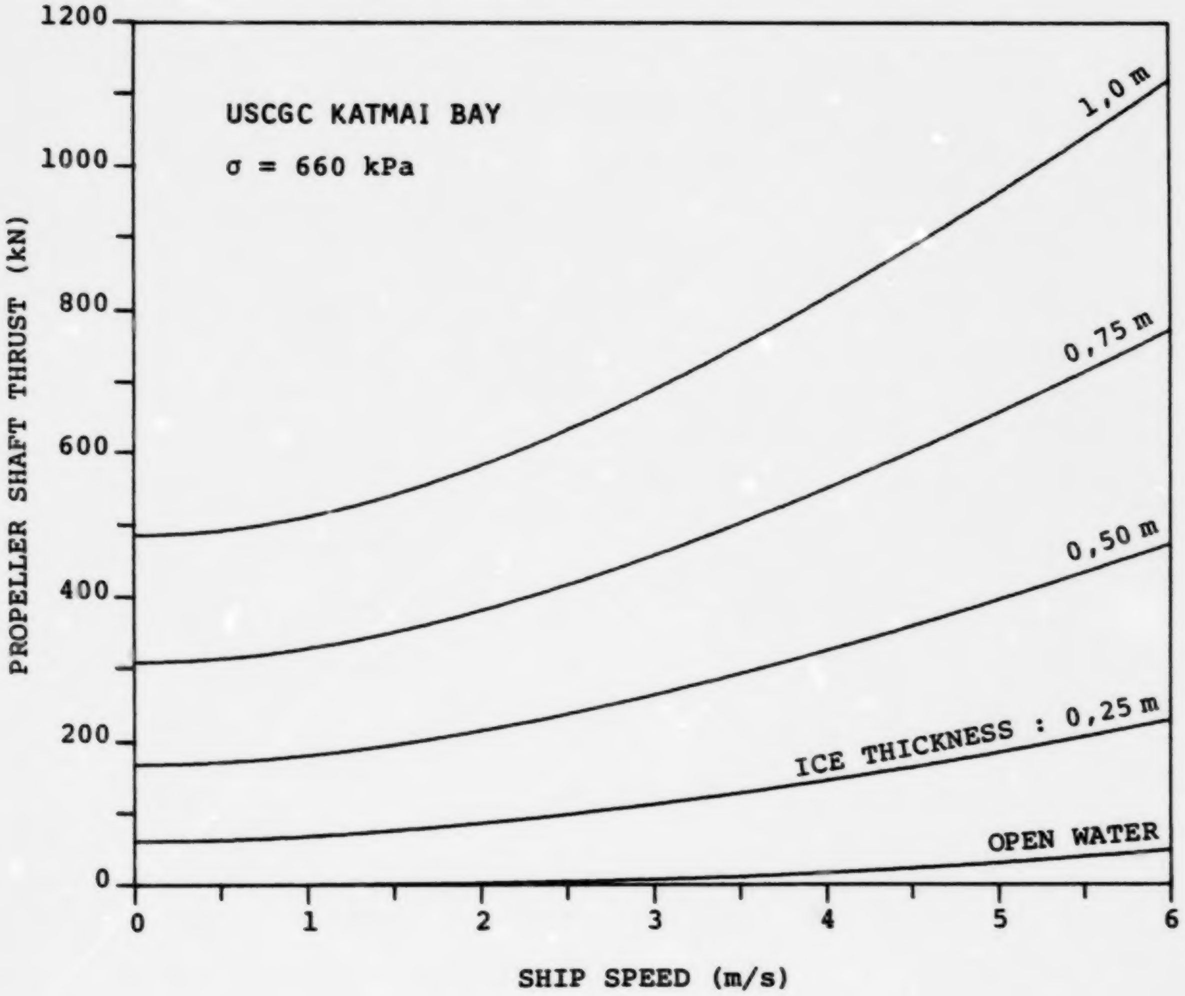

Figure D.6.: Plot of predicted thrust required to overcome level ice resistance versus ship speed. Predicted thrust obtained by using EQ.: 4.1.

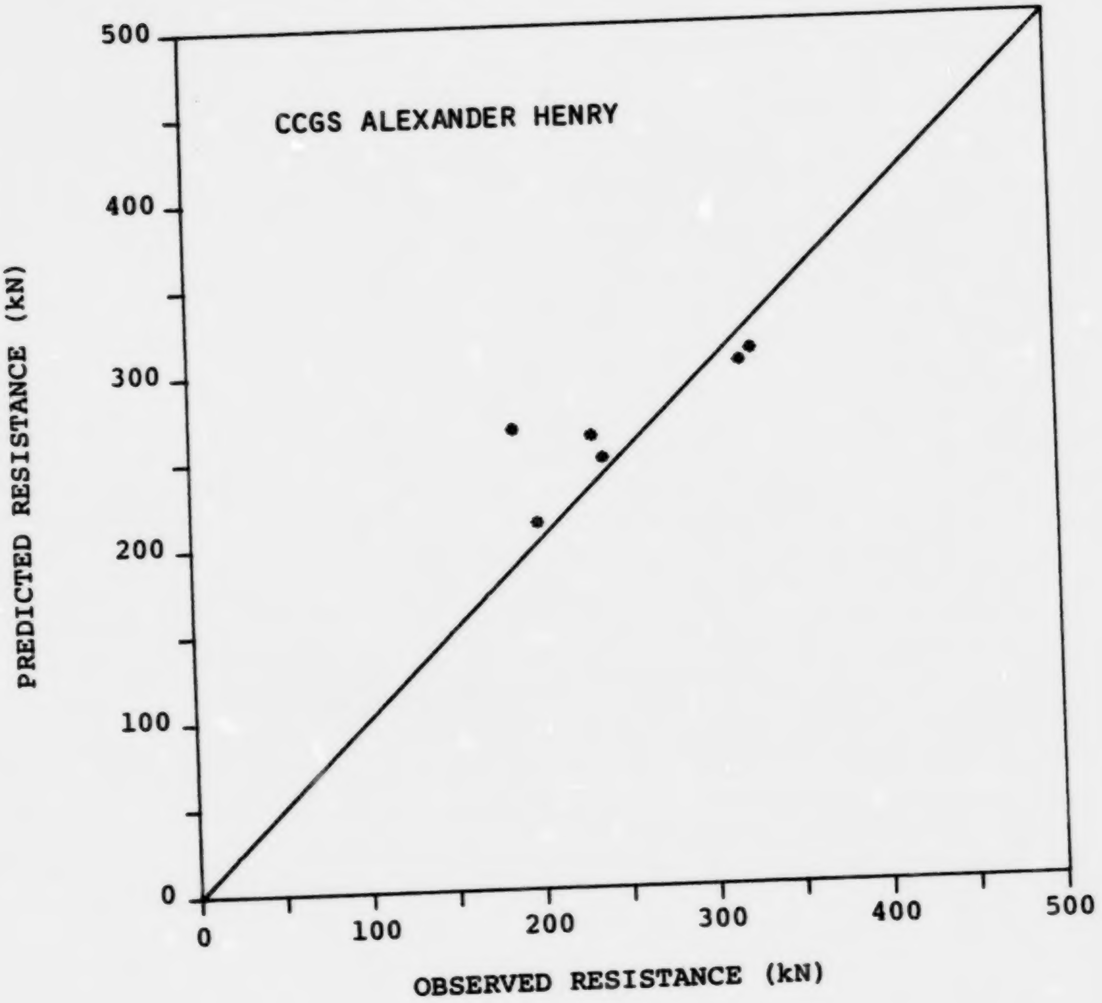

Figure D.7.: Plot of predicted versus observed resistance. Predicted resistance obtained by using EQ.: 4.1.

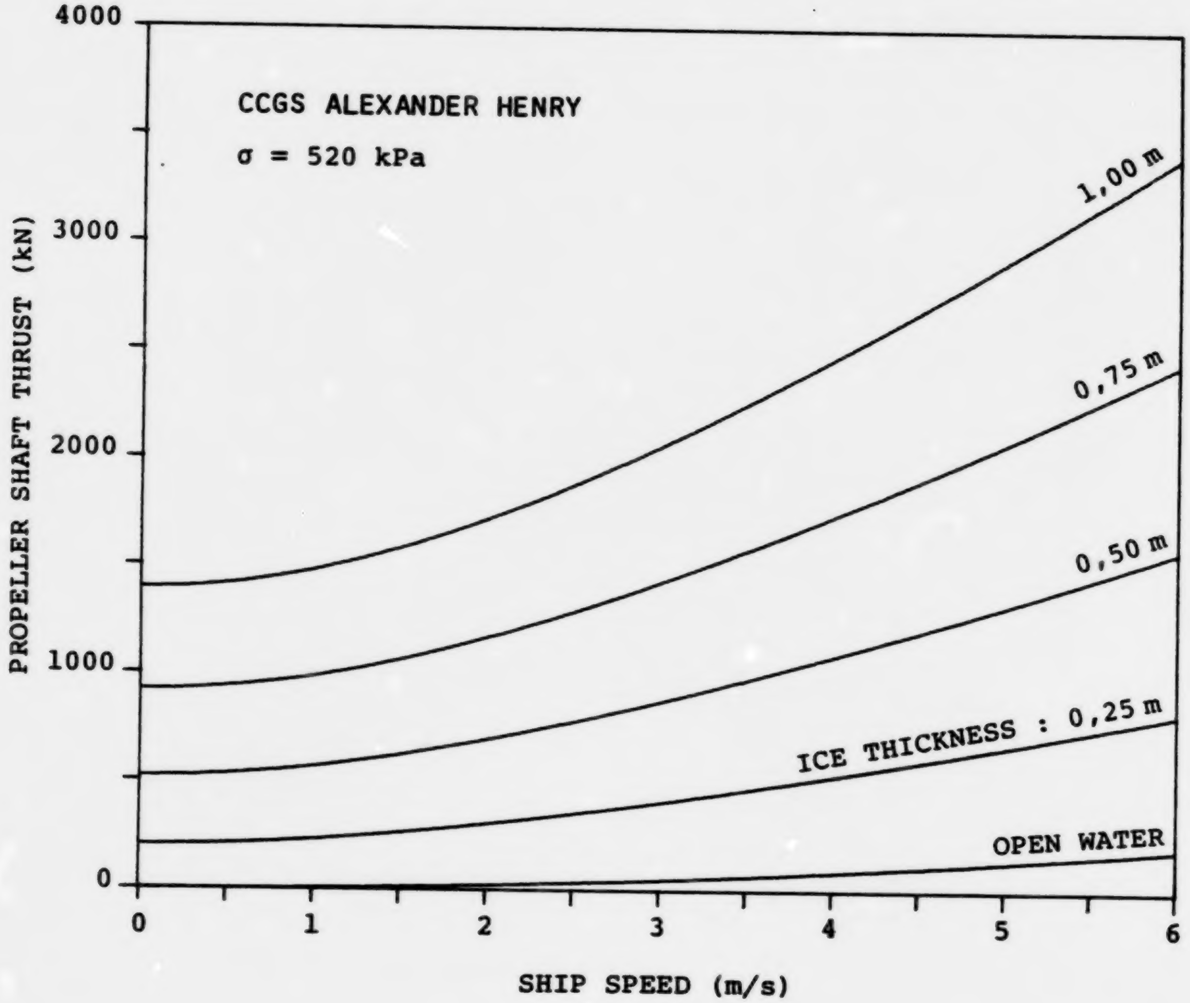

Figure D.8.: Plot of predicted thrust required to overcome level ice resistance versus ship speed. Predicted thrust obtained by using EQ.: 4.1.

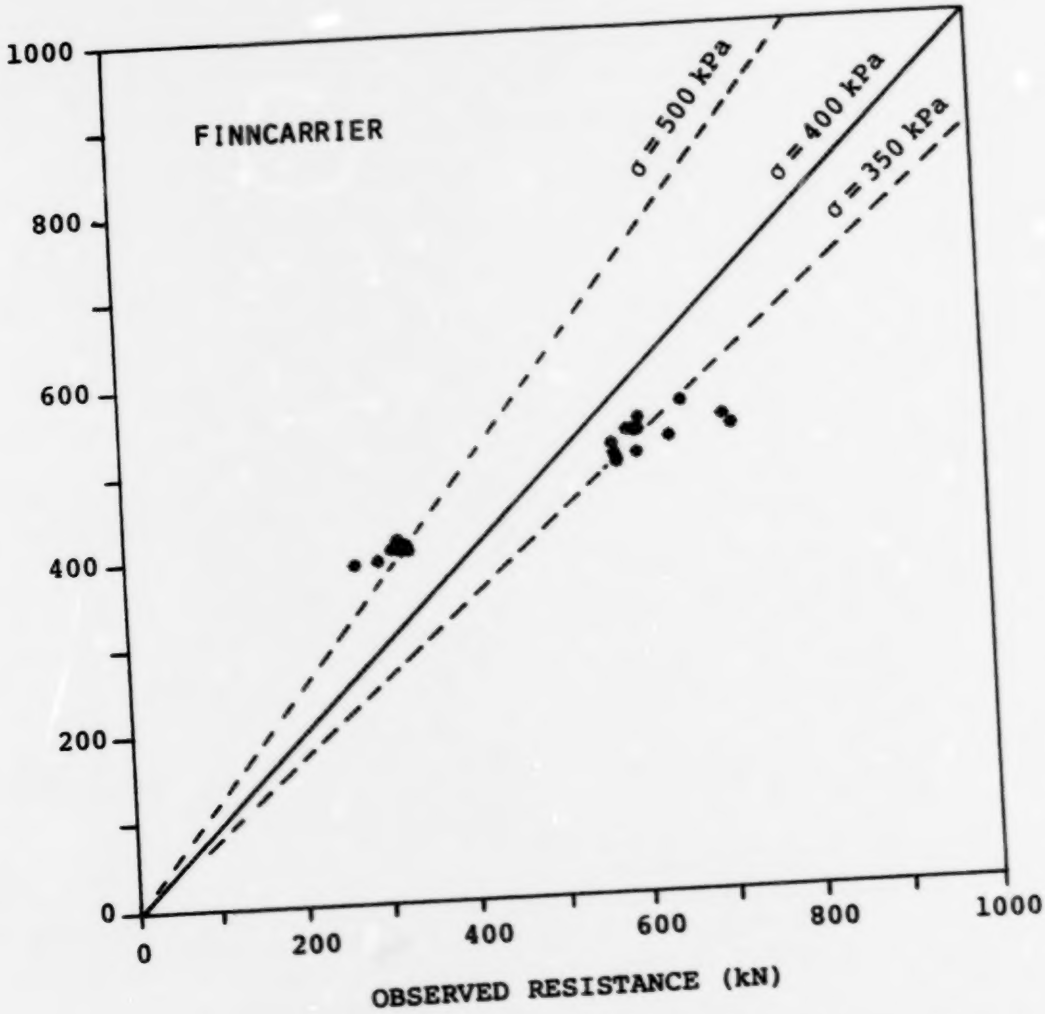

Figure D.9.: Plot of predicted versus observed resistance. Predicted resistance obtained by using EQ.: 4.1.

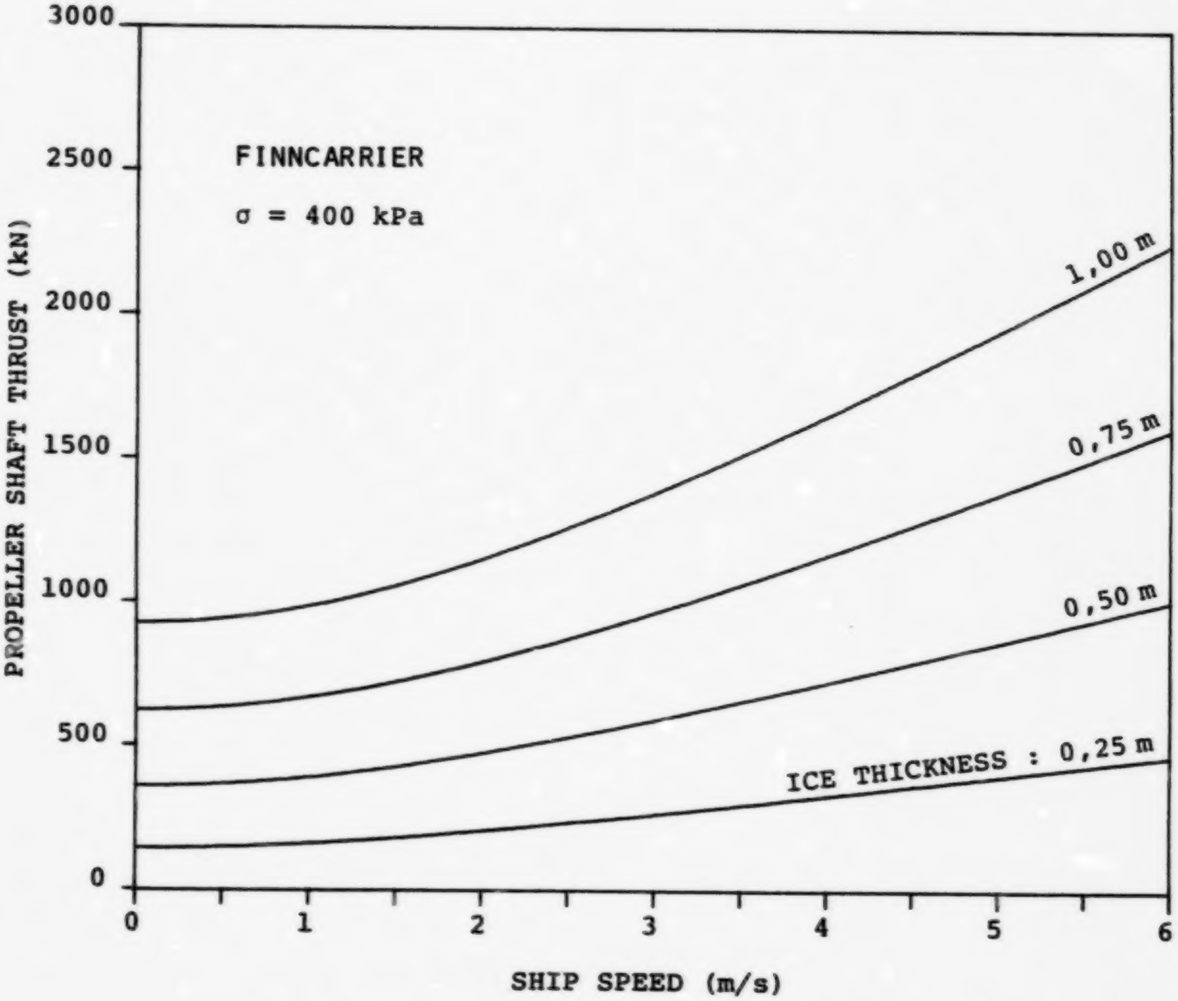

Figure D.10.: Plot of predicted thrust required to overcome level ice resistance versus ship speed. Predicted thrust obtained by using EQ.: 4.1.

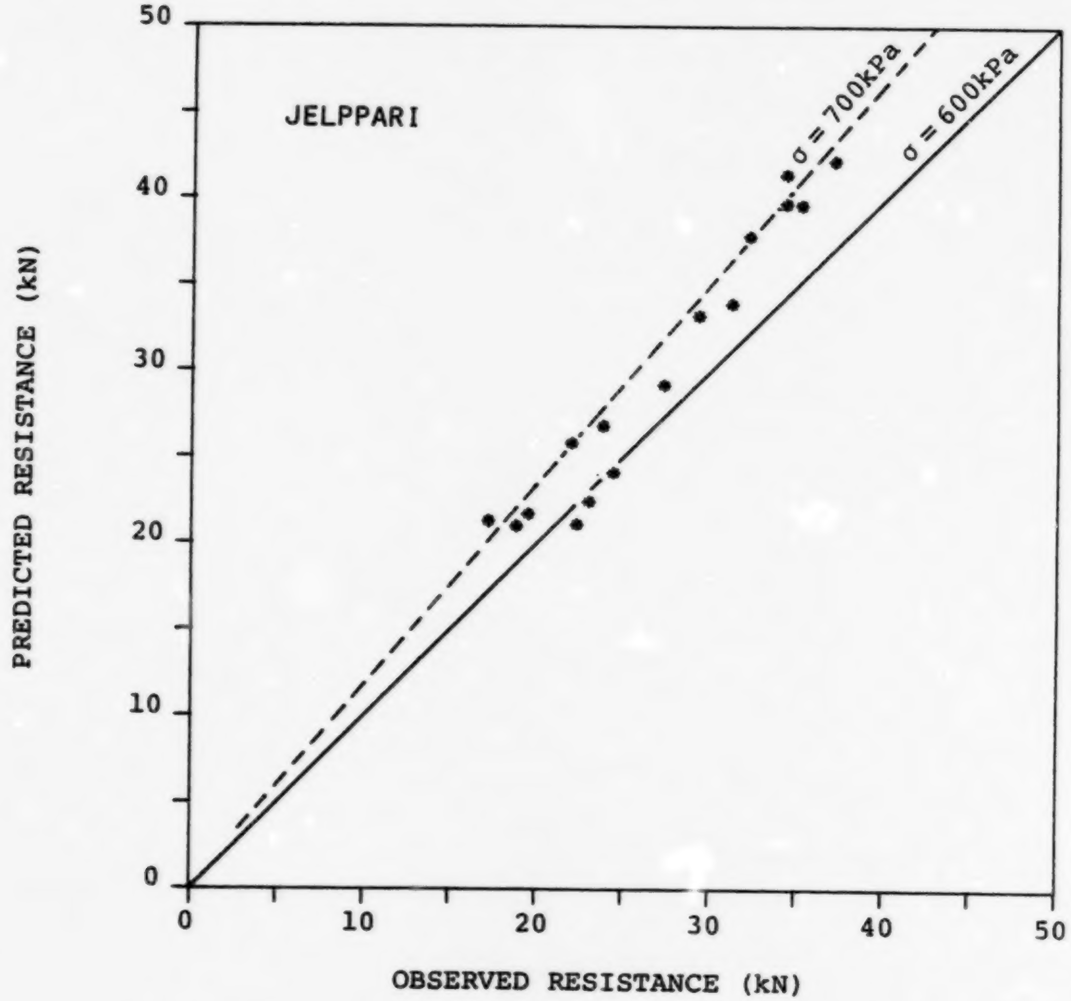

Figure D.11.: Plot of predicted versus observed resistance. Predicted resistance obtained by using EQ.: 4.1.

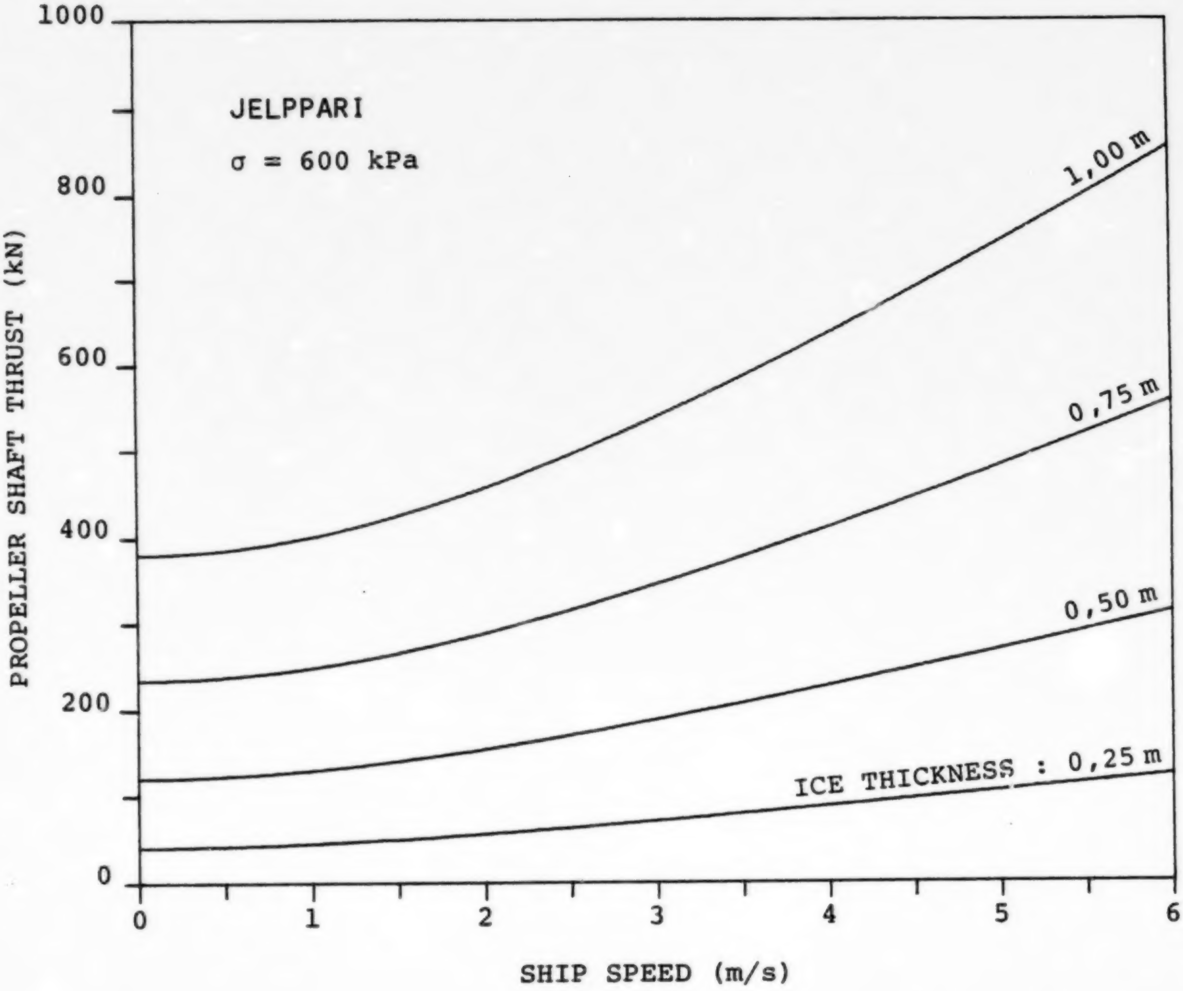

Figure D.12.: Plot of predicted thrust required to overcome level ice resistance versus ship speed. Predicted thrust obtained by using EQ.: 4.1.

- APPENDIX E -

COMPARISON WITH OTHER LEVEL ICE MODELS.

It is generally recognized that the icebreaking resistance is dependent on flexural ice strength. TABLE E.1 presents flexural ice strength data collected under natural conditions reported by various authors.

TABLE E.1

FLEXURAL ICE STRENGTH

Weeks and Assur (1969)	$200 < \sigma < 735$ kPa.
Frankenstein (1961)	$200 < \sigma < 800$ kPa.
Drouin and Michel (1972)	$200 < \sigma < 800$ kPa.
Lavrov (1969)	$140 < \sigma < 830$ kPa.
Enkvist (1972)	$400 < \sigma < 800$ kPa.

The reasonable strength range of ice in which most icebreakers operate seems to vary from 200 to 800 kPa.

Figure E.1 shows the plot of EQ.: 4.2 for USCGC MACKINAW in ice 0,61 m (2 ft) thick. Also shown are comparative resistance values computed using the expressions suggested by Lewis et alt. (1982), Edwards et alt. (1972), Kashteljan et alt. (1968) and the analytical model developed by Milano (1973).

Edwards et alt. (1972) analyzed the MACKINAW full scale data by statistical correlation and regression techniques. A predictor equation was obtained in the following form:

$$\frac{R_i}{\rho g B h^2} = C_0 + C_1 \frac{V}{\sqrt{gh}} + C_2 \frac{V^2}{gh} + C_3 \frac{h_s}{h} \qquad \text{EQ.: E.1}$$

where $C_0 = 5{,}259$; $C_1 = 4.350$; $C_2 = 1{,}676$; $C_3 = 5{,}464$ for the MACKINAW particular conditions.

Lewis et alt. (1982) using different candidate variables obtained by statistical correlation and regression techniques a predictor equation in a different form:

$$\frac{R_i}{\rho g B h^2} = C_0 + C_1 \frac{L}{h} \frac{V}{\sqrt{gB}} \qquad \text{EQ.: E.2}$$

where $C_0 = 7{,}1612$; $C_1 = 0{,}2215$ for the particular MACKINAW full scale data set.

Since these two semi-empirical equations are "custom tailored" by statistical correlation and regression techniques to the particular MACKINAW data set, they will be used as reference lines to represent full scale data.

It must be pointed out that the semi-empirical models are, as shown by the above equations, dependent on the selected candidate parameters. The influence of ship parameters, ice characteristics, and interaction variables are implicitly included in the values of the coefficients. Such predictor equations derived for a particular data set strictly apply for the conditions under which they were derived. Hence, extrapolation is prohibited.

The equation proposed by Kashteljan et alt. (1968) takes into consideration the influence of the hull geometry but neglects the influence of the friction coefficient. It can be seen, from Figure E.1, that the predicted values underestimate the ice resistance even if flexural ice strength as high as 800 kPa is used.

The purely analytical model developed by Milano (1973) considers, in every detail, the energy components absorbed during the icebreaking process. Unfortunately, Milano's model cannot be forced to match full scale data even by using flexural ice strength as high as 1722 kPa.

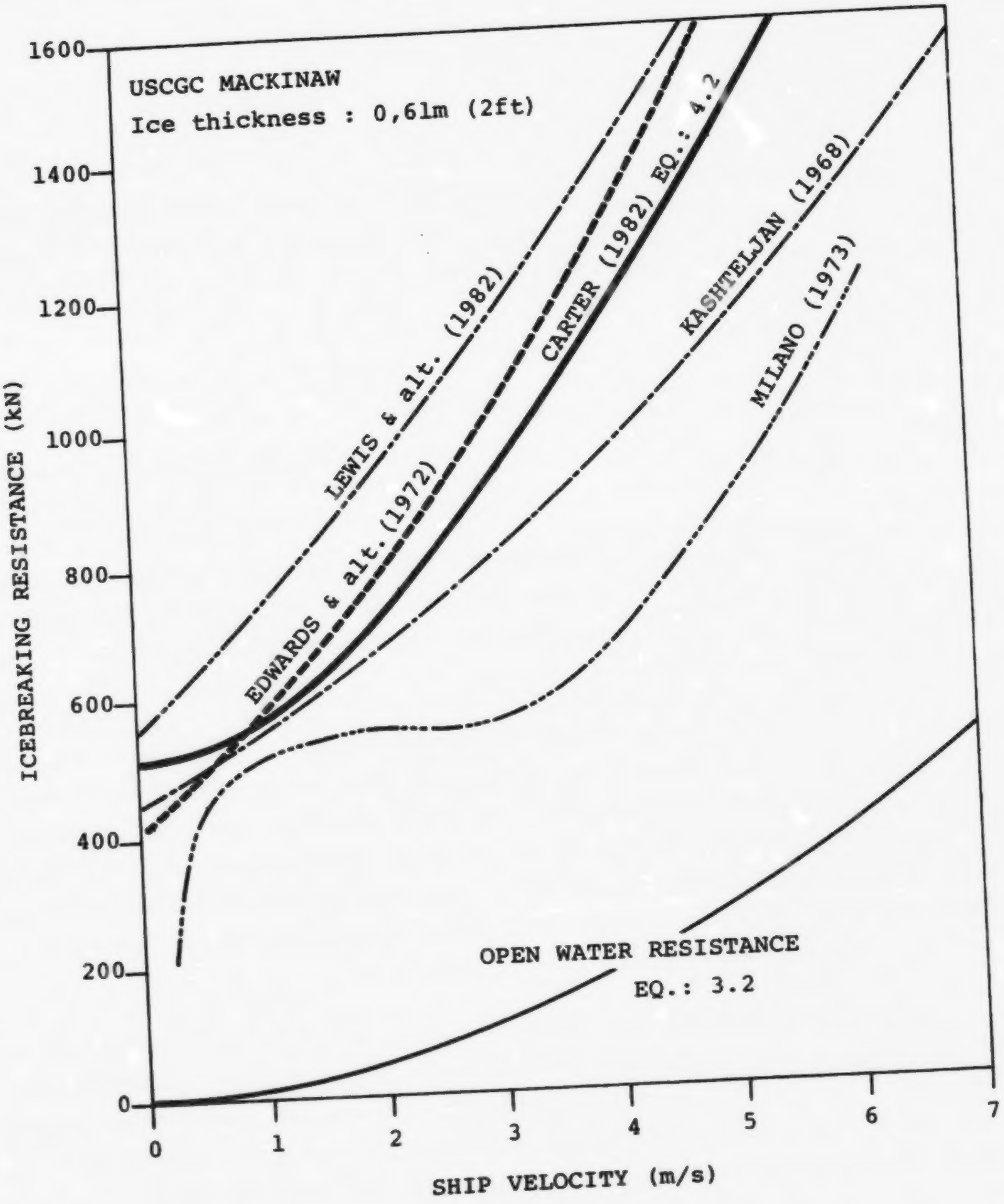

Figure E.1.: Icebreaking resistance versus ship speed for USCGC MACKINAW as predicted by various formulations.

It is thought that the discrepancy between the predicted and observed values may be explained by the failure criterion used by the author. In the absence of a more appropriate ice failure criterion, Milano used the Nevel's criterion which was derived for a load uniformly distributed for a certain distance on a floating ice wedge. (See Figure A.5). The situation corresponding to the force exerted by an icebreaker hull is more properly represented by a force applied at the edge of a truncated floating ice wedge. (See Figure A.12). It would be very interesting to introduce a more appropriate ice failure criterion into Milano's analytical model.

As seen from Figure E.1, the proposed model, EQ.: 4.2, closely reproduces the experimental data when the measured friction coefficient, 0,145, and realistic flexural ice strength, 400 kPa, are used.

REFERENCES.

Drouin,M.,and Michel,B., 1972, La Résistance en Flexion de la Glace du St-Laurent déterminée en Nature. Rapport GCT-72-09-26 préparé pour Min. des Transports, Div. du Chenal Maritime du St-Laurent. Univ. Laval, Génie civil, Québec, Canada. 55p.

Edwards,R.Y.Jr., Lewis,J.W., Wheaton,J.W. and Coburn,J.Jr., Full Scale and Model Tests of a Great Lake Icebreaker.SNAME paper no 5, presented at the Annual Meeting, New York, November 16 17, 1975

Enkvist,E., 1972, On the Ice Resistance Encountered by Ships Operating in the Continuous Mode Of Icebreaking, The Swedish Academy of Engineering Sciences in Finland, Report no 24, Helsinky.

Frankenstein,G.E. 1961, Strength data on Lake Ice, SIPRE, Tech. report 80, 18 p.

Kashteljan,V.I., Poznjak,I.I., Ryvlin,A.Ja,1968, Ice Resistance to Motion of a Ship. Sudostroenie, Leningrad, (translation)

Lavrov,V.V. 1969, Deformation and Strength of Ice. Translated from Russian, Israel Program for Scientific Tranlations, U.S. Dept. of Commerce, N.T.I.S., Springfield,Va.

Lewis,J.W., Bulat,V., Glen,I.F., Kotras,T., 1982, Development of a Semi Empirical Model for Predicting Resistance and Determining Thrust Requirements for Ships in Level Ice. Jointly sponsored project by Transport-Canada, Transportation Development Centre, and US MARAD performed by Arctec Canada Ltd and Arctec Inc.,

Milano,V.R., 1973, Ship Resistance to Continuous Motion in Ice, Paper presented at the Annual Meeting, New York, N.Y., November 15-17, 1973, of the SNAME.

Weeks,W.F.,and Assur,A., 1969 Fracture of Lake and Sea Ice, Research Report 269, CRREL, Hanover, New Hampshire, U.S.A.

- APPENDICE F -

OPTIMUM CHARACTERISTICS OF THE HULL-ICE INTERFACE

The objective of the work described in this Appendice is to investigate the possibility of reducing the continuous level icebreaking by optimizing the characteristics of the hull-ice interface. Hydrostatical and hydrodynamical considerations are beyond the scope of the present work.

The thrust requirements to overcome the ice resistance will be determined by making use of the math model developed previously in Chapter 3. The model considers the ice force at a given point as resolved into two components: the normal and tangential components. When the ice cover is about to fail, the tangential component, i.e. the friction force, acts in a direction defined by the line of intersection of the two following planes:

- tangent plane at the considered point;
- plane defined by the normal at the considered point and by the direction of ship motion.

From our math model, the following general trends can be drawn: (See Figures 3.6 & 3.7)

Forebody Characteristics	Influence on Level Ice Resistance
Ship Beam, B	Intermediate
Ratio Forebody Length / Beam	Intermediate
Stem Angle, β	Intermediate for $\beta < 30°$ Strong for $\beta > 30°$
Spread angle, θ	Small
Flare angle at midship, γ	Strong for $\gamma < 15°$ Intermediate for $\gamma > 20°$
Coefficient of friction, f	Strong

It is emphasized that the aimed objectives are to optimize ice passage capability not to design a viable real ship.

Considering that the ship beam is generally set by mission requirements and that the ratio "Forebody Length / Beam" must be greater than 1 / tan θ in order to avoid a point of inflection, the following characteristics were retained for the "OPTIMUM HULL" which minimizes the thrust requirements to overcome the level ice resistance.

Hull Shape Variables	Selected Values
Maximum Beam, B	60 ft (18,29 m)
Forebody Length	80 ft (24,38 m)
Ship Length	250 ft (76,2 m)
Stem Angle, β	18°
Flare Angle at Midship, γ	20°
Spread Angle, θ	45°

The hull shape being defined at the maximum beam section and at the stem, the waterline shape was then interpolated by the method of elliptical arcs outlined in Chapter 1. As shown in Figures F.1 and F.2, the elliptical approximations are very consistent with the forebody characteristics for icebreakers of conventional form. The calculated DWL OFFSETS and BOW ANGLES for the "OPTIMUM HULL" are given in Table F.1. A schematic representation of the hull-ice interface and a graphical representation of the hull angles are respectively shown in Figures F.3 and F.4.

The ice load distribution on the hull was then evaluated making use of EQ.: 3.9 and numerically integrated. The results are shown in Figure F.5. It can be seen that resistance due to friction varies from 50 to 70% of the total resistance. This observation is in accordance with the fact that the predictor models which neglect friction forces consistently underestimate ice resistance by a factor 2.

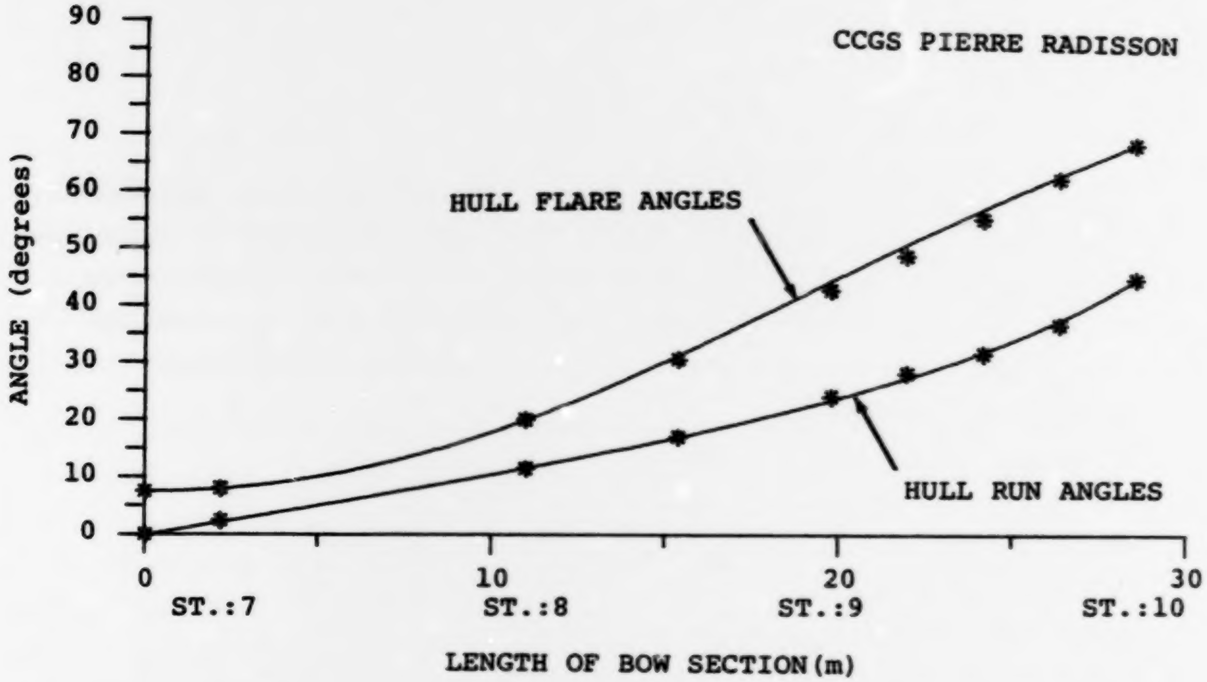

Figure F.1.: Comparison of approximations to hull run angles and hull flare angles with data measured from lines plan. CCGS RADISSON

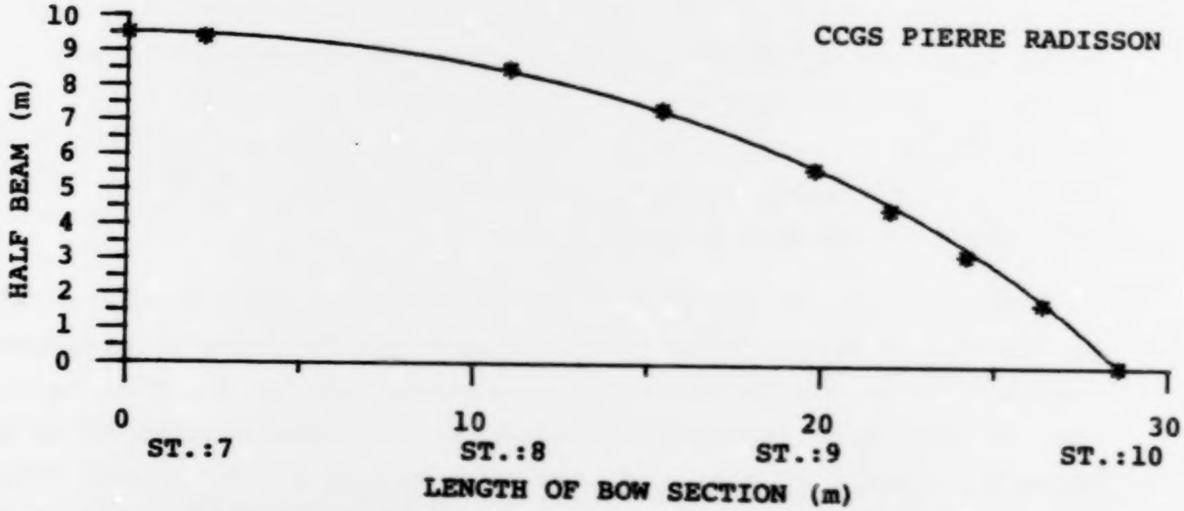

Figure F.2.: Comparison of elliptical approximation to the waterline with data measured from lines plan. CCGS RADISSON.

TABLE F.1

DWL OFFSETS AND BOW ANGLES FOR THE "OPTIMUM HULL".

STATION #	OFFSETS (1)	WATER-LINE ANGLES θ	BUTTOCK LINE ANGLES β	FLARE ANGLES γ	ANGLES (2) r	ANGLES (3) s	ANGLES (4) t
6,75	1,200	0,00	0,58	20,00	90,00	20,00	90,00
6,875	1,199	0,81	2,35	20,05	89,19	35,30	89,34
7	1,196	2,15	5,82	20,38	87,85	36,47	88,27
7,125	1,190	3,50	9,07	21,00	86,50	37,43	87,22
7,25	1,181	4,85	11,93	21,92	85,15	38,71	86,21
7,375	1,169	6,22	14,33	23,11	83,78	40,31	85,26
7,5	1,154	7,59	16,25	24,58	82,41	42,20	84,38
7,625	1,136	8,98	17,73	26,31	81,02	44,32	83,59
7,75	1,114	10,39	18,83	28,27	79,61	46,61	82,88
7,875	1,090	11,82	19,59	30,45	78,18	49,01	82,28
8	1,062	13,27	20,09	32,81	76,73	51,46	81,78
8,125	1,031	14,75	20,37	35,33	75,25	53,90	81,37
8,25	0,996	16,26	20,49	37,97	73,74	56,29	81,06
8,375	0,958	18,81	20,48	40,69	72,19	58,59	80,83
8,5	0,916	19,40	20,37	43,46	70,60	60,79	80,67
8,625	0,870	21,03	20,20	46,25	68,97	62,86	80,58
8,75	0.819	22,72	19,98	49,01	67,28	64,79	80,53
8,875	0,765	24,47	19,74	51,73	65,53	66,58	80,52
9	0,706	26,29	19,48	54,38	63,71	68,23	80,55
9,125	0,641	28,18	19,21	56,95	61,82	69,74	80,59
9,25	0,571	30,16	18,95	59,41	59,84	71,13	80,65
9,375	0,496	32,25	18,71	61,76	57,75	72,39	80,71
9,5	0,414	34,46	18,49	64,01	55,54	73,54	80,77
9,625	0,324	36,80	18,29	66,15	53,20	74,57	80,83
9,75	0,226	39,32	18,14	68,19	50,68	75,50	80,87
9,875	0,119	42,04	18,04	70,13	47,96	76,33	80,89
10	0,000	45,00	18,00	71,99	45,00	77,06	80,89

(1) OFFSETS ÷ STATION SPACING ; (2),(3),(4) See Figure 1.1

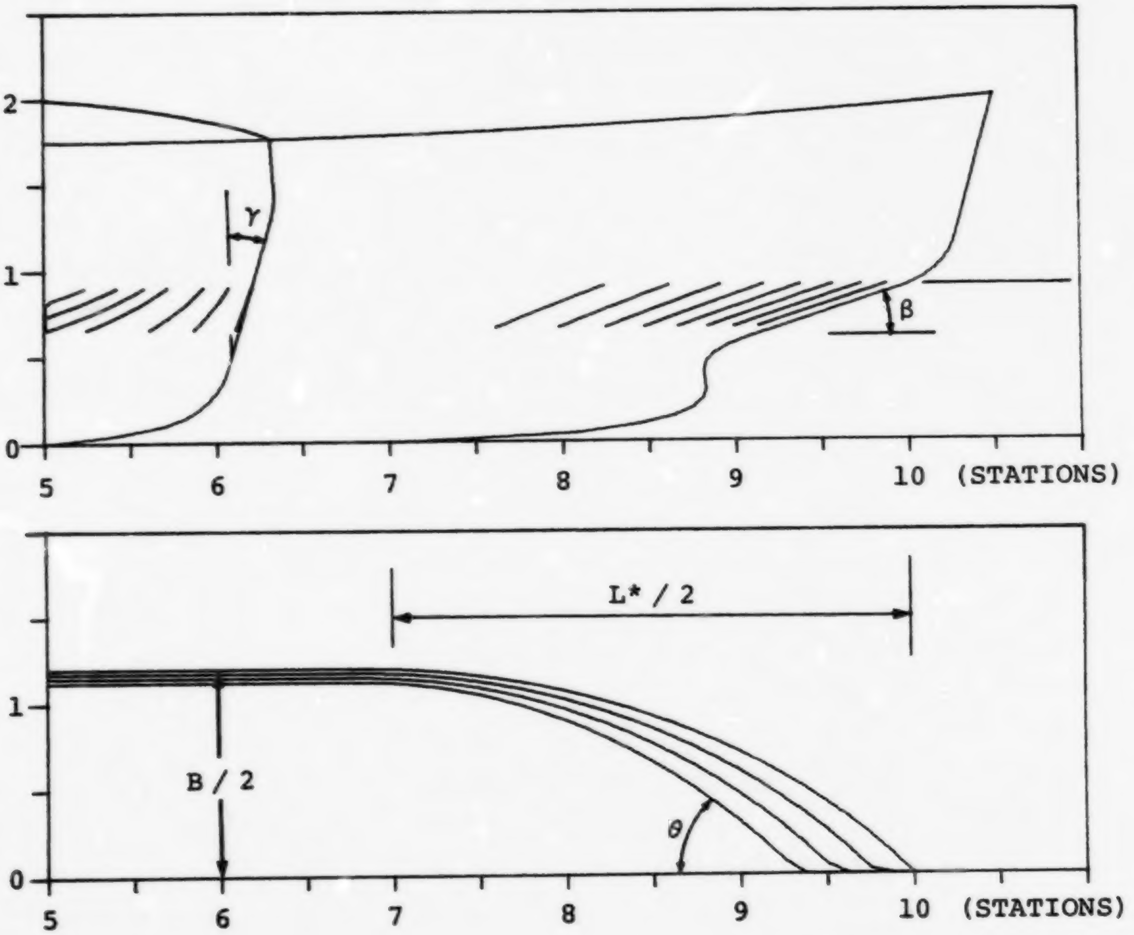
2
1
0
γ
β
5
6
7
8
9
10 (STATIONS)
L* / 2
1
B / 2
θ
0
5
6
7
8
9
10 (STATIONS)

Figure F.3.: Schematic representation of the hull-ice interface for the "OPTIMUM HULL".

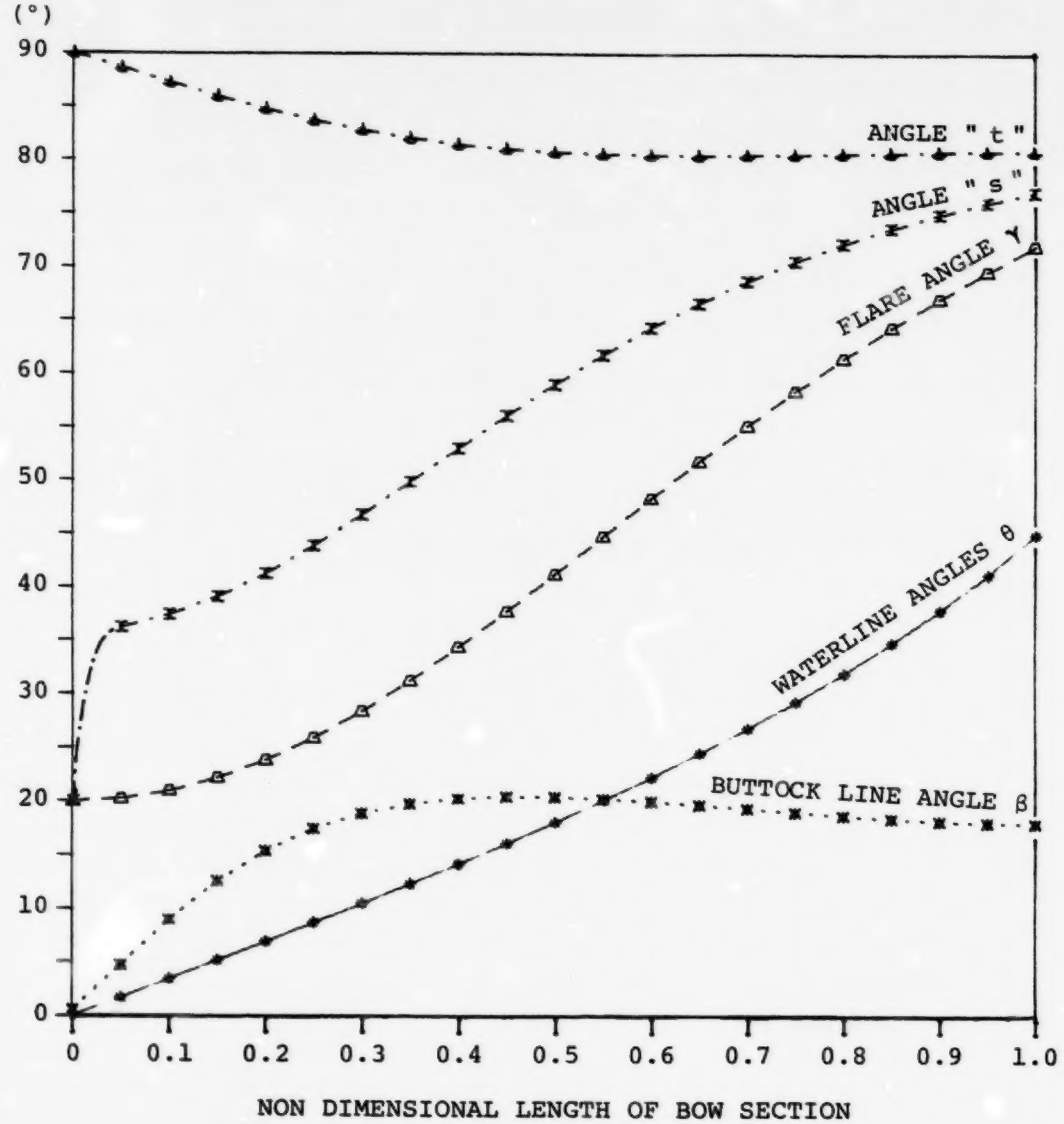

Figure F.4.: Hull Angles for the "OPTIMUM HULL".

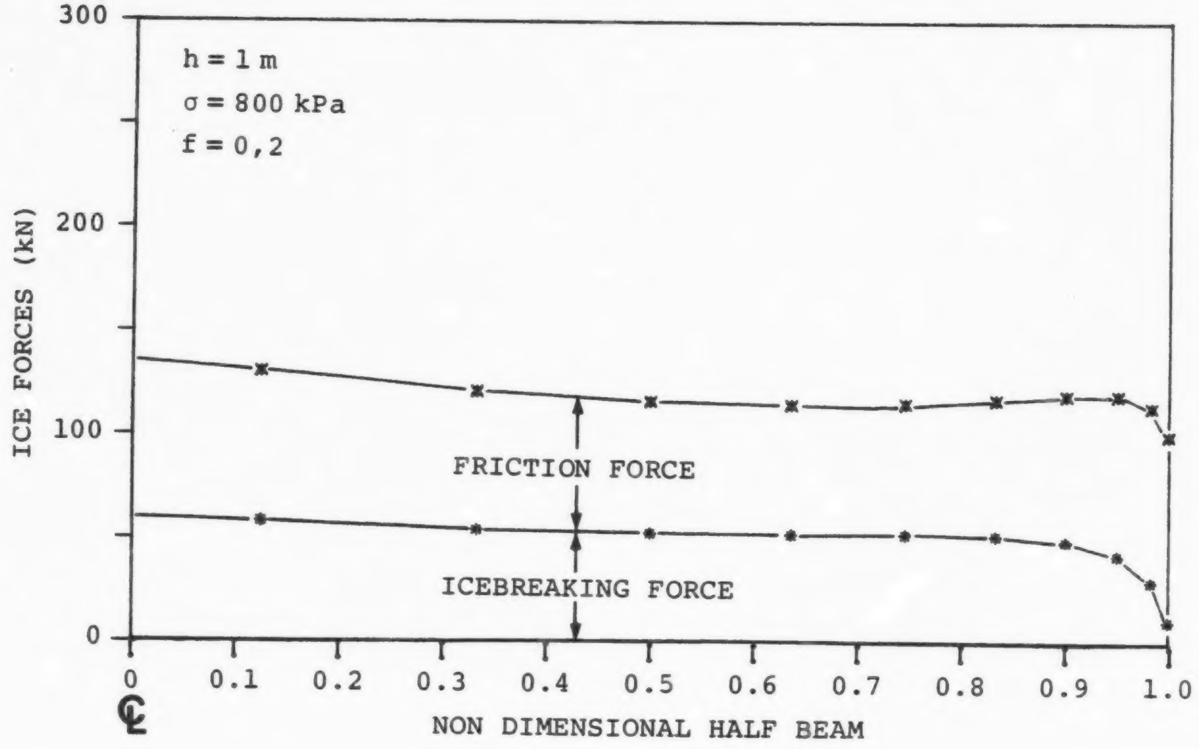

Figure F.5.: Components of the load distribution associated respectively with icebreaking and friction forces.
- "OPTIMUM HULL" -

Figure F.6 shows the tremendous increase of the thrust requirement when the flare angle at midship is varied from 20° to 0°.

In Figure F.7, the load distribution for the "OPTIMUM HULL" is compared with that of four different ships. It is seen that, for a properly designed forebody section, the thrust required to overcome ice resistance may be reduced by a factor as high as 7.

Figure F.8 shows a similar adverse effect of $\gamma = 0°$ as obtained by a quite different math model.

It is concluded that the hull shape and dimension can have a very significant impact on the thrust required to overcome level ice resistance. The results obtained indicate that, to be efficient, the characteristics of an icebreaker forebody section should be kept, when possible, within the following ranges:

Variables	Ranges of Variation
Beam	As small as possible
Forebody Length / Beam	1,5 → 2,5
Bow Stem Angle, β	18° → 30°
Spread Angle, θ	30° → 45°
Flare Angle at Midship, γ	15° → 20°
Coefficient of friction, f	As low as possible

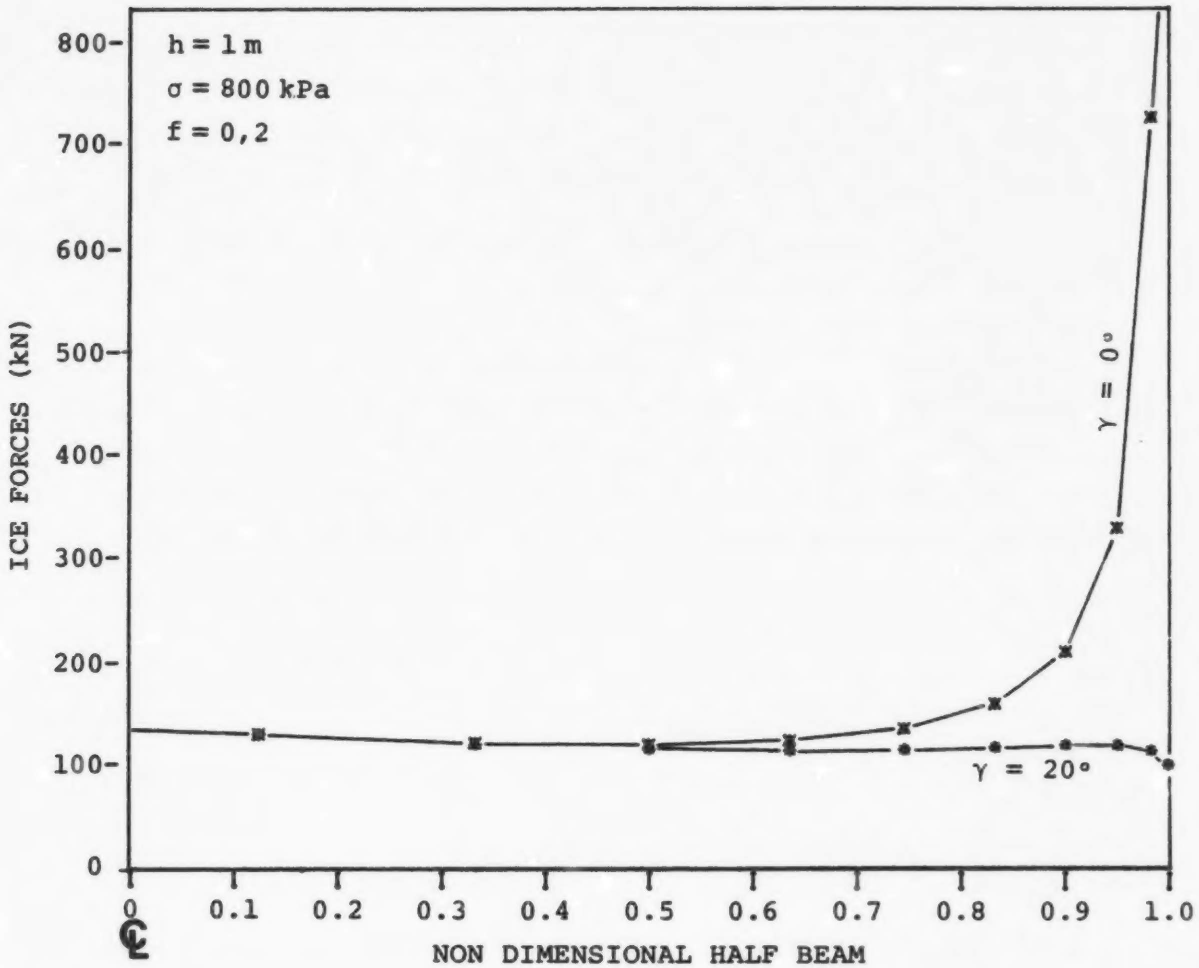

Figure F.6.: Influence of flare angle at midship. The relative thrust required to overcome ice resistance is as follows:
"OPTIMUM HULL" with γ = 20°: 1,0
"OPTIMUM HULL" with γ = 0°: 4,6

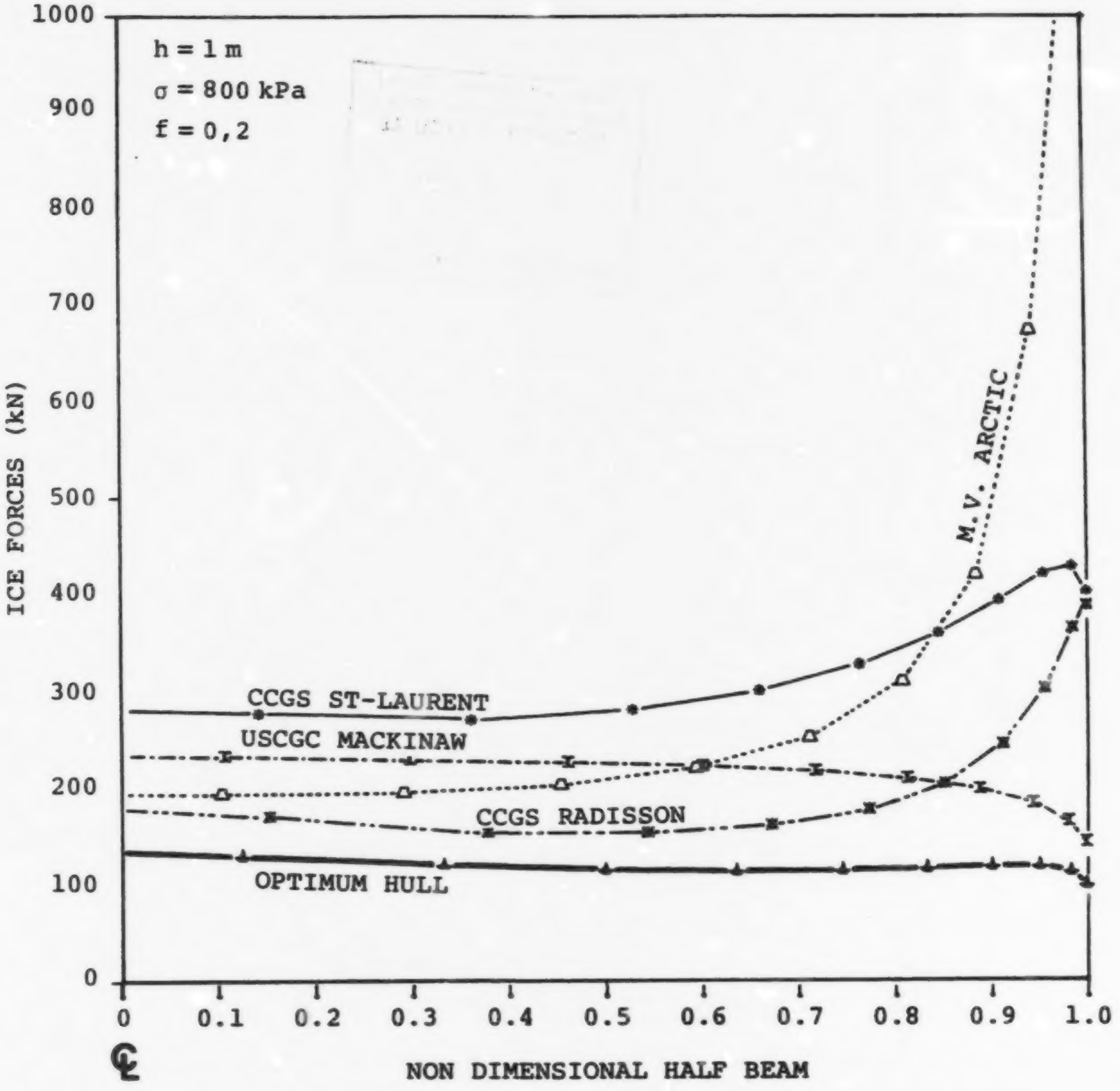

Figure F.7.: Load distributions for four different ships as compared to that of "OPTIMUM HULL". With BEAM EQUAL to that of "OPTIMUM HULL", the relative thrust required to overcome ice resistance would be as follows: "OPTIMUM HULL"..........: 1,0
USCGC MACKINAW.....: 1,83 ; CCGS RADISSON..........: 1,90
CCGS ST-LAURENT....: 2,89 ; M.V. ARCTIC............: 7,72

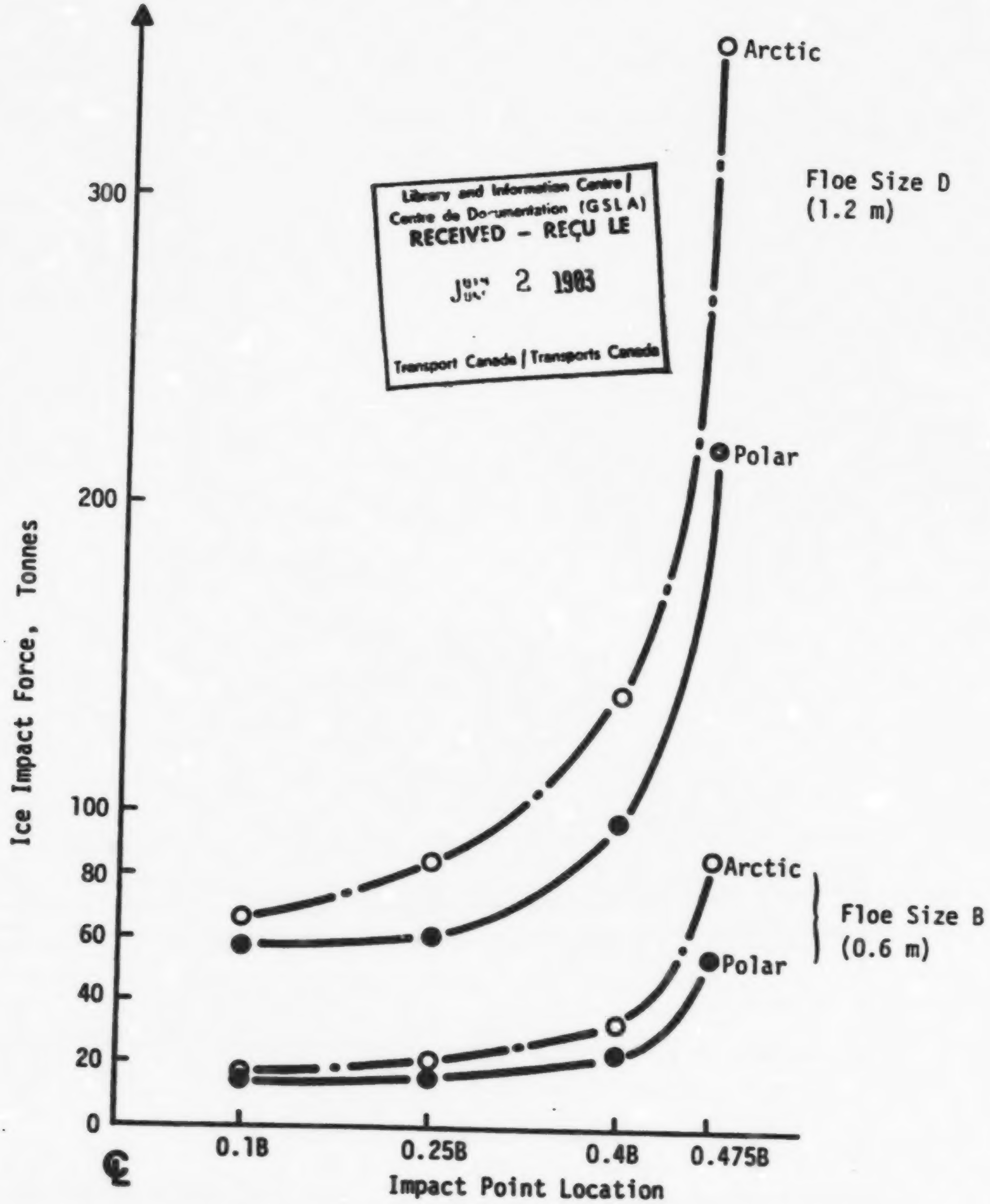

Library and Information Centre / Centre de Documentation (GSLA)
RECEIVED – REÇU LE
J[illegible] 2 1983
Transport Canada / Transports Canada

Figure F.8.: Impact force versus corresponding impact locations as computed by a math model developed by ARCTEC. This figure is reproduced from:

Nawwar, A., and Noble, P., 1980, Final Report on Ice Force Math Model Investigations. Report TP 2596 prepared for the Transportation Development Centre by Arctec Canada, July 5, 1980.

POOR

QUALITY

ORIGINAL